Theory of optical signal amplification and processing by quantum-dot semiconductor optical amplifiers

M. Sugawara,* H. Ebe, N. Hatori, and M. Ishida
Institute of Industrial Science and Nanoelectronics Collaborative Research Center, University of Tokyo, 4-6-1 Komaba, Meguro, Tokyo 127-8172, Japan

Y. Arakawa
Research Center for Advanced Science and Technology, University of Tokyo, 4-6-1 Komaba, Meguro, Tokyo 127-8172, Japan

T. Akiyama, K. Otsubo, and Y. Nakata
Fujitsu Laboratories Ltd. and Fujitsu Ltd., 10-1 Morinosato-Wakamiya, Atsugi 240-01, Japan
and Optoelectronic Industry and Technology Development Association (OITDA), 1-20-10 Sekiguchi, Bunkyo, Tokyo 112-0014, Japan
(Received 24 July 2003; revised manuscript received 24 December 2003; published 30 June 2004)

This work presents a theory of optical signal amplification and processing by quantum-dot semiconductor optical amplifiers (SOA's) based on the density matrix equations to treat electron-light interaction and the optical pulse propagation equations. The theory includes the linear optical response as well as the incoherent and coherent nonlinear response of the new devices with arbitrary spectral and spatial distribution of quantum dots in the active region under the multimode light. The incoherent nonlinear response was due to the incoherent spectral hole burning and the reduction in the carrier density by the stimulated emission. The coherent nonlinearity was due to the dynamic spectral hole burning caused by the population beating at the electronic states resonant to the multimode light and the carrier density pulsation caused by the carrier relaxation dynamics. Based on the theory, we numerically simulated the operation of quantum-dot SOA's, and succeeded in presenting their diverse promising features in a very systematical manner. We expect amplifiers with low power consumption, high saturation power, broad gain bandwidth, and pattern-effect-free operation under gain saturation, and also signal processing devices to realize high-speed (40 to 160 Gb/s) pattern-effect-free wavelength conversion by the cross-gain modulation with low frequency chirping and symmetric highly-efficient 1 to 2 THz wavelength conversion by the nondegenerate four-wave mixing. We point out that the nonlinear optical response due to the spectral hole burning plays a decisive role in the high-speed optical signal processing. Many of the theoretical predictions in this paper agree well with recent experimental demonstrations of device performance. This work will help not only design practical quantum-dot devices working in the photonic networks but also understand how carrier dynamics relates to the optical response of quantum dots with optical gain under current injection.

DOI: 10.1103/PhysRevB.69.235332 PACS number(s): 85.35.Be, 68.65.Hb, 78.67.Hc, 73.21.La

I. INTRODUCTION

Quantum-dot semiconductor optical amplifiers (SOA's) have opened a new frontier in the field of semiconductor optical devices for high-capacity and flexible optical data transmission. Since we first proposed multiwavelength and high-speed pattern-effect-free signal amplification and processing by quantum-dot SOA's based on their nonlinear optical properties[1–5] and our device theory,[6–10] we have discovered and demonstrated diverse promising features both theoretically and experimentally.[11–18] Among them are high saturation power, broad gain bandwidth, pattern-effect-free amplification of single- and multichannel signals, pattern-effect-free high-speed wavelength conversion of optical signals by the cross-gain modulation, and symmetric high-speed wavelength conversion by nondegenerate four-wave mixing. In particular, a series of experimental demonstrations of 1.3-micron quantum-dot SOA's with InAs self-assembled dots in the active region aroused broad interests in this new nanodevice field; We demonstrated 10–40 Gb/s pattern-effect-free amplification,[11–15] 10–40 Gb/s pattern-effect-free wavelength conversion by the cross-gain modulation,[11–15] and the symmetric wavelength conversion by nondegenerate four-wave mixing.[16,17] We expect these promising features of quantum-dot SOA's to provide high-performance amplifiers as well as all-optical switches in the next-generation photonic networks, which will work as regenerators, wavelength converters, and time-division demultiplexers of optical pulse trains at much higher capacity than the bulk or quantum-well counterparts. These pioneering works have been followed by various reports like the wavelength conversion by 1.5-micron InAs quantum-dash SOA's,[19] and the polarization-independent photoluminescence, and thus optical gain, in stacked InAs quantum dots.[20]

Though practical significance of quantum-dot SOA's has now come to be acknowledged, their operation theory has yet to be developed in order to understand their linear and nonlinear optical response more precisely as well as to design best-performance devices. Indispensable prerequisites for the theoretical development is to deal with unique features of quantum dots in the SOA active region, like their spatial localization, inhomogeneous broadening of optical spectra due to their size, composition, shape, and strain distribution, carrier capture from the wetting layer, carrier emis-

sion to the wetting layer, intradot population relaxation, and homogeneous broadening of the optical spectrum at each discrete energy state due to polarization relaxation, etc. In particular, dealing with the population and polarization relaxation at each discrete energy state of each dot under the multimode light is a key to comprehensive understanding of nonlinear optical response, which we expect to be remarkable in quantum-dot SOA's. Such remarkable nonlinearity is due to slower population and polarization relaxation than conventional semiconductors known as the phonon bottleneck[21–23] and due to prevention of direct carrier transfer between spatially localized dots. Though the ultrafast nonlinear phenomena in quantum-dot SOA's has been found by pump-probe and four-wave mixing measurements,[1–5] a large gap between such knowledge on the carrier dynamics of quantum dots and the device performance still remains to be bridged.

The purpose of this work is to present an operation theory of quantum-dot SOA's including all the above mentioned properties unique to quantum dots for precise analyses of the SOA operation, and more generally, to step into a new body of theory, i.e., quantum-dot optical device theory, beyond the conventional one made for bulk or quantum-well active regions. We start by deriving equations for the polarization and the carrier population of the quantum-dot active region under the multimode light using the density matrix equations. Then, we present the optical pulse propagation equations in traveling-type quantum-dot SOA's, which include the spatial position of each dot, inhomogeneous broadening, linear optical susceptibility, and nonlinear optical susceptibilities due to spectral hole burning and carrier density pulsation. Based on the derived theory, we simulate the quantum-dot SOA performance to reveal its promising features in the photonic networks, its superiority to conventional SOA's with bulk or quantum-well active regions, and the physical origins behind the benefits. We add an Appendix to present a theory of SOA's with bulk or quantum-well active regions which describes comprehensively their performance as linear amplifiers and incoherent and coherent switches. This comparative approach will help highlight features of our quantum-dot theory in the main text.

II. THEORY OF OPTICAL PULSE PROPAGATION IN QUANTUM-DOT SOA's

The structure of the quantum-dot SOA is illustrated in Fig. 1. The SOA operates in the way that the current is injected into the active layer including quantum dots, and the input optical signals are amplified via the stimulated emission or processed via the optical nonlinearity by the quantum dots. Figure 1 also shows the cross-sectional and plan-view images of self-assembled InGaAs quantum dots as a typical example of quantum-dot crystals. Self-assembled InGaAs quantum dots on GaAs substrates and their application to semiconductor lasers have been intensively studied since early in the 1990s. They are nanosize semiconductor islands with a wetting layer grown via the Strasnki-Krastanow mode under highly mismatched epitaxy, where the electron energy states are completely quantized due to the three-dimensional

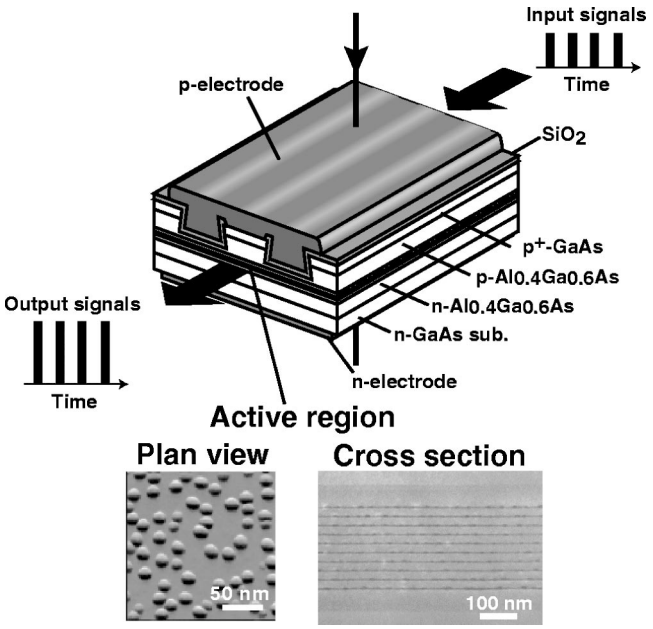

FIG. 1. Structure of the quantum-dot SOA with cross-sectional and plan-view images of self-assembled InGaAs quantum dots.

quantum confinement. Quantum-dot SOA's are novel optical devices using self-assembled quantum dots.

In this section, we develop an operation theory of the quantum-dot SOA's. First, we derive equations for the polarization and the carrier population of the quantum-dot active region under the multimode light using the density matrix equations to treat electron-light interaction in each quantum dot. We consider the two-level system in the quantum dot, which consists of the quantized electronic energy level of the conduction band and that of the valence band to describe the interband transition. We derive both linear and nonlinear polarization, and classify the nonlinear polarization into the incoherent and coherent ones. The incoherent nonlinear polarization is due to the population reduction via the stimulated emission which occurs even under a single light mode, causing the spectral-hole burning in the gain spectrum. We define this type of the spectral-hole burning as the incoherent one. The coherent nonlinear polarization is due to the population beating at the energy states through the optical response to more than two optical modes with different frequencies, and also due to the population beating through the intraband relaxation. We call the former population beating as the dynamic spectral-hole burning, and the latter as the carrier density pulsation according to general usage in bulk semiconductors and quantum wells (see Appendix). We also derive the pulse propagation equation in the quantum-dot SOA's, which work as the bases to describe their various operation modes, including single- and multimode amplification, amplified spontaneous emission, cross-gain and cross-phase modulation, and nondegenerate four-wave mixing. We present rate equations of carrier population in randomly distributed quantum dots, which are solved simultaneously with the pulse propagation equations.

Our theory can describe the linear and nonlinear optical response of the quantum-dot SOA's with arbitrary spectral

and spatial distribution of quantum dots in the active region under the multimode light. What is unique in our theory are as follows. First, we consider that each quantum dot is spatially isolated in the active region, and forms its own electric dipole under the multimode light. Polarization of the quantum-dot active region is formed by summing up the contribution of each quantum dot with different carrier population and under different light electric-field amplitude. We neglect the interdipole interaction between the dots. Second, we take into account the dispersion of the interband transition energy or frequency due to the distribution of size and/or other factors like composition, shape, and strain, which causes inhomogeneous broadening in the optical spectra. We group quantum dots by their ground-state resonant frequency to derive equations of the optical susceptibility in randomly distributed self-assembled quantum dots for practical calculations. Third, we take into account the population relaxation at each energy state of each dot using rate equations which include intradot carrier relaxation, carrier capture from the wetting layer, and carrier emission to the wetting layer. This approach enables us to treat the carrier dynamics in the quantum-dot active region under multimode light, and to derive formulas on the incoherent and coherent nonlinear optical response of the quantum-dot SOA.

The prototype of our quantum-dot optical device theory presented the optical gain formula, and had a great success in describing lasing spectra of self-assembled quantum-dot lasers.[24,25] The optical gain formula introduced the inhomogeneous broadening by grouping dots in terms of their resonant frequency and the homogeneous broadening. By using the separate rate equation of carriers for each dot group, we could treat the Fabry-Pérot multimode interaction through the incoherent carrier population variation in each dot group, and explain the experiments on the narrowing of the lasing spectra as temperature increases. The present work improves the optical gain formula by introducing the coherent nonlinear gain, and the optical electric field intensity at each dot. This improvement enables us to treat the detuning-dependent multimode interaction more quantitatively, and also, to calculated the optical gain of the spatially arbitrarily distributed dots.

A. Electronic states and electric dipole in quantum dots

We describe the state vector of the conduction band as $|c,\mathbf{k}_c\rangle$, and that of the valence band as $|v,\mathbf{k}_v\rangle$, where $\mathbf{k}_c$ is the wave vector of the conduction-band electron, and $\mathbf{k}_v$ is that of the valence-band electron. Under the effective-mass approximation, the state vectors are written as

$$|c,\mathbf{k}_e\rangle = \int d^3\mathbf{r}|\mathbf{r}\rangle \sqrt{\Omega}\varphi_{c,\mathbf{k}_c}(\mathbf{r})u_{c,0} \tag{1}$$

and

$$|v,\mathbf{k}_v\rangle = \int d^3\mathbf{r}|\mathbf{r}\rangle \sqrt{\Omega}\varphi_{v,\mathbf{k}_v}(\mathbf{r})u_{v,0}, \tag{2}$$

where $\varphi_{c,\mathbf{k}_c}(\mathbf{r})$ is the envelope wave function of the conduction band, $\varphi_{v,\mathbf{k}_v}(\mathbf{r})$ is that of the valence band, $u_{c,0}$ is the base function of the conduction-band edge, and $u_{v,0}$ is that of the valence-band edge, and Ω is the unit-cell volume.

The simplest description of the electronic states in the conduction band and the valence band is given by solving the effective-mass equation of

$$\left[-\frac{\hbar^2}{2m_j^*}\nabla + V_j(\mathbf{r})\right]\varphi_{j,\mathbf{k}_j}(\mathbf{r}) = \varepsilon_{j,\mathbf{k}_j}\varphi_{j,\mathbf{k}_j}(\mathbf{r}), \tag{3}$$

where $j=c$ and v, m_j^* is the effective mass, $V_j(\mathbf{r})$ is the confinement potential due to the band offset at the heterojunctions, and $\varepsilon_{j,\mathbf{k}_j}$ is the energy. As long as we are concerned with the interband transition close to the band edge, we have only to treat one conduction band and two valence bands, i.e., the heavy-hole and light-hole bands. When we need detail structures of the energy states, we should do many-band calculations including the interband and intersubband interactions which depend on the size, strain, shape, and confinement potential profiles of the dots. The results of this kind of treatment can be immediately applied to the SOA theory in this paper.

In cubic-shape quantum dots with a volume of $L_xL_yL_z$ and with infinite potential barriers, Eq. (3) gives the wave function of

$$\varphi_{j,\mathbf{k}_j}(\mathbf{r}) = \left(\frac{2}{L}\right)^{3/2}\sin(k_{jx}x)\sin(k_{jy}y)\sin(k_{jz}z), \tag{4}$$

the energy of

$$\varepsilon_{j,\mathbf{k}_j} = \hbar\omega_{j,\mathbf{k}_j} = \frac{\hbar^2 k_j^2}{2m_j^*}, \tag{5}$$

and the wave vector of

$$\mathbf{k}_j = (k_{jx},k_{jy},k_{jz}) = \left(\frac{n_{jx}\pi}{L_x},\frac{n_{jy}\pi}{L_y},\frac{n_{jz}\pi}{L_z}\right), \tag{6}$$

where n_{jx}, n_{jy}, $n_{jz}=1,2,\ldots$. The electronic states are denoted by the band and three independent quantum numbers. Here, we assume the **k** selection rule that the interband transition is possible when $\mathbf{k}_c=\mathbf{k}_v=\mathbf{k}$.

Let us consider the electric dipole at each quantum dot by assigning the serial number of $s=1,2,3\ldots$ to each dot in the active region of SOA's. The position of each dot is denoted by $\mathbf{r}_s$. The electric dipole of $-e\mathbf{r}_s'$ at each dot is formed by the conduction-band and valence-band **k** states under the light electric field. The resonant frequency of each quantum dot for the optical transition between the conduction-band and the valence-band **k** states is $\omega_{cv,\mathbf{k}}^s=\omega_{c,\mathbf{k}}^s-\omega_{v,\mathbf{k}}^s+E_g/\hbar$, where E_g is the band gap of the quantum dot. Then, the matrix element of the electric dipole for the interband transition is given as

$$p_{cv,\mathbf{k}}^{s,\sigma} = -\langle c,\mathbf{k}|e\mathbf{e}_\sigma\cdot\mathbf{r}_s'|v,\mathbf{k}\rangle = \frac{ei}{m_0\omega_{cv,\mathbf{k}}^s}p_{cv,\mathbf{k}}^\sigma, \tag{7}$$

where $\mathbf{e}_\sigma$ is the polarization unit vector, and

$$P_{cv,\mathbf{k}}^\sigma = \langle c,\mathbf{k}|e_\sigma\cdot p|v,\mathbf{k}\rangle. \tag{8}$$

The s dependence of $P^{\sigma}_{cv,\mathbf{k}}$ is neglected. Note that $\omega^{s}_{cv,\mathbf{k}}$ varies dot by dot, resulting in the inhomogeneous broadening of the optical spectra.

B. Linear and nonlinear polarization and carrier population in quantum dots

An advantage of the density-matrix approach in deriving the polarization by electrons under the light electric field is that the relaxation of the polarization can be incorporated phenomenologically without taking into account microscopic elementary processes of electron scattering. As a result, this approach gives general expressions for the linear and nonlinear optical susceptibilities.[26,27]

We write the electric field of the multimode light by superimposing optical modes with different frequencies as

$$E=\frac{1}{2}\sum_{m}\ \mathbf{e}_{\sigma}E_{m}e^{i(\mathbf{q}_{m}\cdot\mathbf{r}-\omega_{m}t)}. \tag{9}$$

Here, the mode is denoted by an integer of m, $\mathbf{q}_{m}$ is the wave vector, and ω_{m} is the frequency. We define that $\omega_{-m}=-\omega_{m}$, $E_{-m}=E^{*}_{m}$, and $\mathbf{q}_{-m}=-\mathbf{q}_{m}$, which guarantee that the electric field is a real number. The index to represent the polarization σ might vary with the mode. Assuming that the light electric field maintains its polarization along the waveguide, and that the induced polarization of the system is parallel to the electric field, we write the polarization as

$$P=\frac{1}{2}\sum_{m}\ \mathbf{e}_{\sigma}P_{m}(\mathbf{r},t)e^{-i\omega_{m}t}, \tag{10}$$

where $P_{-m}(\mathbf{r},t)=P^{*}_{m}(\mathbf{r},t)$. We assume here that the response of the polarization to the electric field is instantaneous.

We consider the interaction of the multimode light of Eq. (9) with the two-level electron system consisting of the conduction-band state, $|c,\mathbf{k}\rangle$, and the valence-band state $|v,\mathbf{k}\rangle$. The density matrix of the sth dot is given as[27,28]

$$\rho(t;s)=\rho_{cc,\mathbf{k}}(t;s)|c,\mathbf{k}\rangle\langle c,\mathbf{k}|+\rho_{vv,\mathbf{k}}(t;s)|v,\mathbf{k}\rangle\langle v,\mathbf{k}| +\rho_{cv,\mathbf{k}}(t;s)|c,\mathbf{k}\rangle\langle v,\mathbf{k}|+\rho_{vc,\mathbf{k}}(t;s)|v,\mathbf{k}\rangle\langle c,\mathbf{k}|. \tag{11}$$

Its equation of motion is

$$\frac{\partial\rho(t;s)}{\partial t}=\frac{1}{i\hbar}[H_{0}+H_{1},\rho(t;s)]+\left[\frac{\partial\rho(t;s)}{\partial t}\right]_{rel}, \tag{12}$$

where H_{0} is the unperturbed Hamilton written as

$$H_{0}=\hbar\omega^{s}_{c,\mathbf{k}}|c,\mathbf{k}\rangle\langle c,\mathbf{k}|+\hbar\omega^{s}_{v,\mathbf{k}}|v,\mathbf{k}\rangle\langle v,\mathbf{k}|, \tag{13}$$

and H_{1} is the Hamiltonian representing the electron-light interaction. The last term of the right-hand side in Eq. (12) is the phenomenological term to describe the relaxation of the density matrix to the steady state without light. The interaction Hamiltonian is written as

$$H_{1}=\mu^{\sigma}_{cv,\mathbf{k}}(\mathbf{r}_{s},t)|c,\mathbf{k}\rangle\langle v,\mathbf{k}|+\mu^{\sigma}_{cv,\mathbf{k}}(\mathbf{r},t)|v,\mathbf{k}\rangle\langle c,\mathbf{k}|, \tag{14}$$

where

$$\mu^{\sigma}_{cv,\mathbf{k}}(\mathbf{r}_{s},t)=\frac{1}{2}\sum_{m}\ \mu^{\sigma,m}_{cv,\mathbf{k}}e^{i(\mathbf{q}_{m}\cdot\mathbf{r}_{s}-\omega_{m}t)} \tag{15}$$

and

$$\mu^{\sigma,m}_{cv,\mathbf{k}}=\frac{eE_{m}}{im_{0}\omega_{m}}P^{\sigma}_{cv,\mathbf{k}}. \tag{16}$$

From Eqs. (11)–(15), the equation of motion for the nondiagonal term is given as

$$\dot{\rho}_{cv,\mathbf{k}}(t;s)=(-i\omega^{s}_{cv,\mathbf{k}}-\Gamma^{s}_{cv,\mathbf{k}})\rho_{cv,\mathbf{k}}(t;s)+\frac{i}{\hbar}[\rho_{cc,\mathbf{k}}(t;s)-\rho_{vv,\mathbf{k}}(t;s)]\mu^{\sigma}_{cv,\mathbf{k}}(\mathbf{r}_{s},t), \tag{17}$$

where $\Gamma^{s}_{cv,\mathbf{k}}$ is the relaxation rate of the nondiagonal term of $\rho_{cv,\mathbf{k}}(t;s)$. Similarly, the equation of motion of the diagonal term in the conduction band is given as

$$\dot{\rho}_{cc,\mathbf{k}}(t;s)=-\frac{i}{\hbar}[\rho_{vc,\mathbf{k}}(t;s)\mu^{\sigma}_{cv,\mathbf{k}}(\mathbf{r}_{s},t)-\rho_{cv,\mathbf{k}}(t;s)\mu^{\sigma}_{vc,\mathbf{k}}(\mathbf{r}_{s},t)]+g_{c,\mathbf{k}}(t;s) \tag{18}$$

with

$$g_{c,\mathbf{k}}(t;s)=-T^{s}_{cc,\mathbf{k}}[\rho_{cc,\mathbf{k}}(t;s)-\tilde{\tilde{\rho}}_{cc,\mathbf{k}}(t;s)]-R^{s}_{cc,\mathbf{k}}[\rho_{cc,\mathbf{k}}(t;s)-\tilde{\rho}_{cc,\mathbf{k}}(t;s)], \tag{19}$$

and that in the valence band is given as

$$\dot{\rho}_{vv,\mathbf{k}}(t;s)=\frac{i}{\hbar}[\rho_{vc,\mathbf{k}}(t;s)\mu^{\sigma}_{cv,\mathbf{k}}(\mathbf{r}_{s},t)-\rho_{cv,\mathbf{k}}(t;s)\mu^{\sigma}_{vc,\mathbf{k}}(\mathbf{r}_{s},t)]+g_{v,\mathbf{k}}(t;s), \tag{20}$$

with

$$g_{v,\mathbf{k}}(t;s)=-T^{s}_{vv,\mathbf{k}}[\rho_{vv,\mathbf{k}}(t;s)-\tilde{\tilde{\rho}}_{vv,\mathbf{k}}(t;s)]-R^{s}_{vv,\mathbf{k}}[\rho_{vv,\mathbf{k}}(t;s)-\tilde{\rho}_{vv,\mathbf{k}}(t;s)], \tag{21}$$

where $\tilde{\rho}_{jj,\mathbf{k}}$ $(j=c,v)$ is the diagonal term under the thermal equilibrium state, $\tilde{\tilde{\rho}}_{jj,\mathbf{k}}$ is that under the quasithermal equilibrium state under a given injection current, $R^{s}_{jj,\mathbf{k}}$ is the carrier recombination rate toward thermal equilibrium state, and $T^{s}_{jj,\mathbf{k}}$ is the intraband carrier relaxation rate toward the quasithermal equilibrium state.

Since the interaction term is a perturbation to H_{0}, we can solve Eqs. (17)–(21) by conventional perturbation expansion of $\rho=\rho^{(0)}+\rho^{(1)}+\rho^{(2)}\ldots$, where the number in the parenthesis represents how many times the electron has interacted with the light. By grouping terms with the same perturbation order, we obtain a series of equations for $\dot{\rho}^{(n)}_{cv,\mathbf{k}}$ and $\dot{\rho}^{(n)}_{jj,\mathbf{k}}$. The

initial condition is that terms other than $\rho^{(0)}_{jj,\mathbf{k}}$ are zero. Then, the time derivative of the zeroth-order diagonal term is given as

$$\dot{\rho}^{(0)}_{jj,\mathbf{k}}(t;s) = -T^{s}_{jj,\mathbf{k}}[\rho^{(0)}_{jj,\mathbf{k}}(t;s) - \tilde{\rho}_{jj,\mathbf{k}}(t;s)] - R^{s}_{jj,\mathbf{k}}[\rho^{(0)}_{jj,\mathbf{k}}(t;s) - \tilde{\rho}_{jj,\mathbf{k}}(t;s)]. \quad (22)$$

For $n=1,2,3,...$, we obtain

$$\dot{\rho}^{(2n-1)}_{cv,\mathbf{k}}(t;s) = [-i\omega^{s}_{cv,\mathbf{k}} - \Gamma^{s}_{cv,\mathbf{k}}]\rho^{(2n-1)}_{cv,\mathbf{k}}(t;s) + \frac{i}{\hbar}[\rho^{(2n-2)}_{cc,\mathbf{k}}(t;s) - \rho^{(2n-2)}_{vv,\mathbf{k}}(t;s)]\mu^{\sigma}_{cv,\mathbf{k}}(\mathbf{r}_s,t), \quad (23)$$

$$\dot{\rho}^{(2n)}_{cc,\mathbf{k}}(t;s) = -\frac{i}{\hbar}[\rho^{(2n-1)}_{vc,\mathbf{k}}(t;s)\mu_{cv,\mathbf{k}}(\mathbf{r}_s,t) - \rho^{(2n-1)}_{cv,\mathbf{k}}(t;s)\mu_{vc,\mathbf{k}}(\mathbf{r}_s,t)] + g^{(2n)}_{c,\mathbf{k}}(t;s), \quad (24)$$

and

$$\dot{\rho}^{(2n)}_{vv,\mathbf{k}}(t;s) = \frac{i}{\hbar}[\rho^{(2n-1)}_{vc,\mathbf{k}}(t;s)\mu_{cv,\mathbf{k}}(\mathbf{r}_s,t) - \rho^{(2n-1)}_{cv,\mathbf{k}}(t;s)\mu_{vc,\mathbf{k}}(\mathbf{r}_s,t)] + g^{(2n)}_{v,\mathbf{k}}(t;s), \quad (25)$$

where

$$g^{(2n)}_{j,\mathbf{k}}(t;s) = -T^{s}_{jj,\mathbf{k}}\rho^{(2n)}_{jj,\mathbf{k}}(t;s) - R^{s}_{jj,\mathbf{k}}\rho^{(2n)}_{jj,\mathbf{k}}(t;s). \quad (26)$$

Note that odd diagonal terms and even nondiagonal terms are zero, which is due to the two-level electronic system assumed here. By expanding each term as $\rho^{(2n-1)}_{cv,\mathbf{k}}(t:s) = \Sigma_m \rho^{(2n-1)}_{cv,\mathbf{k}}(\omega_m;s)e^{-i\omega_m t}$ and $\rho^{(2n)}_{jj,\mathbf{k}}(t;s) = \Sigma_m \rho^{(2n)}_{jj,\mathbf{k}}(\omega_m;s)e^{-i\omega_m t}$, and inserting them into Eqs. (23)–(25), we obtain each frequency component. Note that m is an integer and that $\omega_{-m} = -\omega_m$.

The polarization of the mth mode at the perturbation order of $2n-1$ is given by the diagonal summation of the product of the density matrix and the electric dipole as

$$P^{(2n-1)}_{m}(\mathbf{r},t)/2 = 2\sum_{c,v,\mathbf{k},s}\rho^{(2n-1)}_{cv,\mathbf{k}}(\omega_m;s)p^{s,\sigma}_{vc,\mathbf{k}}\delta(\mathbf{r}-\mathbf{r}_s) + \text{h.c.}, \quad (27)$$

where the factor of 2 on the right-hand side represents the degeneracy due to spin. The delta function of $\delta(\mathbf{r}-\mathbf{r}_s)$ will be eliminated when we integrate the polarization by $\mathbf{r}$ to obtain its average in the local area.

The total polarization is given by the sum of each perturbation-order term as

$$P_m(\mathbf{r},t) = \sum_{n=1} P^{(2n-1)}_{m}(\mathbf{r},t). \quad (28)$$

and is divided into

$$P_m(\mathbf{r},t) = P^{(1)}_{m}(\mathbf{r},t) + P^{inc}_{m}(\mathbf{r},t) + P^{coh}_{m}(\mathbf{r},t), \quad (29)$$

where $P^{(1)}_{m}(\mathbf{r},t)$ is the linear polarization, $P^{inc}_{m}(\mathbf{r},t)$ is the incoherent nonlinear polarization, and $P^{coh}_{m}(\mathbf{r},t)$ is the coherent nonlinear polarization. Here, we use the term of "incoherent" when the phase of some of the participating light modes is lost, and the term of "coherent" when the phase of all the participating light modes is preserved. We derived each polarization term as follows.

1. Linear polarization

By substituting

$$\rho^{(1)}_{cv,\mathbf{k}}(t;s) = \sum_{m}\rho^{(1)}_{cv,\mathbf{k}}(\omega_m;s)e^{-i\omega_m t} \quad (30)$$

into Eq. (23) with $n=1$, the first-order nondiagonal term is derived as

$$\rho^{(1)}_{cv,\mathbf{k}}(\omega_m;s) = \frac{[\rho^{(0)}_{vv,\mathbf{k}}(t;s) - \rho^{(0)}_{cc,\mathbf{k}}(t;s)]\mu^{\sigma,m}_{cv,\mathbf{k}}e^{i\mathbf{q}_m\cdot\mathbf{r}_s}}{2\hbar(\omega_m - \omega^{s}_{cv,\mathbf{k}} + i\Gamma^{s}_{cv,\mathbf{k}})}. \quad (31)$$

By substituting Eqs. (16) and (31) into Eq. (27) with $n=1$, the linear polarization is given as

$$P^{(1)}_{m}(\mathbf{r},t) = \varepsilon_0\chi^{(1)}_{\sigma}(\mathbf{r},t,\omega_m)E_m e^{i\mathbf{q}_m\cdot\mathbf{r}}, \quad (32)$$

where the first-order susceptibility is

$$\chi^{(1)}(\mathbf{r},t,\omega_m) = \sum_{c,v,\mathbf{k},s}\chi^{(1)}_{\sigma}(t,\omega_m;cv\mathbf{k}s)\delta(\mathbf{r}-\mathbf{r}_s) \quad (33)$$

and

$$\chi^{(1)}_{\sigma}(t,\omega_m;cv\mathbf{k}s) = \frac{2e^2|P^{\sigma}_{cv,\mathbf{k}}|^2[\rho^{(0)}_{cc,\mathbf{k}}(t;s) - \rho^{(0)}_{vv,\mathbf{k}}(t;s)]}{\varepsilon_0\hbar m_0^2\omega_m\omega^{s}_{cv,\mathbf{k}}} \times\left[\frac{1}{\omega_m - \omega^{s}_{cv,\mathbf{k}} + i\Gamma^{s}_{cv,\mathbf{k}}} + \frac{1}{\omega_m + \omega^{s}_{cv,\mathbf{k}} + i\Gamma^{s}_{cv,\mathbf{k}}}\right]. \quad (34)$$

Note that $e^{i\mathbf{q}_m\cdot\mathbf{r}_s}$ is replaced by $e^{i\mathbf{q}_m\cdot\mathbf{r}}$ in Eq. (32) considering the delta function in Eq. (33). (This kind of treatment often appears below.)

2. Second-order diagonal terms

By substituting Eqs. (15), (16), (30), and (31) into Eq. (24) with $n=1$, we obtain

$$\begin{aligned}\dot{\rho}^{(2)}_{cc,\mathbf{k}}(t;s) &\equiv -\frac{i}{4\hbar}\sum_{\substack{m,m'\\(>0)}}\frac{e^2[\rho^{(0)}_{cc,\mathbf{k}}(t;s) - \rho^{(0)}_{vv}(t;s)]|P^{\sigma}_{cv,\mathbf{k}}|^2}{\hbar m_0^2\omega_m\omega_{m'}(\omega_m - \omega^{s}_{cv,\mathbf{k}} + i\Gamma^{s}_{cv,\mathbf{k}})} \\ &\times E_m E^{*}_{m'}e^{i(\mathbf{q}_m - \mathbf{q}_{m'})\cdot\mathbf{r}}e^{-i(\omega_m - \omega_{m'})t} \\ &+ \text{c.c.} + g^{(2)}_{c,\mathbf{k}}(t;s) \\ &\cong -\frac{\varepsilon_0 i}{8\hbar}\sum_{\substack{m,m'\\(>0)}}\chi^{(1)}_{\sigma}(t,\omega_m;cv\mathbf{k}s)E_m E^{*}_{m'} \\ &\times e^{i(\mathbf{q}_m - \mathbf{q}_{m'})\cdot\mathbf{r}_s}e^{-i(\omega_m - \omega_{m'})t} + \text{c.c.} + g^{(2)}_{c,\mathbf{k}}(t;s)\end{aligned} \quad (35)$$

for the electron in the conduction band. In deriving the second equation of Eq. (35), we neglected nonresonant terms and the high-frequency terms of $e^{-i(\omega_m+\omega_{m'})t}$, and used Eq. (34) with $\omega^s_{cv,\mathbf{k}} \cong \omega_{m'}$. The time derivative of the second-order diagonal term can be divided as

$$\dot{\rho}^{(2)}_{cc,\mathbf{k}}(t;s) = \dot{\rho}^{(2)pop}_{cc,\mathbf{k}}(t;s) + \dot{\rho}^{(2),beat}_{cc,\mathbf{k}}(t;s), \tag{36}$$

where the population term which does not include the oscillating components is

$$\dot{\rho}^{(2)pop}_{cc,\mathbf{k}}(t;s) \cong \frac{\varepsilon_0}{4\hbar} \sum_{\substack{m \\ (>0)}} \mathrm{Im}\,\chi^{(1)}_\sigma(t,\omega_m;cv\mathbf{k}s)|E_m|^2 - T^s_{cc,\mathbf{k}}\rho^{(2),inc}_{cc,\mathbf{k}}(t;s) - R^s_{cc,\mathbf{k}}\rho^{(2),inc}_{cc,\mathbf{k}}(t;s) \tag{37}$$

and the beating term which oscillates with the frequency of $\omega_m - \omega_{m'}$ is

$$\dot{\rho}^{(2),beat}_{cc,\mathbf{k}}(t;s) \cong -\frac{\varepsilon_0 i}{8\hbar} \sum_{\substack{m,m' \\ (m\neq m',>0)}} \chi^{(1)}_\sigma(t,\omega_m;cv\mathbf{k}s)E_m E^*_{m'} \times e^{i(\mathbf{q}_m-\mathbf{q}_{m'})\cdot\mathbf{r}_s} e^{-i(\omega_m-\omega_{m'})t} + \text{c.c.} - T^s_{cc,\mathbf{k}}\rho^{(2),beat}_{cc,\mathbf{k}}(t;s) - R^s_{cc,\mathbf{k}}\rho^{(2),beat}_{cc,\mathbf{k}}(t;s). \tag{38}$$

The expression for the valence band can be derived from Eq. (25) in the same way, and is divided into $\dot{\rho}^{(2)}_{vv,\mathbf{k}}(t;s) = \dot{\rho}^{(2)pop}_{vv,\mathbf{k}}(t;s) + \dot{\rho}^{(2),beat}_{vv,\mathbf{k}}(t;s)$.

Higher order diagonal terms can also be classified into population and oscillating terms. We write the population terms as $\rho^{(2n+2),pop}_{cc,\mathbf{k}}(t;s)$ and $\rho^{(2n+2),pop}_{vv,\mathbf{k}}(t;s)$, and beating terms between two optical modes as $\rho^{(2n+2),beat}_{cc,\mathbf{k}}(t;s)$ and $\rho^{(2n+2),beat}_{vv,\mathbf{k}}(t;s)$, where $n \geqslant 1$. We neglect the diagonal terms consisting of more than three optical-mode frequencies.

3. Incoherent nonlinear polarization due to spectral hole burning

The second-order population term of Eq. (37) becomes negative when $\rho^{(0)}_{cc,\mathbf{k}}(t;s) > \rho^{(0)}_{vv,\mathbf{k}}(t;s)$ [see Eq. (34)] due to the stimulated emission, leading to the reduction in the population of the $\mathbf{k}$ state at the sth dot. This is the nonlinear polarization known as spectral hole burning. In the sense that the population shows no beating oscillation and that the phase of the optical waves are lost, we call this nonlinear polarization and the spectral hole burning "incoherent."

The $(2n+1)$th order incoherent nonlinear polarization $(n \geqslant 1)$ originates from the $(2n+1)$th order nondiagonal term of $\rho^{(2n+1),inc}_{cv,\mathbf{k}}(t;s)$ derived by Eq. (23) with the $(2n)$th order population terms of $\rho^{(2n),pop}_{cc,\mathbf{k}}(t;s)$ and $\rho^{(2n),pop}_{vv,\mathbf{k}}(t;s)$. By substituting the Fourier expansion of

$$\rho^{(2n+1),inc}_{cv,\mathbf{k}}(t;s) = \sum_m \rho^{(2n+1),inc}_{cv,\mathbf{k}}(\omega_m;s)e^{-i\omega_m t} \tag{39}$$

into Eq. (23), we obtain the Fourier component of $(2n+1)$th order nondiagonal term as

$$\rho^{(2n+1),inc}_{cv,\mathbf{k}}(\omega_m;s) = \frac{[\rho^{(2n),pop}_{vv,\mathbf{k}}(t;s) - \rho^{(2n),pop}_{cc,\mathbf{k}}(t;s)]\mu^{\sigma,m}_{cv,\mathbf{k}}e^{i\mathbf{q}_m\cdot\mathbf{r}_s}}{2\hbar(\omega_m - \omega^s_{cv,\mathbf{k}} + i\Gamma^s_{cv,\mathbf{k}})}. \tag{40}$$

By substituting Eq. (40) into Eq. (27), we obtain the $(2n+1)$th order incoherent nonlinear polarization as

$$P^{(2n+1),inc}_m(\mathbf{r},t) = \varepsilon_0\chi^{(2n+1),inc}_\sigma(\mathbf{r},t,\omega_m)E_m e^{i\mathbf{q}_m\cdot\mathbf{r}}, \tag{41}$$

where

$$\chi^{(2n+1),inc}_\sigma(\mathbf{r},t,\omega_m) = \sum_{c,v,\mathbf{k},s} \chi^{(2n+1),inc}_\sigma(t,\omega_m;cv\mathbf{k}s) \times \delta(\mathbf{r}-\mathbf{r}_s) \tag{42}$$

and

$$\chi^{(2n+1),inc}_\sigma(t,\omega_m,cv\mathbf{k}s) = \frac{2e^2|P^\sigma_{cv,\mathbf{k}}|^2[\rho^{(2n),pop}_{cc,\mathbf{k}}(t;s) - \rho^{(2n),pop}_{vv,\mathbf{k}}(t;s)]}{\varepsilon_0\hbar m_0^2\omega_m\omega^s_{cv,\mathbf{k}}} \times \left[\frac{1}{\omega_m - \omega^s_{cv,\mathbf{k}} + i\Gamma^s_{cv,\mathbf{k}}} + \frac{1}{\omega_m + \omega^s_{cv,\mathbf{k}} + i\Gamma^s_{cv,\mathbf{k}}}\right]. \tag{43}$$

Then, the total incoherent nonlinear polarization is

$$P^{inc}_m(\mathbf{r},t) = \sum_{n=1} P^{(2n+1),inc}_m(\mathbf{r},t). \tag{44}$$

By substituting Eqs. (15), (16), (39), and (40) into Eq. (24), the $(2n+2)$th order population term becomes $(n \geqslant 1)$

$$\dot{\rho}^{(2n+2),pop}_{cc,\mathbf{k}}(t;s) \cong \frac{\varepsilon_0}{4\hbar} \sum_{\substack{m \\ (>0)}} \mathrm{Im}\,\chi^{(2n+1),inc}_\sigma(t,\omega_m;cv\mathbf{k}s)|E_m|^2 - T^s_{cc,\mathbf{k}}\rho^{(2n+2),pop}_{cc,\mathbf{k}}(t;s) - R^s_{cc,\mathbf{k}}\rho^{(2n+2),pop}_{cc,\mathbf{k}}(t;s). \tag{45}$$

From Eqs. (32)–(34) and (41)–(44), the total polarization due to the linear polarization and the incoherent nonlinear polarization becomes

$$P^{pop}_m(\mathbf{r},t) = P^{(1)}_m(\mathbf{r},t) + P^{inc}_m(\mathbf{r},t) \equiv \varepsilon_0\chi^{pop}_\sigma(\mathbf{r},t,\omega_m)E_m e^{i\mathbf{q}_m\cdot\mathbf{r}}, \tag{46}$$

where

$$\chi_{\sigma}^{pop}(\mathbf{r},t,\omega_m)=\sum_{c,v,\mathbf{k},s}\chi_{\sigma}^{pop}(t,\omega_m;cv\mathbf{k}s)\,\delta(\mathbf{r}-\mathbf{r}), \quad (47)$$

$$\chi_{\sigma}^{pop}(t,\omega_m;cv\mathbf{k}s)=\chi_{\sigma}^{(1)}(t,\omega_m;cv\mathbf{k}s)+\sum_{n=1}\chi_{\sigma}^{(2n+1),inc}(t,\omega_m;cv\mathbf{k}s)$$
$$=\frac{2e^2|P_{cv,\mathbf{k}}^{\sigma}|^2[\rho_{cc,\mathbf{k}}^{pop}(t;s)-\rho_{vv,\mathbf{k}}^{pop}(t;s)]}{\varepsilon_0\hbar m_0^2\omega_m\omega_{cv,\mathbf{k}}^{s}}\times\left[\frac{1}{\omega_m-\omega_{cv,\mathbf{k}}^{s}+i\Gamma_{cv,\mathbf{k}}^{s}}+\frac{1}{\omega_m+\omega_{cv,\mathbf{k}}^{s}+i\Gamma_{cv,\mathbf{k}}^{s}}\right], \quad (48)$$

and

$$\rho_{cc,\mathbf{k}}^{pop}(t;s)=\rho_{cc,\mathbf{k}}^{(0)}(t;s)+\rho_{cc,\mathbf{k}}^{(2)pop}(t;s)+\sum_{n=1}\rho_{cc,\mathbf{k}}^{(2n+2),pop}(t;s). \quad (49)$$

By using Eqs. (22), (37), (45), and (49), the time derivative of $\rho_{cc,\mathbf{k}}^{pop}(t;s)$ is given as

$$\dot{\rho}_{cc,\mathbf{k}}^{pop}(t;s)=\frac{\varepsilon_0}{4\hbar}\sum_{\substack{m\\(>0)}}\mathrm{Im}\,\chi_{\sigma}^{pop}(t,\omega_m;cv\mathbf{k}s)|E_m|^2-T_{cc,\mathbf{k}}^{s}[\rho_{cc,\mathbf{k}}^{pop}(t;s)-\tilde{\tilde{\rho}}_{cc,\mathbf{k}}(t;s)]-R_{cc,\mathbf{k}}^{s}[\rho_{cc,\mathbf{k}}^{pop}(t;s)-\tilde{\rho}_{cc,\mathbf{k}}(t;s)]. \quad (50)$$

The expressions for the valence band, $\rho_{vv,\mathbf{k}}^{pop}(t;s)$, and its time derivative can be derived in the same way.

4. Coherent nonlinear polarization due to spectral hole burning

The beating diagonal terms under the two optical modes of different frequencies form the dynamic spectral-hole burning, and mix with the third light to cause nonlinear polarization. We call this nonlinear polarization coherent in the sense that the phase of all the optical waves is preserved.

Let us derive the coherent nonlinear polarization from $\rho_{cc,\mathbf{k}}^{(2),beat}(t;s)$, $\rho_{cc,\mathbf{k}}^{(2n+2),beat}(t;s)$, $\rho_{vv,\mathbf{k}}^{(2),beat}(t;s)$, and $\rho_{vv,\mathbf{k}}^{(2n+2),beat}(t;s)$. The total beating term in the conduction band is

$$\rho_{cc,\mathbf{k}}^{beat}(t;s)=\rho_{cc,\mathbf{k}}^{(2),beat}(t;s)+\sum_{n=1}\rho_{cc,\mathbf{k}}^{(2n+2),beat}(t;s). \quad (51)$$

The time derivative of the second order term of $\rho_{cc,\mathbf{k}}^{(2),beat}(t;s)$ is given by Eq. (38). By substituting Eqs. (15), (16), (39), and (40) into Eq. (24), we obtain

$$\dot{\rho}_{cc,\mathbf{k}}^{(2n+2),beat}(t;s)\cong-\frac{\varepsilon_0 i}{8\hbar}\sum_{\substack{m,m'\\(m\neq m',>0)}}\chi_{\sigma}^{(2n+1),inc}(t,\omega_m;cv\mathbf{k}s)\times E_m E_{m'}^{*}e^{i(\mathbf{q}_m-\mathbf{q}_{m'})\cdot\mathbf{r}_s}e^{-i(\omega_m-\omega_{m'})t}+\text{c.c.}-T_{cc,\mathbf{k}}^{s}\rho_{cc,\mathbf{k}}^{(2n+2),beat}(t;s)-R_{cc,\mathbf{k}}^{s}\rho_{cc,\mathbf{k}}^{(2n+2),beat}(t;s). \quad (52)$$

As in Eq. (35), we neglected nonresonant terms and the high-frequency terms of $e^{-i(\omega_m+\omega_{m'})t}$, and used Eq. (43) with $\omega_{cv,\mathbf{k}}\cong\omega_{m'}$. Then, using Eqs. (38), (48), (51), and (52), we obtain the total beating term as

$$\dot{\rho}_{cc,\mathbf{k}}^{beat}(t;s)\cong-\frac{\varepsilon_0 i}{8\hbar}\sum_{\substack{m,m'\\(m\neq m',>0)}}\chi_{\sigma}^{pop}(t,\omega_m;cv\mathbf{k}s)\times E_m E_{m'}^{*}e^{i(\mathbf{q}_m-\mathbf{q}_{m'})\cdot\mathbf{r}_s}e^{-i(\omega_m-\omega_{m'})t}+\text{c.c.}-T_{cc,\mathbf{k}}^{s}\rho_{cc,\mathbf{k}}^{beat}(t;s)-R_{cc,\mathbf{k}}^{s}\rho_{cc,\mathbf{k}}^{beat}(t;s). \quad (53)$$

By substituting the second-order diagonal beating term of

$$\rho_{cc,\mathbf{k}}^{(2),beat}(t;s)=\sum_{\substack{m',m''\\(m\neq m',>0)}}\rho_{cc,\mathbf{k}}^{(2),beat}(\omega_{m'}-\omega_{m''};s)\times e^{-i(\omega_{m'}-\omega_{m''})t}+\text{c.c.} \quad (54)$$

into Eq. (38), we obtain

$$\rho_{cc,\mathbf{k}}^{(2),beat}(\omega_{m'}-\omega_{m''};s)=\frac{\varepsilon_0}{8\hbar}\frac{\chi_{\sigma}^{(1)}(t,\omega_{m'};cv\mathbf{k}s)}{[\omega_{m'}-\omega_{m''}+i(T_{cc,\mathbf{k}}^{s}+R_{cc,\mathbf{k}}^{s})]}E_{m'}E_{m''}^{*}\times e^{i(\mathbf{q}_{m'}-\mathbf{q}_{m''})\cdot\mathbf{r}_s}. \quad (55)$$

Similarly, by substituting the $(2n+2)$-order diagonal beating term of

$$\rho_{cc,\mathbf{k}}^{(2n+2),beat}(t;s)=\sum_{\substack{m,m'\\(m\neq m',>0)}}\rho_{cc,\mathbf{k}}^{(2n+2),beat}(\omega_{m'}-\omega_{m''};s)\times e^{-i(\omega_{m'}-\omega_{m''})t}+\text{c.c.} \quad (56)$$

into Eq. (52), we obtain

$$\rho_{cc,\mathbf{k}}^{(2n+2),beat}(\omega_{m'}-\omega_{m''};s)=\frac{\varepsilon_0}{8\hbar}\frac{\chi_{\sigma}^{(2n+1),inc}(t,\omega_{m'};cv\mathbf{k}s)}{[\omega_{m'}-\omega_{m''}+i(T_{cc,\mathbf{k}}^{s}+R_{cc,\mathbf{k}}^{s})]}\times E_m E_{m'}^{*}e^{i(\mathbf{q}_{m'}-\mathbf{q}_{m''})\cdot\mathbf{r}_s}. \quad (57)$$

From Eq. (23), the coherent nondiagonal terms due to dynamic spectral hole burning are given by

$$\dot{\rho}^{(3),dshb}_{cv,\mathbf{k}}(t;s)=[-i\omega^{s}_{cv,\mathbf{k}}-\Gamma^{s}_{cv,\mathbf{k}}]\rho^{(3),dshb}_{cv,\mathbf{k}}(t;s)+\frac{i}{\hbar}[\rho^{(2),beat}_{cc,\mathbf{k}}(t;s)-\rho^{(2),beat}_{vv,\mathbf{k}}(t;s)]\mu^{\sigma}_{cv,\mathbf{k}}(\mathbf{r},t) \tag{58}$$

and

$$\dot{\rho}^{(2n+3),dshb}_{cv,\mathbf{k}}(t;s)=[-i\omega^{s}_{cv,\mathbf{k}}-\Gamma^{s}_{cv,\mathbf{k}}]\rho^{(2n+3),dshb}_{cv,\mathbf{k}}(t;s)+\frac{i}{\hbar}[\rho^{(2n+2),beat}_{cc,\mathbf{k}}(t;s)-\rho^{(2n+2),beat}_{vv,\mathbf{k}}(t;s)]\mu^{\sigma}_{cv,\mathbf{k}}(\mathbf{r}_s,t). \tag{59}$$

By substituting $\rho^{(3),dshb}_{cv,\mathbf{k}}(t;s)=\Sigma_{m',m'',m'''}\rho^{(3)dshb}_{cv,\mathbf{k}}(\omega_m=\omega_{m'}+\omega_{m''}+\omega_{m'''};s)e^{-i(\omega_{m'}+\omega_{m''}+\omega_{m'''})t}$ into Eq. (58) and $\rho^{(2n+3),dshb}_{cv,\mathbf{k}}(t;s)=\Sigma_{m',m'',m'''}\rho^{(2n+3),dshb}_{cv,\mathbf{k}}(\omega_m=\omega_{m'}+\omega_{m''}+\omega_{m'''};s)e^{-i(\omega_{m'}+\omega_{m''}+\omega_{m'''})t}$ into Eq. (59) and using Eq. (15), we obtain the Fourier components of $\rho^{dshb}_{cv,\mathbf{k}}(t;s)=\rho^{(3),dshb}_{cv,\mathbf{k}}(t;s)+\Sigma_{n=1}\rho^{(2n+3),dshb}_{cv,\mathbf{k}}(t;s)$. The component at the frequency of $\omega_m=\omega_{m'}-\omega_{m''}+\omega_{m'''}$ with m', m'', $m'''>0$ and $m'\neq m''$ is given as

$$\rho^{dshb}_{cv,\mathbf{k}}(\omega_m=\omega_{m'}-\omega_{m''}+\omega_{m'''};s)=\rho^{(3),dshb}_{cv,\mathbf{k}}(\omega_m=\omega_{m'}-\omega_{m''}+\omega_{m'''};s)+\sum_{n=1}\rho^{(2n+3),dshb}_{cv,\mathbf{k}}(\omega_m=\omega_{m'}-\omega_{m''}+\omega_{m''};s)$$

$$=\frac{e\varepsilon_0 iP^{\sigma}_{cv,\mathbf{k}}}{16m_0\omega_{m''}\hbar^2}\frac{[\chi^{pop}_{\sigma}(t,\omega_{m'};cv\mathbf{k}s)-\chi^{pop}_{\sigma}(t,\omega_{m''};cv\mathbf{k}s)^*]}{[(\omega_{m'}-\omega_{m''}+\omega_{m'''}-\omega^{s}_{cv,\mathbf{k}})+i\Gamma_{cv,\mathbf{k}}]}\times\left\{\frac{1}{[\omega_{m'}-\omega_{m''}+i(T^{i}_{cc,\mathbf{k}}+R^{t}_{cc,\mathbf{k}})]}\right.$$

$$\left.+\frac{1}{[\omega_{m'}-\omega_{m''}+i(T^{s}_{vv,\mathbf{k}}+R^{s}_{vv,\mathbf{k}})]}\right\}\times E_{m'}E^{*}_{m''}E_{m''}e^{i(\mathbf{q}_{m'}-q_{m''}+\mathbf{q}_{m'''})\cdot\mathbf{r}_s}. \tag{60}$$

Note that the series expansion of the nondiagonal terms by the perturbation order in Eq. (60) is often used to obtain nonlinear gain coefficient in lasers.

Then, by the diagonal summation of Eq. (27), we obtain the coherent nonlinear polarization due to dynamic spectral hole burning as

$$P^{dshb}_{m}(\mathbf{r},t)=\sum_{n=1}P^{(2n+1),dshb}_{m}(\mathbf{r},t)=\varepsilon_0\sum_{\substack{m',m''m'''\\(m'\neq m'',>0)}}\chi^{dshb}_{\sigma}(\mathbf{r},t,\omega_m=\omega_{m'}-\omega_{m''}+\omega_{m'''})E_{m'}E^{*}_{m''}E_{m'''}e^{i(\mathbf{q}_{m'}-\mathbf{q}_{m''}+\mathbf{q}_{m'''})\cdot\mathbf{r}}, \tag{61}$$

where

$$\chi^{dshb}_{\sigma}(\mathbf{r},t,\omega_m=\omega_{m'}-\omega_{m''}+\omega_{m'''})=\sum_{c,v,\mathbf{k},s}\chi^{dshb}_{\sigma}(t,\omega_m=\omega_{m'}-\omega_{m''}+\omega_{m'''};cv\mathbf{k}s)\,\delta(\mathbf{r}-\mathbf{r}_s) \tag{62}$$

and

$$\chi^{dshb}_{\sigma}(\mathbf{r},t,\omega_m=\omega_{m'}-\omega_{m''}+\omega_{m'''};cv\mathbf{k}s)$$

$$=\frac{e^2|P^{\sigma}_{cv,\mathbf{k}}|^2}{4m^2_0\omega_{m'''}\omega^{s}_{cv,\mathbf{k}}\hbar^2}\frac{\chi^{pop}_{\sigma'}(t,\omega_{m'};cv\mathbf{k}s)-\chi^{pop}_{\sigma'}(t,\omega_{m''};cv\mathbf{k}s)^*}{\omega_{m'}-\omega_{m''}+\omega_{m'''}-\omega^{s}_{cv,\mathbf{k}}+i\Gamma_{cv,\mathbf{k}}}x\left\{\frac{1}{\omega_{m'}-\omega_{m''}+i(T^{s}_{cc,\mathbf{k}}+R^{s}_{cc,\mathbf{k}})}\right.$$

$$\left.+\frac{1}{\omega_{m'}-\omega_{m''}+i(T^{s}_{vv,\mathbf{k}}+\mathbf{R}^{s}_{vv,\mathbf{k}})}\right\}. \tag{63}$$

Note that we added prime on the population susceptibility since the polarization of the m'' mode, σ, can be different from that of the m' and m'' modes, σ'.

C. Coherent nonlinear polarization due to population beating via intraband relaxation: carrier density pulsation

The light-induced population beating at the conduction-band $\mathbf{k}$ state described by Eq. (53) causes the population beating in other energy states in the conduction band via the intraband electron relaxation, generating another source for coherent nonlinear polarization besides the dynamic spectral hole burning of Eq. (61). This is also the case in the valence band. We call this source of nonlinearity as carrier density pulsation according to the general usage in conventional semiconductors (see Appendix). We treat the time-dependent population at the $|c,\mathbf{k}_l\rangle$ state of the sth dot taking into account all the intraband relaxation processes related to other intradot states denoted by the index of $i \neq l$ and the wetting layer state denoted by the index of w (Fig. 2). Then, using Eqs. (50) and (53), we obtain the time derivative of the population at $|c,\mathbf{k}_l\rangle$ state as

$$\begin{aligned}\dot{\rho}_{cc,\mathbf{k}_l}(t;s) &= \dot{\rho}^{pop}_{cc,\mathbf{k}_l}(t;s) + \dot{\rho}^{beat}_{cc,\mathbf{k}_l}(t;s) \\ &= \frac{\varepsilon_0}{4\hbar} \sum_{\substack{m \\ (>0)}} \mathrm{Im}\,\chi^{pop}_{\sigma}(t,\omega_m;cv\mathbf{k}_l s)|E_m|^2 \\ &\quad - \frac{\varepsilon_0 i}{8\hbar} \sum_{\substack{m,m' \\ (m\neq m',>0)}} \chi^{pop}_{\sigma}(t,\omega_m;cv\mathbf{k}_l s) E_m E^*_{m'} \\ &\quad \times e^{i(\mathbf{q}_m - \mathbf{q}_{ml})\cdot \mathbf{r}_s} e^{-i(\omega_m - \omega_{m'})t} + \text{c.c.} \\ &\quad - T^s_{cc,\mathbf{k}_l}[\rho_{cc,\mathbf{k}_l}(t;s) - \tilde{\tilde{\rho}}_{cc,\mathbf{k}_l}(t;s)] \\ &\quad - R^s_{cc,\mathbf{k}_l}[\rho_{cc,\mathbf{k}_l}(t;s) - \tilde{\rho}_{cc,\mathbf{k}_l}(t;s)], \end{aligned} \tag{64}$$

where

$$T^s_{cc,\mathbf{k}_l} = \sum_{i\neq l} T^{s,c}_{il} + T^c_{wl}, \tag{65}$$

$$T^{s,c}_{il} = \rho_{cc,\mathbf{k}_l}(t;s)\tau^{-1}_{i\to l,0} + [1 - \rho_{cc,\mathbf{k}_l}(t;s)]\tau^{-1}_{l\to i,0}, \tag{66}$$

$$T^c_{wl} = \frac{N^{\mathrm{tot}}_{c,w}}{2N_D}\tau^{-1}_{w\to l,0} + \left(1 - \frac{N^{\mathrm{tot}}_{c,w}}{2D_{c,w}}\right)\tau^{-1}_{l\to w,0}, \tag{67}$$

and

$$\tilde{\tilde{\rho}}_{cc,\mathbf{k}_l}(t;s) = {T^s_{cc,\mathbf{k}_l}}^{-1}\left[\sum_{i\neq l}\rho_{cc,\mathbf{k}_l}(t;s)\tau^{-1}_{i\to l,0} + \frac{N^{\mathrm{tot}}_{c,w}}{2N_D}\tau^{-1}_{w\to l,0}\right]. \tag{68}$$

Here, $\tau_{i\to l,0}$ is the relaxation lifetime from the $|c,\mathbf{k}_i\rangle$ state to the $|c,\mathbf{k}_l\rangle$ state, vice versa, $\tau_{w\to l,0}$ is the relaxation lifetime from the wetting layer to the $|c,\mathbf{k}_l\rangle$ state, vice versa, N_D is the dot density, and $N^{\mathrm{tot}}_{c,w}$ is the total electron density in the conduction band of the wetting layer. The lifetimes are assumed to be common in each dot, and their band index, conduction or valence band, is omitted. We suppose one energy level with the degeneracy of $D_{c,w}$ in the conduction band of the wetting layer for simplicity. The rate equation of the wetting-layer electron density is

$$\begin{aligned}\frac{dN^{\mathrm{tot}}_{c,w}}{dt} &= \frac{J}{ed_w} - \sum_{s,l}\frac{N^{\mathrm{tot}}_{c,w}}{2N_D}[1-\rho_{cc,\mathbf{k}_l}(t;s)]\tau^{-1}_{w\to l,0} \\ &\quad + \sum_{s,l}\rho_{cc,\mathbf{k}_l}(t;s)\left(1 - \frac{N^{\mathrm{tot}}_{c,w}}{2D_{c,w}}\right)\tau^{-1}_{l\to w,0} - R^c_w N^{\mathrm{tot}}_{c,w}, \end{aligned} \tag{69}$$

where J is the current density, d_w is the total thickness of the wetting layer, R^c_w is the electron recombination rate in the wetting layer, and the summation on the dot number, s, is taken per unit volume, and the summation on l is taken over all the energy states at each dot.

We obtain the amplitude of the population beating at the $|c,\mathbf{k}_l\rangle$ state in the sth dot by substituting

$$\rho_{cc,\mathbf{k}_l}(t;s) = \rho^{pop}_{cc,\mathbf{k}_l}(t;s) + \sum_{\substack{m',m'' \\ (m\neq m',>0)}} \rho_{cc,\mathbf{k}_l}(\omega_{m'} - \omega_{m''};s)e^{-i(\omega_{m'}-\omega_{m''})t} + \text{c.c.} \tag{70}$$

and

$$N^{\mathrm{tot}}_{c,w} = N_{c,w} + \sum_{\substack{m',m'' \\ (m\neq m',>0)}} \Delta N_{c,w}(\omega_{m'} - \omega_{m''})e^{-i(\omega_{m'}-\omega_{m''})t} + \text{c.c.} \tag{71}$$

into Eq. (64) as

$$\begin{aligned}\rho_{cc,\mathbf{k}_l}(\omega_{m'} - \omega_{m''};s) &= \rho^{beat}_{cc,\mathbf{k}_l}(\omega_{m'} - \omega_{m''};s) + \sum_{i\neq l} i\frac{T^{s,c}_{li}}{\omega_{m'} - \omega_{m''} + i(T^s_{cc,\mathbf{k}_l} + R^s_{cc,\mathbf{k}_l})}\rho_{cc,\mathbf{k}_l}(\omega_{m'} - \omega_{m''};s) \\ &\quad + i\frac{T^c_w}{\omega_{m'} - \omega_{m''} + i(T^s_{cc,\mathbf{k}_l} + R^s_{cc,\mathbf{k}_l})}\Delta N_{c,w}(\omega_{m'} - \omega_{m''}), \end{aligned} \tag{72}$$

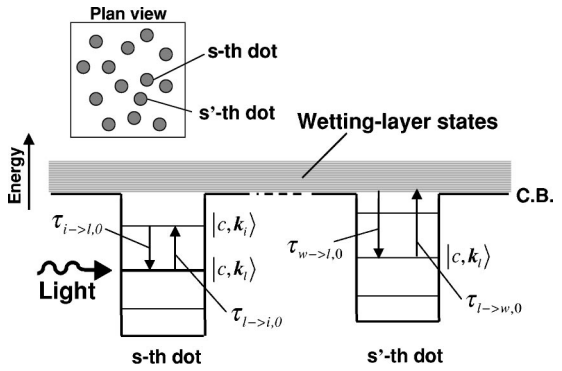

FIG. 2. Conduction-band energy diagram of quantum-dot active region, and intraband relaxation processes of the $|c,\mathbf{k}_1\rangle$ state due to other intradot states denoted by the index of $i \neq l$ and the wetting layer state denoted by the index of w.

where

$$T_w^c = \sum_{s,l} \left[\frac{\rho_{cc,\mathbf{k}_l}(t;s)}{2D_{c,w}} \tau_{l\to w,0}^{-1} + \frac{1-\rho_{cc,\mathbf{k}_l}(t;s)}{2N_D} \tau_{w\to l,0}^{-1} \right]. \tag{73}$$

Never mix up i to describe the state index and the complex number. In Eq. (72), we used the Fourier component of the light-induced beating term of $\rho_{cc,\mathbf{k}_l}^{beat}(t;s)$ given by Eqs. (55) and (57) as

$$\rho_{cc,\mathbf{k}_l}^{beat}(\omega_{m'} - \omega_{m''};s) = \frac{\varepsilon_0}{8\hbar} \frac{\chi_\sigma^{pop}(t,\omega_m;cv\mathbf{k}_l s)}{[\omega_{m'} - \omega_{m''} + i(T_{cc,\mathbf{k}_l}^s + R_{cc,\mathbf{k}_l}^s)]} \times E_m E_{m'}^* e^{i(\mathbf{q}_{m'} - \mathbf{q}_{m'})\cdot \mathbf{r}_s}. \tag{74}$$

Similarly, from Eq. (69), we obtain

$$\Delta N_{c,w}(\omega_{m'} - \omega_{m''}) = i \sum_{s,l} \frac{T_{wl}^c \rho_{cc,\mathbf{k}_l}(\omega_{m'} - \omega_{m''};s)}{\omega_{m'} - \omega_{m''} + i(T_w^c + R_w^c)}. \tag{75}$$

Equations (72), (74), and (75) are the linear simultaneous equations, and can be solved numerically.

We can obtain an analytical and approximate solution of Eqs. (72), (74), and (75) by the successive approximation with the form of

$$\rho_{cc,\mathbf{k}_l}(\omega_{m'} - \omega_{m''};s) = \rho_{cc,\mathbf{k}_l}^{beat}(\omega_{m'} - \omega_{m''};s) + \rho_{cc,\mathbf{k}_l}^{cdp}(\omega_{m'} - \omega_{m''};s), \tag{76}$$

where

$$\rho_{cc,\mathbf{k}_l}^{cdp}(\omega_{m'} - \omega_{m''};s) = \sum_{i,s'} A_{li}^c(\omega_{m'} - \omega_{m''};ss') \times \rho_{cc,\mathbf{k}_l}^{beat}(\omega_{m'} - \omega_{m''};ss'). \tag{77}$$

Here, $A_{li}^c(\omega_{m'} - \omega_{m''};ss')$ represents the population pulsation at the $\mathbf{k}_l$ state of the sth dot caused by the light-induced beating at the $\mathbf{k}_i$ state of the s'th dot, and is a complex number to cause phase shift from the light-induced beating. Thus, $A_{li}^c(\omega_{m'} - \omega_{m''};ss')$ with $s \neq s'$ represents the interdot interaction via the wetting layer, and cannot be neglected when the electron diffusion length in the wetting layer within the beating period is longer than the interdot distance. Note that

$$A_{li}^c(\omega_{m'} - \omega_{m''};ss') = A_{li}^{c*}(\omega_{m''} - \omega_{m'};ss'). \tag{78}$$

By substituting Eqs. (76) and (77) into Eq. (75), we obtain $\Delta N_{c,w}(\omega_{m'} - \omega_{m''})$.

The beating at the $\mathbf{k}_l$ state causes the coherent nondiagonal term of $\rho_{cv,\mathbf{k}_l}(t;s)$ via Eq. (17) with $\mathbf{k} = \mathbf{k}_l$ as

$$\dot{\rho}_{cv,\mathbf{k}_l}^{coh}(t;s) = [-i\omega_{cv,\mathbf{k}_l}^s - \Gamma_{cv,\mathbf{k}_l}^s]\rho_{cv,\mathbf{k}_l}^{coh}(t;s) + \frac{i}{\hbar}[\rho_{cc,\mathbf{k}_l}(t;s) - \rho_{vv,\mathbf{k}_l}(t;s)]\mu_{cv,\mathbf{k}_l}^\sigma(\mathbf{r}_s,t). \tag{79}$$

By substituting

$$\rho_{cv,\mathbf{k}_l}^{coh}(t;s) = \sum_{m',m'',m'''} \rho_{cv,\mathbf{k}_l}^{coh}(\omega_m = \omega_{m'} + \omega_{m''} + \omega_{m'''};s) e^{-i(\omega_{m'} + \omega_{m''} + \omega_{m'''})t}, \tag{80}$$

$\rho_{cc,\mathbf{k}_l}(t;s)$ of Eq. (70), and

$$\rho_{vv,\mathbf{k}_l}(t;s) = \rho_{vv,\mathbf{k}_l}^{pop}(t;s) + \sum_{\substack{m',m'' \\ (m\neq m',>0)}} \rho_{vv,\mathbf{k}_l}(\omega_{m'} - \omega_{m''};s) e^{-i(\omega_{m'} - \omega_{m''})t} + \text{c.c.} \tag{81}$$

into Eq. (79) with Eq. (15), we obtain the component with the frequency of $\omega_m = \omega_{m'} - \omega_{m''} + \omega_{m'''}$ with $m', m'', m''' > 0$ and $m' \neq m''$ as

$$\rho^{coh}_{cv,\mathbf{k}_l}(\omega_m=\omega_{m'}-\omega_{m''}+\omega_{m'''};s)=\rho^{dshb}_{cv,\mathbf{k}_l}(\omega_m=\omega_{m'}-\omega_{m''}+\omega_{m'''};s)+\rho^{cdp}_{cv,\mathbf{k}_l}(\omega_m=\omega_{m'}-\omega_{m''}+\omega_{m'''};s), \tag{82}$$

where

$$\rho^{cdp}_{cv,\mathbf{k}_l}(\omega_m=\omega_{m'}-\omega_{m''}+\omega_{m'''};s)=\frac{i\varepsilon_0 e P^{\sigma}_{cv,\mathbf{k}_l}}{16m_0\omega_{m''}\hbar^2}\sum_{i,s'}\frac{\chi^{pop}_{\sigma}(t,\omega_{m'};cv\mathbf{k}_l s')-\chi^{pop*}_{\sigma}(t,\omega_{m''};cv\mathbf{k}_l s')}{[(\omega_{m'}-\omega_{m''}+\omega_{m'''}-\omega^{s}_{cv,\mathbf{k}_l})+i\Gamma_{cv,\mathbf{k}_l}]}$$
$$\times\left[\frac{A^{c}_{li}(\omega_{m'}-\omega_{m''};ss')}{\omega_{m'}-\omega_{m''}+i(T^{s'}_{cc,\mathbf{k}_i}+R^{s'}_{cc,\mathbf{k}_i})}+\frac{A^{v}_{li}(\omega_{m'}-\omega_{m''};ss')}{\omega_{m'}-\omega_{m''}+i(T^{s'}_{vv,\mathbf{k}_i}+R^{s'}_{vv,\mathbf{k}_i})}\right]$$
$$\times E_{m'}E^{*}_{m''}E_{m'''}e^{i(\mathbf{q}_{m'}-\mathbf{q}_{m''}+\mathbf{q}_{m'''})\cdot\mathbf{r}_s}. \tag{83}$$

We neglected nonresonant terms, and assumed $e^{-i(\mathbf{q}_{m'}-\mathbf{q}_{m''})\cdot(\mathbf{r}_s-\mathbf{r}_{s'})}\cong 1$. Terms related to the valence band like $A^{v}_{li}(\omega_{m'}-\omega_{m''};ss')$ can be derived in the same way as the conduction band. The total coherent nonlinear polarization, given by the diagonal summation of Eq. (27) with $\rho^{(2n-1)}_{cv,\mathbf{k}}(\omega_m;s)$ replaced by $\rho^{coh}_{cv,\mathbf{k}_l}(\omega_m=\omega_{m'}-\omega_{m''}+\omega_{m'''};s)$, is the sum of the contribution by the dynamic spectral hole burning, $P^{dshb}_{m}(\mathbf{r},t)$, and the carrier density pulsation in the dots, $P^{cdp}_{m}(\mathbf{r},t)$, and in the wetting layer, $P^{wet}_{m}(\mathbf{r},t)$, as

$$P^{coh}_{m}(\mathbf{r},t)=P^{dshb}_{m}(\mathbf{r},t)+P^{cdp}_{m}(\mathbf{r},t)+P^{wet}_{m}(\mathbf{r},t)=\varepsilon_0\sum_{\substack{m',m'',m'''\\(m'\neq m''>0)}}\chi^{coh}_{\sigma}(\mathbf{r},t,\omega_m=\omega_{m'}-\omega_{m''}+\omega_{m'''})E_{m'}E^{*}_{m''}E_{m'''}e^{i(\mathbf{q}_{m'}-\mathbf{q}_{m''}+\mathbf{q}_{m'''})\cdot\mathbf{r}}, \tag{84}$$

where

$$\chi^{coh}_{\sigma}(\mathbf{r},t,\omega_m=\omega_{m'}-\omega_{m''}+\omega_{m'''})=\chi^{dshb}_{\sigma}(\mathbf{r},t,\omega_m=\omega_{m'}-\omega_{m''}+\omega_{m'''})+\chi^{cdp}_{\sigma}(\mathbf{r},t,\omega_m=\omega_{m'}-\omega_{m''}+\omega_{m'''})$$
$$+\chi^{wet}_{\sigma}(\mathbf{r},t,\omega_m=\omega_{m'}-\omega_{m''}+\omega_{m'''}), \tag{85}$$

$$\chi^{cdp}_{\sigma}(\mathbf{r},t,\omega_m=\omega_{m'}-\omega_{m''}+\omega_{m'''})=\sum_{c,v,\mathbf{k}_l,s}\chi^{cdp}_{\sigma}(t,\omega_m=\omega_{m'}-\omega_{m''}+\omega_{m'''};cv\mathbf{k}_l s)\,\delta(\mathbf{r}-\mathbf{r}_s), \tag{86}$$

$$\chi^{cdp}_{\sigma}(\mathbf{r},t,\omega_m=\omega_{m'}-\omega_{m''}+\omega_{m'''};cv\mathbf{k}_l s)=\frac{e^2|P^{\sigma}_{cv,\mathbf{k}_l}|^2}{4m_0^2\omega_{m'''}\omega^{s}_{cv,\mathbf{k}_l}\hbar^2}\sum_{i,s'}\frac{\chi^{pop}_{\sigma'}(t,\omega_{m'};cv\mathbf{k}_l s')-\chi^{pop*}_{\sigma'}(t,\omega_{m};cv\mathbf{k}_l s')}{\omega_{m'}-\omega_{m''}+\omega_{m'''}-\omega^{s}_{cv,\mathbf{k}_l}+i\Gamma_{cv,\mathbf{k}_l}}$$
$$\times\left[\frac{A^{c}_{li}(\omega_{m'}-\omega_{m''};ss')}{\omega_{m'}-\omega_{m''}+i(T^{s'}_{cc,\mathbf{k}_i}+R^{s'}_{cc,\mathbf{k}_i})}+\frac{A^{v*}_{li}(\omega_{m'}-\omega_{m''};ss')}{\omega_{m'}-\omega_{m''}+i(T^{s'}_{vv,\mathbf{k}_i}+R^{s'}_{vv,\mathbf{k}_i})}\right], \tag{87}$$

and

$$\chi^{wet}_{\sigma}(N_{c,w},N_{v,w},\omega_m=\omega_{m'}-\omega_{m''}+\omega_{m'''})$$
$$=\sum_{i=c,v}\frac{\partial\chi^{pop}_{\sigma}(N_{c,w},N_{v,w},\omega_{m'''})}{\partial N_{i,w}}$$
$$\times[\Delta N_{i,w}(\omega_{m'}-\omega_{m''})+\Delta N^{*}_{i,w}(\omega_{m''}-\omega_{m'})]$$
$$\times E^{-1}_{m'}E^{*-1}_{m''}e^{-i(\mathbf{q}_{m'}-\mathbf{q}_{m''})\cdot\mathbf{r}}. \tag{88}$$

Note that we added prime on the population susceptibility in Eq. (87) since the polarization of the m'' mode, σ, can be different from that of the m' and m'' modes, σ'.

D. Optical pulse propagation in the waveguide

We derive the equations for light pulse propagation in the wave guide of SOA's. The direction of the wave guide with the length of L and with the cross sectional area of the active region of D is taken as the z axis and its perpendicular direction is the x-y plane. The refractive index of the wave guide is represented by $n(x,y,\omega_m)$.

The wave equation of light is derived from Maxwell's equations as

$$\nabla^2\mathbf{E}=c^{-2}\partial^2\mathbf{E}/\partial t^2+\mu_0\sigma\partial\mathbf{E}/\partial t+\mu_0\partial^2\mathbf{P}/\partial t^2, \tag{89}$$

where $\mathbf{P}$ is the polarization of the material induced by the electric field. We write the electric field of the light pulse as

$$\mathbf{E}=\frac{1}{2}\sum_{m>0}\mathbf{e}[E_m(\mathbf{r},t)e^{-i\omega_m t}+\text{c.c.}]. \tag{90}$$

We assume a trial solution of the form of

$$E_m(\mathbf{r},t)=H(x,y)R_m(z,t)\exp[iq_m z], \tag{91}$$

where the real wave number in the z direction is

$$q_m=q_0(\omega_m)\equiv\frac{\omega_m n_{\text{eff}}(\omega_m)}{c} \tag{92}$$

and the transverse mode distribution in the x-y plane, $H(x,y)$, is determined by the conventional wave guide equation of

$$\left(\frac{d^2}{dx^2}+\frac{d^2}{dy^2}\right)H(x,y)+\left\{\frac{\omega^2 n^2(x,y,\omega_m)}{c^2}-q_0^2(\omega_m)\right\}H(x,y)=0. \tag{93}$$

We omitted the transverse mode index in $H(x,y)$ for simplicity. The polarization of Eq. (10) is divided into

$$\mathbf{P}=\mathbf{P}^{pop}+\mathbf{P}^{coh}+\mathbf{P}^{b}. \tag{94}$$

where $\mathbf{P}^{pop}+\mathbf{P}^{coh}$ is the polarization of the active region due to the interband transition, $\mathbf{P}^{pop}$ is the sum of the linear polarization and incoherent nonlinear polarization, $\mathbf{P}^{coh}$ is the coherent nonlinear polarization, and $\mathbf{P}^{b}$ is the background polarization. The photon flux density, i.e., the number of photons that pass the unit area of the waveguide cross section per unit time is

$$S_m=\frac{\varepsilon_0 c n_{\text{eff}}(\omega_m)}{2\hbar\omega_m D}\int_{cav}|E_m(\mathbf{r},t)|^2dxdy. \tag{95}$$

From Eqs. (89)–(94), we obtain the propagation equation as[29]

$$\frac{\partial}{\partial z}R_m(z,T)=\frac{\Gamma_m}{2}[\eta^{pop}(z,T,\omega_m)+\eta^{coh}(z,T,\omega_m=\omega_{m'}-\omega_{m''}+\omega_{m'''})]R_m(z,T)-\frac{\alpha_{loss}(\omega_m)}{2}R_m(z,T), \tag{96}$$

where we made the transformation of $T=t-q_0(\omega_m)z$ to employ a frame of reference moving with the pulse at the group velocity of $q_0(\omega_m)^{-1}$ and neglected the term of the group velocity dispersion. In Eq. (96), the optical confinement factor is

$$\Gamma_m=\frac{\int_{act}|H(x,y)|^2dxdy}{\int_{cav}|H(x,y)|^2dxdy}, \tag{97}$$

the contribution of the population term is

$$\eta^{pop}(z,T,\omega_m)=i\frac{\omega_m}{n_{\text{eff}}(\omega_m)c}\frac{\int_{act}\chi_\sigma^{pop}(\mathbf{r},T,\omega_m)|H(x,y)|^2dxdy}{\int_{act}|H(x,y)|^2dxdy}, \tag{98}$$

the contribution of the coherent nonlinear polarization term is

$$\eta^{coh}(z,T,\omega_m=\omega_{m'}-\omega_{m''}+\omega_{m'''})=i\frac{\omega_m}{n_{\text{eff}}(\omega_m)c}\sum_{\substack{m',m'',m'''\\(m'\neq m'',>0)}}\frac{\int_{act}\chi_\sigma^{coh}(\mathbf{r},T,\omega_m=\omega_{m'}-\omega_{m''}+\omega_{m'''})|H(x,y)|^4dxdy}{\int_{act}|H(x,y)|^2dxdy}\times R_{m'}(z,T)R_{m''}^{*}(z,T)R_{m'''}(z,T)R_m^{-1}(z,T)e^{i(q_{m'}-q_{m''}+q_{m'''}-q_m)z}, \tag{99}$$

and the internal loss is defined as $\alpha_{loss}(\omega_m)=\mu_0\sigma\omega/q_0(\omega_m)$. The integration of ''act'' is done over the cross section of the active region, and that of ''cav'' is done over the cross section of the waveguide in Eqs. (97)–(99).

Let us decompose the population term into k

$$\eta^{pop}(z,T,\omega_m)=g(z,T,\omega_m)+i\xi(z,T,\omega_m), \tag{100}$$

where

$$g(z,T,\omega_m)=-\frac{\omega_m}{n_{\text{eff}}(\omega_m)c}\frac{\int_{act}\text{Im}\,\chi_\sigma^{pop}(\mathbf{r},T,\omega_m)|H(x,y)|^2dxdy}{\int_{act}|H(x,y)|^2dxdy} \tag{101}$$

is the optical gain, and

$$\xi(z,T,\omega_m)=\frac{\omega_m}{n_{\text{eff}}(\omega_m)c}\frac{\int_{act}\text{Re}\,\chi_\sigma^{pop}(\mathbf{r},T,\omega_m)|H(x,y)|^2dxdy}{\int_{act}|H(x,y)|^2dxdy} \tag{102}$$

is related to the phase of the optical pulse. When $\chi_\sigma^{pop}(\mathbf{r},T,\omega_m)$ is replaced with $\chi_\sigma^{(1)}(\mathbf{r},T,\omega_m)$, Eq. (101) gives the linear gain of $g^{(1)}(\omega_m)$.

The amplitude of the optical pulse propagating in the z direction is affected by the terms of $\eta_m^{pop}(z,T)$ and $\eta_m^{coh}(z,T)$ as seen in Eq. (96). By averaging Eq. (98) with Eq. (47) over the small distance of Δz, we obtain

$$\eta^{pop}(z,T,\omega_m)=i\frac{\omega_m}{n_{\text{eff}}(\omega_m)c}\frac{\sum_{c,v,\mathbf{k},s}\int_{act}dxdy\int_z^{z+\Delta z}dz\chi_\sigma^{pop}(z,T,\omega_m;cv\mathbf{k}s)\delta(\mathbf{r}-\mathbf{r}_s)|H(x,y)|^2}{\Delta z\int_{act}|H(x,y)|^2dxdy}$$

$$=i\frac{\omega_m}{n_{\text{eff}}(\omega_m)c}\sum_{\substack{c,v,\mathbf{k},s\\(z\sim z+\Delta z)}}\chi_\sigma^{pop}(z,T,\omega_m;cv\mathbf{k}s)\frac{|H(x_s,y_s)|^2}{\Delta z\int_{act}|H(x,y)|^2dxdy}. \tag{103}$$

Here, the summation over s is limited to the dots between z and $z+\Delta z$, where Δz should satisfy $\Delta z\partial R_m(z,T)/\partial z \ll R_m(z,T)$. Similarly, from Eqs. (85) and (99), we obtain

$$\eta^{coh}(z,T,\omega_m=\omega_{m'}-\omega_{m''}+\omega_{m'''})=\eta^{cshb}(z,T,\omega_m=\omega_{m'-\omega_{m''}+\omega_{m'''}})+\eta^{cdp}(z,T,\omega_m=\omega_{m'}-\omega_{m''}+\omega_{m'''})$$
$$+\eta^{wet}(z,T,\omega_m=\omega_{m'}-\omega_{m''}+\omega_{m'''}), \tag{104}$$

where

$$\eta^{cshb}(z,T,\omega_m=\omega_{m'}-\omega_{m''}+\omega_{m'''})=i\frac{\omega_m}{n_{\text{eff}}(\omega_m)c}\sum_{\substack{m',m'',m'''\\(m'\neq m'',>0)}}\sum_{\substack{c,v,\mathbf{k},s\\(z\sim z+\Delta z)}}\chi_\sigma^{cshb}(z,T,\omega_m=\omega_{m'}-\omega_{m''}+\omega_{m''};cv\mathbf{k}s)$$
$$\times\frac{|H(x_s,y_s)|^4}{\Delta z\int_{act}|H(x,y)|^2dxdy}R_{m'}(z,T)R_{m''}^*(z,T)R_{m'''}(z,T)R_m^{-1}(z,T)e^{i(q_{m'}-q_{m''}+q_{m'''}-q_m)z}, \tag{105}$$

$$\eta^{cdp}(z,T,\omega_m=\omega_{m'}-\omega_{m''}+\omega_{m'''})=i\frac{\omega_m}{n_{\text{eff}}(\omega_m)c}\sum_{\substack{m',m'',m'''\\(m'\neq m'',>0)}}\sum_{\substack{c,v,\mathbf{k},\mathbf{k}_l,s\\(z-z+\Delta z)}}\chi_\sigma^{cdp}(z,T,\omega_m=\omega_{m'}-\omega_{m''}+\omega_{m'''};cv\mathbf{k}s)$$
$$\times\frac{|H(x_s,y_s)|^4}{\Delta z\int_{act}|H(x,y)|^2dxdy}R_{m'}(z,T)R_{m''}^*(z,T)R_{m'''}(z,T)R_m^{-1}(z,T)e^{i(q_{m'}-q_{m''}+q_{m'''}-q_m)z}, \tag{106}$$

and

$$\eta^{wet}(z,T,\omega_m=\omega_{m'}-\omega_{m''}+\omega_{m'''})=i\frac{\omega_m}{n_{\text{eff}}(\omega_m)c}\sum_{\substack{m',m'',m'''\\(m'\neq m'',>0)}}\frac{\int_{act}\chi_\sigma^{wet}(N_{c,w},N_{v,w},\omega_m=\omega_{m'}-\omega_{m''}+\omega_{m'''})|H(x,y)|^4dxdy}{\int_{act}|H(x,y)|^2dxdy}$$
$$\times R_{m'}(z,T)R_{m''}^*(z,T)R_{m'''}(z,T)R_m^{-1}(z,T)e^{i(q_{m'}-q_{m''}+q_{m'''}-q_m)z}. \tag{107}$$

In order to calculate Eqs. (103) and (104), we need to know the position, the energy states and the carrier population of each dot.

E. Amplified spontaneous emission and noise figure

Spontaneous emission is one of the major recombination processes of electrons and holes injected into the active region besides stimulated emission and nonradiative recombination. Based on the Weisskopf and Wigner theory in the three-dimensional symmetric continuous optical modes, the spontaneous emission shows an exponential irreversible decay with a time constant of about one nanosecond.[28,30] Some of the spontaneous emission propagate in the waveguide being amplified via the stimulated emission. As a result, we observe amplified spontaneous emission light from the edge of the waveguide superimposed to the output signals.[29,31,32]

The propagation equation of the spontaneous emission being amplified in the cavity is given as

$$\frac{d}{dz}S_{sp}(z,T,\omega_{sp})=[\Gamma_{sp}g(z,T,\omega_{sp})-\alpha_{loss}(\omega_{sp})]$$
$$\times S_{sp}(z,T,\omega_{sp})$$
$$+\Gamma_{sp}g_{spon}(z,T,\omega_{sp})S_{vac}(\omega_{sp}), \tag{108}$$

where $S_{sp}(z,T,\omega_{sp})$ is the photon flux density of the spontaneous emission with the frequency between ω_{sp} and $\omega_{sp}+\Delta\omega_{sp}$, $\alpha_{loss}(\omega_{sp})$ is the loss, the optical gain of $g(z,T,\omega_{sp})$ is given by Eq. (101) with ω_m replaced by ω_{sp}, Γ_{sp} is the optical confinement factor, $S_{vac}(\omega_{sp})=\Delta\omega_{sp}/(2\pi D)$ is the photon flux density of the vacuum field with a frequency between ω_{sp} and $\omega_{sp}+\Delta\omega_{sp}$, $g_{spon}(z,T,\omega_{sp})$ is given by $g(z,T,\omega_{sp})$ with the distribution

function of $\rho^{pop}_{cc,\mathbf{k}}(z,T;s)-\rho^{pop}_{vv,\mathbf{k}}(z,T;s)$ replaced with $\rho^{pop}_{cc,\mathbf{k}}(z,T;s)[1-\rho^{pop}_{vv,\mathbf{k}}(z,T;s)]$ to described the stimulated emission by the vacuum field. We used the concept that the spontaneous emission is the stimulated emission by the vacuum field.[33]

Under the linear condition, where the gain is independent of z and T, we write $g(z,T,\omega_{sp})=g^{(1)}(\omega_{sp})$ and $g_{spon}(z,T,\omega_{sp})=g^{(1)}_{spon}(\omega_{sp})$. Then, we obtain an analytical solution of Eq. (108); by integrating Eq. (108) in the waveguide between 0 and L, we obtain the output of[29,31,32]

$$S_{sp}(L,T,\omega_{sp})=[G^{(1)}(\omega_{sp})-1]n_{sp}(\omega_{sp})S_{vac}(\omega_{sp}) + G^{(1)}(\omega_{sp})S_{sp}(0,T,\omega_{sp}), \tag{109}$$

where $S_{sp}(0,T,\omega_{sp})$ is the photon flux density of the input spontaneous emission, the linear amplifier gain is

$$G^{(1)}(\omega_{sp})=\exp\{[\Gamma_{sp}g^{(1)}(\omega_{sp})-\alpha_{loss}(\omega_{sp})]L\}, \tag{110}$$

and the population inversion parameter is

$$n_{sp}(\omega_{sp})=n^{(1)}(\omega_{sp})n^{(2)}(\omega_{sp}) \tag{111}$$

with

$$n^{(1)}(\omega_{sp})=\frac{g^{(1)}_{spon}(\omega_{sp})}{g^{(1)}(\omega_{sp})} \tag{112}$$

and

$$n^{(2)}(\omega_{sp})=\frac{\Gamma^{sp}g^{(1)}(\omega_{sp})}{\Gamma_{sp}g^{(1)}(\omega_{sp})-\alpha_{loss}(\omega_{sp})}. \tag{113}$$

The population inversion parameter of Eq. (111) takes the minimum value of one when $\rho^{pop}_{cc,\mathbf{k}}(z;s)=1$, $\rho^{pop}_{vv,\mathbf{k}}(z;s)=0$, and $\alpha_{loss}(\omega_{sp})=0$.

The signal-to-noise ratio (SNR) degrades in SOA's because of the beating noise that comes from the beating of the signal with the spontaneous emission light, and from the beating between the amplified spontaneous emission of different frequencies.[29,31,32] The noise figure (NF) of the SOA is given as

$$\mathrm{NF}=\frac{1+2\,\eta_{out}S_{sp}(L,T,\omega_m)/S_{vac}(\omega_m)}{\eta_{in}\eta_{out}G_m(T)}, \tag{114}$$

where η_{in} is the input coupling coefficient, and η_{out} is the output coupling coefficient. In the linear region, using $G_m(T)=G^{(1)}_m=\exp\{[\Gamma_m g^{(1)}(\omega_m)-\alpha_{loss}(\omega_m)]L\}$ and Eq. (109) with $S_{sp}(0,T,\omega_m)=0$, we obtain

$$\mathrm{NF}=\frac{1+2\,\eta_{out}[G^{(1)}_m-1]n_{sp}(\omega_m)}{\eta_{in}\eta_{out}G^{(1)}_m}\cong\frac{2n_{sp}(\omega_m)}{\eta_{in}}. \tag{115}$$

The noise figure is proportional to the population inversion parameter and inversely proportional to the input coupling coefficient. Its minimum is NF=3 dB when $n_{sp}(\omega_m)=\eta_{in}=1$.

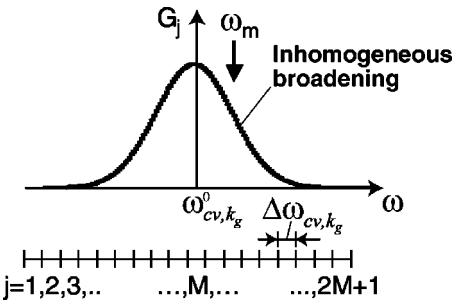

FIG. 3. Grouping of quantum dots in terms of their resonant frequency of the ground-state interband transition.

F. Optical susceptibility and carrier population in randomly distributed quantum dots with inhomogeneous broadening

In order to simplify the calculation of the susceptibilities described by Eqs. (103) and (104), we group quantum dots by their resonance energies or frequencies; let us divide the dot ensemble into $2M+1$ groups depending on their resonant frequency for the ground-state interband transition (Fig. 3). Taking the central frequency of the ground-state transition as $\omega^0_{cv,\mathbf{k}_g}$ and the frequency width of each group as $\Delta\omega_{cv,\mathbf{k}_g}$, the frequency of the ground state of the jth group is represented by

$$\omega^0_{cv,\mathbf{k}_g}=\omega^0_{cv,\mathbf{k}_g}-(M-j)\Delta\omega_{cv,\mathbf{k}_g}, \tag{116}$$

where $j=0,1,2,...,$ and $2M$ [do not confuse the index of j with what was used to describe the electronic bands in Eq. (3)]. We should choose M to make $\Delta\omega_{cv,\mathbf{k}_g}$ much smaller than the dephasing rate, say, $\Delta\omega_{cv,\mathbf{k}_g}\ll\Gamma_{cv,\mathbf{k}_g}$ so that the dots in one group behave in the same way under the light. We use the inhomogeneous broadening function of

$$G_j=G(\omega^j_{cv,\mathbf{k}_g}-\omega^0_{cv,\mathbf{k}_g})\Delta\omega_{cv,\mathbf{k}_g} \tag{117}$$

to describe the distribution of the interband transition frequency at the ground state. Note that G_j is normalized as $\Sigma_{j=0}^{2M+1}G_j=1$. In self-assembled quantum dots, G_j often obeys Gaussian distribution. The frequency of the lth excited state of the jth group is represented by

$$\omega^j_{cv,\mathbf{k}_l}=\omega^0_{cv,\mathbf{k}_l}-(M-j)\Delta\omega_{cv,\mathbf{k}_l}, \tag{118}$$

where $\omega^0_{cv,\mathbf{k}_l}$ is the central frequency and $\Delta\omega_{cv,\mathbf{k}_l}$ is the frequency width of each group ($\Delta\omega_{cv,\mathbf{kl}}$ might vary with j). We assume the following; First, each resonant frequency group has the same spatial distribution in the xy plane. Second, quantum dots in the same resonant frequency group have the same population. Third, each group has the same relaxation and recombination rates, which we denote by j instead of s, like $\Gamma^j_{cv,\mathbf{k}}$ instead of $\Gamma^s_{cv,\mathbf{k}}$ for example. Let us call this treatment a random distribution approximation.

We assume in Eq. (118), for simplicity, that the higher the ground-state resonant frequency is, the higher the excited-state frequency. This might not be the case when the inhomogeneous broadening is caused by multiple factors like the

size, alloy composition, shape, and strain of quantum dots. Then, the grouping should take into account the various combination of the ground- and excited-state frequencies. Tsiper treated this case by deriving the formula on the probability density for the combination of the ground- and excited-state frequencies, and presented the way to know the statistical distribution of the each energy state from the photoluminescence and photoluminescence excitation experiments.[34]

By taking the summation of j and s independently, Eq. (103) becomes

$$\eta^{pop}(z,T,\omega_m)=\sum_{c,v,\mathbf{k}}\sum_{j=1}^{2M+1}\eta^{pop}(z,T,\omega_m;cv\mathbf{k}j), \tag{119}$$

where

$$\eta^{pop}(z,T,\omega_m;cv\mathbf{k}j) = i\frac{\omega_m}{n_{\text{eff}}(\omega_m)c}N_D(z)\chi_\sigma^{pop}(z,T,\omega_m;cv\mathbf{k}j)G_j, \tag{120}$$

$$\chi_\sigma^{pop}(z,T,\omega_m;cv\mathbf{k}j) = \frac{2e^2|P_{cv,\mathbf{k}}^\sigma|^2[\rho_{cc,\mathbf{k}}^{pop}(z,T;j)-\rho_{vv,\mathbf{k}}^{pop}(z,T;j)]}{\varepsilon_0\hbar m_0^2\omega_m\omega_{cv,\mathbf{k}}^j} \times\left[\frac{1}{\omega_m-\omega_{cv,\mathbf{k}}^j+i\Gamma_{cv,\mathbf{k}}^j}+\frac{1}{\omega_m+\omega_{cv,\mathbf{k}}^j+i\Gamma_{cv,\mathbf{k}}^j}\right], \tag{121}$$

and

$$N_{Dk}(z)=\sum_{\substack{s\\(z-z+\Delta z)}}\frac{|H(x_s,y_s)|^2}{\Delta z\int_{act}|H(x,y)|^2dxdy}. \tag{122}$$

Here, $\rho_{cc,\mathbf{k}}^{pop}(z,T;j)$ is the common population of the jth group in the conduction band state, $\rho_{vv,\mathbf{k}}^{pop}(z,T;j)$ is that in the valence band state, and $\Gamma_{cv,\mathbf{k}}^j$ is the common polarization relaxation rate of the jth group. Note that $N_D(z)$ of Eq. (122) becomes the dot density of N_D when $H(x,y)$ is constant over the active region.

In the same way, from Eqs. (100) and (119), we obtain the optical gain as

$$g(z,T,\omega_m)=\sum_{c,v,\mathbf{k}}\sum_{j=1}^{2M+1}g(z,T,\omega_m;cv\mathbf{k}j), \tag{123}$$

where

$$g(z,T,\omega_m;cv\mathbf{k}j) = -\frac{\omega_m}{n_{\text{eff}}(\omega_m)c}N_D(z)\text{Im}\,\chi_\sigma^{pop}(z,T,\omega_m;cv\mathbf{k}j)G_j \tag{124}$$

and

$$\text{Im}\,\chi_\sigma^{pop}(z,T,\omega_m;cv\mathbf{k}j) = -\frac{2\pi e^2|P_{cv,\mathbf{k}}^\sigma|^2[\rho_{cc,\mathbf{k}}^{pop}(z,T;j)-\rho_{vv,\mathbf{k}}^{pop}(z,T;j)]}{\varepsilon_0\hbar m_0^2\omega_m\omega_{cv,\mathbf{k}}^j} \times\frac{\Gamma_{cv,\mathbf{k}}^j/\pi}{(\omega_m-\omega_{cv,\mathbf{k}}^j)^2+\Gamma_{cv,\mathbf{k}}^{j^2}}. \tag{125}$$

The nonresonant term was omitted. The formulas for $g_{spon}(z,T,\omega_{sp})$ can be obtained in the similar way.

By taking the summation of j and s independently, Eq. (104) becomes

$$\eta^{coh}(z,T,\omega_m) = \sum_{\substack{m',m''m'''\\(m'\neq m''>0)}}\sum_{c,v,\mathbf{k},\mathbf{k}_j}\sum_{j=1}^{2M+1}[\eta^{dshb}(z,T,\omega_m;cv\mathbf{k}j) + \eta^{cdp}(z,T,\omega_m;cv\mathbf{k}_lj)] \times R_{m'}(z,T)R_{m''}^*(z,T)R_{m'''}(z,T)R_m^{-1}(z,T) \times e^{i(q_{m'}-q_{m''}+q_{m'''}-q_m)z}+\eta^{wet}(z,T,\omega_m), \tag{126}$$

where

$$\eta^{dshb}(z,T,\omega_m;cv\mathbf{k}j)=i\frac{\omega_m}{n_{\text{eff}}(\omega_m)c}N_D^{coh}(z)\chi_\sigma^{dshb}(z,T,\omega_m;cv\mathbf{k}j)G_j, \tag{127}$$

$$\chi_\sigma^{dshb}(z,T,\omega_m=\omega_{m'}-\omega_{m''}+\omega_{m'''};cv\mathbf{k}j)=\frac{e^2|P_{cv,\mathbf{k}}^\sigma|^2}{4m_0^2\omega_{m'''}\omega_{cv,\mathbf{k}}^j\hbar^2}\frac{\chi_{\sigma'}^{pop}(z,T,\omega_{m'};cv\mathbf{k}j)-\chi_{\sigma'}^{pop}(z,T,\omega_{m''};cv\mathbf{k}j)^*}{\omega_{m'}-\omega_{m''}+\omega_{m'''}-\omega_{cv,\mathbf{k}}^j+i\Gamma_{cv,\mathbf{k}}^j} \times\left\{\frac{1}{\omega_{m'}-\omega_{m''}+i(T_{cc,\mathbf{k}}^j+R_{cc,\mathbf{k}}^j)}+\frac{1}{\omega_{m'}-\omega_{m''}+i(T_{vv,\mathbf{k}}^j+R_{vv,\mathbf{k}}^j)}\right\}, \tag{128}$$

$$\eta^{cdp}(z,T,\omega_m;cv\mathbf{k}_lj)=i\frac{\omega_m}{n_{\text{eff}}(\omega_m)c}N_D^{coh}(z)\chi_\sigma^{cdp}(z,T,\omega_m;cv\mathbf{k}_lj)G_j, \tag{129}$$

$$\chi_{\sigma}^{cdp}(z,T,\omega_m=\omega_{m'}-\omega_{m''}+\omega_{m''};cv\mathbf{k}_l j)=\frac{e^2|P_{cv,\mathbf{k}_l}^{\sigma}|^2}{4m_0^2\omega_{m''}\omega_{cv,\mathbf{k}_l}^{j}\hbar^2}\sum_{i,j'}\frac{\chi_{\sigma'}^{pop}(z,T,\omega_{m'};cv\mathbf{k}_i j')-\chi_{\sigma'}^{pop*}(z,T,\omega_{m'};cv\mathbf{k}_i j')}{\omega_{m'}-\omega_{m''}+\omega_{m'''}-\omega_{cv,\mathbf{k}_i}^{j}+i\Gamma_{cv,\mathbf{k}_i}^{j}}$$
$$\times\left\{\frac{A_{li}^{c}(\omega_{m'}-\omega_{m''};jj')}{\omega_{m'}-\omega_{m''}+i(T_{cc,\mathbf{k}_i}^{j'}+R_{cc,\mathbf{k}_i}^{j'})}+\frac{A_{li}^{v*}(\omega_{m'}-\omega_{m''};jj')}{\omega_{m'}-\omega_{m''}+i(T_{vv,\mathbf{k}_i}^{j'}+R_{vv,\mathbf{k}_i}^{j'})}\right\} \tag{130}$$

and

$$N_D^{coh}(z)=\sum_{\substack{s\\(z-z+\Delta z)}}\frac{|H(x_s,y_s)|^4}{\Delta z\int_{act}|H(x,y)|^2dxdy}. \tag{131}$$

From Eqs. (72)–(75) with s replaced by j, the amplitude of $A_{li}^{c}(\omega_{m'}-\omega_{m''};j)$ is given by solving

$$\rho_{cc,\mathbf{k}_l}(\omega_{m'}-\omega_{m''};j)=\rho_{cc,\mathbf{k}_l}^{beat}(\omega_{m'}-\omega_{m''};j)+\sum_{i\neq l}i\frac{T_{li}^{j,c}}{\omega_{m'}-\omega_{m''}+i(T_{cc,\mathbf{k}_i}^{j}+R_{cc,\mathbf{k}_i}^{j})}$$
$$\times\rho_{cc,\mathbf{k}_i}(\omega_{m'}-\omega_{m''};j)+i\frac{T_w^c}{\omega_{m'}-\omega_{m''}+i(T_{cc,\mathbf{k}_i}^{j}+R_{cc,\mathbf{k}_i}^{j})}\Delta N_{c,w}(\omega_{m'}-\omega_{m''}) \tag{132}$$

and

$$\Delta N_{c,w}(\omega_{m'}-\omega_{m''})=i\sum_{j,l}\frac{2N_D G_j T_{wl}^{c}}{\omega_{m'}-\omega_{m''}+i(T_w^c+R_w^c)}\rho_{cc,\mathbf{k}_l}(\omega_{m'}-\omega_{m''};j) \tag{133}$$

under the successive approximation as

$$\rho_{cc,\mathbf{k}_l}(\omega_{m'}-\omega_{m''};j)=\rho_{cc,\mathbf{k}_l}^{beat}(\omega_{m'}-\omega_{m''};j)+\rho_{cc,\mathbf{k}_l}^{cdp}(\omega_{m'}-\omega_{m''};j) \tag{134}$$

and

$$\rho_{cc,\mathbf{k}_l}^{cdp}(\omega_{m'}-\omega_{m''};j)=\sum_{i,j'}A_{li}^{c}(\omega_{m'}-\omega_{m''};jj')\rho_{cc,\mathbf{k}_l}^{beat}(\omega_{m'}-\omega_{m''};j'). \tag{135}$$

Here, $A_{li}^{c}(\omega_{m'}-\omega_{m''};jj')$ represents the population pulsation at the $\mathbf{k}_l$ state of the jth dot group caused by the light-induced beating at the $\mathbf{k}_i$ state of the j'th dot group, and is a complex number to cause phase shift from the light-induced beating. Thus, $A_{li}^{c}(\omega_{m'}-\omega_{m''};jj')$ with $j\neq j'$ represents the interdot group interaction via the wetting layer, and cannot be neglected when the electron diffusion length in the wetting layer within the beating period is longer than the interdot distance. Note that

$$A_{li}^{c}(\omega_{m'}-\omega_{m''};jj')=A_{li}^{c*}(\omega_{m''}-\omega_{m'};jj'). \tag{136}$$

Under the random distribution approximation, the electron density of the jth dot group in the active region at the position of z is given as

$$N_{c,\mathbf{k}}(z,T;j)=2N_D G_j\rho_{cc,\mathbf{k}}^{pop}(z,T;j)=2(D\Delta z)^{-1}\sum_{s\in j}\sum_{v}\int_{act}dxdy\int_{z}^{z+\Delta z}dz\rho_{cc,\mathbf{k}}^{pop}(z,T;s)\,\delta(\mathbf{r}-\mathbf{r}_s), \tag{137}$$

where the summation of s is done when dots are in the jth group. Note that we added the summation on the valence-band $\mathbf{k}_v$ state. The degeneracy due to spin is taken into account. Using Eq. (50), we obtain the time derivative of Eq. (137) as

$$\frac{dN_{c,\mathbf{k}}(z,T;j)}{dt}=\frac{\varepsilon_0}{2\hbar}(D\Delta z)^{-1}\sum_{s\in i}\sum_{v}\sum_{\substack{m\\(>0)}}\int_{act}dxdy\int_{z}^{z+\Delta z}dz\,\mathrm{Im}\,\chi^{pop}(z,T,\omega_m;cv\mathbf{k}s)\,\delta(\mathbf{r}-\mathbf{r}_s)|E_m(\mathbf{r},t)|^2-T_{cc,\mathbf{k}}^{j}[N_{c,k}(z,T;j)$$
$$-\tilde{\tilde{N}}_{c,\mathbf{k}}(z,T;j)]-R_{cc,\mathbf{k}}^{j}[N_{c,\mathbf{k}}(z,T;j)-\tilde{N}_{c,\mathbf{k}}(z,T;j)], \tag{138}$$

where $\tilde{\tilde{N}}_{c,\mathbf{k}}(z,T;j)$ and $\tilde{N}_{c,\mathbf{k}}(z,T;j)$ are given in the same way as Eq. (138) under the random distribution approximation. Using Eqs. (95) and (124), Eq. (138) becomes

$$\frac{dN_{c,\mathbf{k}}(z,T;j)}{dt} = -\sum_{v}\sum_{\substack{m \\ (>0)}} \Gamma_m S_m g(z,T,\omega_m;cv\mathbf{k}j) - T^j_{cc,\mathbf{k}}[N_{c,\mathbf{k}}(z,T;j) - \tilde{\tilde{N}}_{c,\mathbf{k}}(z,T;j)] - R^j_{cc,\mathbf{k}}[N_{c,\mathbf{k}}(z,T;j) - \tilde{N}_{c,\mathbf{k}}(z,T;j)]. \tag{139}$$

The first term of Eq. (139) represents the reduction of the carrier density by the stimulated emission. The rate equation of the carrier density in the valence band, $N_{v,\mathbf{k}}(z,T;j)$, can be derived in the same way.

III. MODEL OF CARRIER RELAXATION

In order to calculate the light propagation in the waveguide and the carrier density in the active region using the formulas in Sec. II, we need to know the population relaxation rates of $T^j_{cc,\mathbf{k}}$, T^c_w, T^c_{wl}, T^c_{lw}, and $T^{j,c}_{li}$ in the conduction band, the same rates in the valence band, the recombination rates of $R^j_{cc,\mathbf{k}}$, $R^j_{vv,\mathbf{k}}$, R^c_w, and R^v_w, and the polarization relaxation rate of $\Gamma^j_{cv,\mathbf{k}}$ at each conduction-band and valence-band $\mathbf{k}$ state in each dot group. These parameters can be evaluated by many experimental approaches to study the light-matter interaction, like time-resolved photoluminescence, pump-probe, and four-wave mixing techniques, etc.

By time-resolved pump-probe transmission spectra, Akiyama *et al.*[5] reported the incoherent spectral hole burning width, i.e., homogeneous broadening width, to be 10–15 meV in the SOA with 1.15-micron self-assembled InGaAs quantum-dot active region at room temperature, giving us the relaxation lifetime of $(\Gamma^j_{cv,\mathbf{k}})^{-1} = 90$–$130$ fs. The authors found that the spectral hole broadened as the injection current increased, which can be attributed to the enhancement of carrier-carrier scattering rates. By analyzing lasing spectra of the quantum-dot lasers with the same active region based on the prototype of our present theory, Sugawara *et al.* obtained similar values of homogeneous broadening under lasing.[25] By time-resolved four-wave mixing, Borri *et al.* evaluated the polarization relaxation rate at the 1.25-micron ground state of the quantum-dot SOA to be about 150 fs under the current injection condition.[35,36] The authors claimed that this 150-fs value is due to equal contributions from population relaxation and elastic dephasing, and is more than three-time longer than less-confined dots indicating that the strong confinement can reduce the homogeneous broadening under current injection.

The carrier recombination rates of $R^j_{cc,\mathbf{k}}$, $R^j_{cc,\mathbf{k}}$, R^c_w, and R^v_w are 0.1–1 ns in semiconductors. This is due to the spontaneous emission and other nonradiative recombination processes.

Gain saturation recovery of the incoherent spectral hole, which is caused by the population relaxation, was studied by Akiyama *et al.*[5] and Borri *et al.*[3,4,35] in self-assembled InGaAs quantum-dot SOA's. In general, the measured gain as a function of time showed complete recovery of saturation within a few picoseconds or less, and a fast gain recovery component with a time constant of 100–300 fs. The slow recovery component can be attributed to the carrier capture process to quantum dots, which is also evaluated by the rise time of time-resolved photoluminescence.[37] The fast component corresponds to the population relaxation time of $(T^j_{cc,\mathbf{k}})^{-1}$ and $(T^j_{vv,\mathbf{k}})^{-1}$ in our theory. Borri *et al.* analyzed their data to eliminate the superimposed two-photon absorption contribution, and show that the fast recovery component has the time constant of 115 fs in 1.1-micron small-size dots, and 140 fs in 1.25-micron large-size dots.

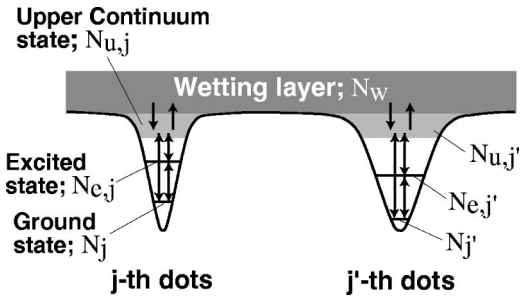

FIG. 4. Conduction band structure of quantum dots including the wetting layer. We take into account the ground state, the excited state, and the upper continuum state in each dot.

Note that the time constants of 100–300 fs are one order of magnitude longer than typical carrier scattering rates of 10–50 fs in conventional semiconductors like quantum wells and bulk materials.[37,38] The slower gain recovery leads to remarkable incoherent and dynamic spectral hole burning in quantum-dot SOA's, which is the principle of the high-speed switching.

Knowledge we are still lacking for simulating quantum-dot SOA performance is about how the carrier population at each $\mathbf{k}$ state and in the wetting layer depends on the current density and the optical intensity. So, we present here a model of the electronic band structure of the quantum-dot active region, and then, a series of rate equations on the population.

Figure 4 shows a model of the conduction-band structure of quantum dots with a wetting layer. The wetting layer is commonly observed in the self-assembled InGaAs quantum dots grown via Stranski-Krastanow mode.[28] In each dot, we take into account three energy states, which we name the ground state, the excited state, and the upper continuum state. The continuum state means the ensemble of dense energy states in each dot which merges into the two-dimensional energy states of the wetting layer. Carriers are injected into the wetting layer by currents, captured by the continuum states, and then, relax into the dots. We describe the center of the interband transition energy, $\mathbf{k}$ vector and the degeneracy as $E_g = \hbar\omega^0_{cv,\mathbf{k}_g}$, $\mathbf{k}_g$ and D_g for the ground state, and $E_e = \hbar\omega^0_{cv,\mathbf{k}_e}$, $\mathbf{k}_e$ and D_e for the excited state. For simplicity, we also represent the upper continuum state by the interband transition energy of $E_u = \hbar\omega^0_{cv,\mathbf{k}_u}$ and the degeneracy of D_u, and the wetting layer by the interband transition energy of $E_w = \hbar\omega_w$ and the degeneracy of D_w. The time constants of the carrier relaxation processes denoted by the arrows in Fig. 4 are given in the Appendix of Ref. 18.

Main assumptions here are as follows. We use random

distribution approximation defined in Sec. II G. We consider one conduction band and one valence band, and use the charge neutrality condition of $\rho^{pop}_{cc,\mathbf{k}}(z,T;j)+\rho^{pop}_{vv,\mathbf{k}}(z,T;j)=1$ at each $\mathbf{k}$ state and $N_{c,w}=N_{v,w}=N_w(z,T)$ in the wetting layer. We write the carrier density of the upper continuum state at the jth dot group as $N_{u,j}(z,T)=2D_uN_DG_j\rho^{pop}_{cc,\mathbf{k}_u}(z,T;j)$, that of the excited state as $N_{e,j}(z,T)=2D_eN_DG_j\rho^{pop}_{cc,\mathbf{k}_e}(z,T;j)$, and that of the ground state as $N_{g,j}(z,T)=2D_eN_DG_j\rho^{pop}_{cc,\mathbf{k}_g}(z,T;j)$. We use the relaxation rates common for each conduction-band and valence-band $\mathbf{k}$ state, instead of treating the relaxation of electrons and holes separately. For example, the population relaxation rates of $T^j_{cc,\mathbf{k}_s}$ and $T^j_{vv,\mathbf{k}_g}$ are written as T^j_g, the recombination rates of $R^j_{cc,\mathbf{k}_g}$ and $R^j_{vv,\mathbf{k}_g}$ as R^j_g, and the polarization relaxation rate of $\Gamma^j_{cv,\mathbf{k}_g}$ as Γ^j_g. We suppose that only the ground state is resonant to the light, i.e., the stimulated emission and the light-induced population beating occurs only in the ground state.

A. Rate equations of carrier density

The rate equations of carriers at each energy state are given in Ref. 18. The intraband relaxation rates used in this paper's notation are given as

$$T_w=\sum_j\left[\frac{N_{u,j}(z,T)}{2D_w}\tau^{-1}_{u\to w,0}+\left(1-\frac{N_{u,j}}{2D_uN_DG_j}\right)G_j\tau^{-1}_{w\to u,0}\right] \tag{140}$$

for the wetting layer,

$$T^j_u(z,T)=T_{wu}(z,T)+T^j_{gu}(z,T)+T^j_{eu}(z,T), \tag{141}$$

$$T_{wu}(z,T)=\frac{N_w(z,T)}{2D_uN_D}\tau^{-1}_{w\to u,0}+\left(1-\frac{N_w}{2D_w}\right)\tau^{-1}_{u\to w,0}, \tag{142}$$

$$T^j_{gu}(z,T)=\frac{N_j(z,T)}{2D_uN_DG_j}\tau^{-1}_{g\to u,0}+\left(1-\frac{N_j}{2D_gN_DG_j}\right)\tau^{-1}_{u\to g,0}, \tag{143}$$

$$T^j_{eu}(z,T)=\frac{N_{e,j}(z,T)}{2D_uN_DG_j}\tau^{-1}_{e\to u,0}+\left(1-\frac{N_{e,j}}{2D_eN_DG_j}\right)\tau^{-1}_{u\to e,0}, \tag{144}$$

for the upper continuum state, and

$$T^j_e(z,T)=T^j_{ge}(z,T)+T^j_{ue}(z,T), \tag{145}$$

$$T^j_{ge}(z,T)=\frac{N_j(z,T)}{2D_eN_DG_j}\tau^{-1}_{g\to e,0}+\left(1-\frac{N_j}{2D_gN_DG_j}\right)\tau^{-1}_{e\to g,0}, \tag{146}$$

$$T^j_{ue}(z,T)=\frac{N_{u,j}(z,T)}{2D_eN_DG_j}\tau^{-1}_{u\to e,0}+\left(1-\frac{N_{u,j}}{2D_uN_DG_j}\right)\tau^{-1}_{e\to u,0}, \tag{147}$$

for the excited state. The carrier recombination rate at each state is written as R_w, R^j_c, and R^j_e.

The rate equation of the ground state is

$$\begin{aligned}\frac{dN_{g,j}(z,T)}{dT}=&-\sum_{\substack{m\\(>0)}}\Gamma_mS_mg(z,T,\omega_m;cvgj)\\&-T^j_g(z,T)[N_{g,j}(z,T)-\tilde{\tilde{N}}_{g,j}(z,T)]\\&-R^j_g[N_{g,j}(z,T)-\tilde{N}_{g,j}(z,T)],\end{aligned} \tag{148}$$

where

$$g(z,T,\omega_m;cvgj)=D_gg(z,T,\omega_m;cv\mathbf{k}_gj), \tag{149}$$

$$\tilde{\tilde{N}}_{g,j}(z,T)=[N_{u,j}(z,T)\tau^{-1}_{u\to g,0}+N_{e,j}(z,T)\tau^{-1}_{e\to g,0}]T^j_g(z,T)^{-1}, \tag{150}$$

$$T^j_g(z,T)=T^j_{eg}(z,T)+T^j_{ug}(z,T), \tag{151}$$

$$T^j_{eg}(z,T)=\frac{N_{e,j}(z,T)}{2D_gN_DG_j}\tau^{-1}_{e\to g,0}+\left(1-\frac{N_{e,j}}{2D_eN_DG_j}\right)\tau^{-1}_{g\to e,0}, \tag{152}$$

$$T^j_{ug}(z,T)=\frac{N_{u,j}(z,T)}{2D_gN_DG_j}\tau^{-1}_{c\to g,0}+\left(1-\frac{N_{u,j}}{2D_uN_DG_j}\right)\tau^{-1}_{g\to u,0}, \tag{153}$$

and R^j_g is the carrier recombination rate in the excited state.

B. Nonlinear polarization due to carrier density pulsation in wetting layer

Under the model of carrier relaxation in this section, let us derive the contribution of the wetting layer to the nonlinear polarization due to carrier density pulsation, i.e., $\eta^{wet}(z,T,\omega_m)$ in Eq. (126). Using $\Delta N_{c,w}(\omega_{m'}-\omega_{m''})=\Delta N_{v,w}(\omega_{m'}-\omega_{m''})=\Delta N_w(\omega_{m'}-\omega_{m''})$ under the charge neutrality condition, Eq. (88) becomes

$$\begin{aligned}\chi^{wet}_\sigma(N_w,\omega_m=\omega_{m'}-\omega_{m''}+\omega_{m'''})&\\=\frac{\partial\chi^{pop}_\sigma(N_w,\omega_{m'''})}{\partial N_w}&[\Delta N_w(\omega_{m'}-\omega_{m''})\\&+\Delta N^*_w(\omega_{m''}-\omega_{m'})]E^{-1}_{m'}E^{*-1}_{m''}e^{-i(\mathbf{q}_{m'}-\mathbf{q}_{m''})\cdot\mathbf{r}},\end{aligned} \tag{154}$$

where

$$\begin{aligned}\Delta N_w(\omega_{m'}-\omega_{m''})=i\sum_{j=1}^{2M+1}&\frac{T_{wu}}{\omega_{m'}-\omega_{m''}+i(T_w+R_w)}\\&\times\Delta N_u(\omega_{m'}-\omega_{m''};j).\end{aligned} \tag{155}$$

Equation (155) comes from Eq. (133) when only the upper continuum state is taken into account with the beating amplitude of $\Delta N_u(\omega_{m'}-\omega_{m''};j)=2D_uN_DG_j\rho^{cdp}_{cc,\mathbf{k}_u}(\omega_{m'}-\omega_{m''};j)$. Since only the ground state is under light-induced beating, Eq. (135) with $i=g$, $l=u$, and s replaced by j and Eq. (77) with s replaced by j give

$$\Delta N_u(\omega_{m'}-\omega_{m''};j)=\frac{\varepsilon_0}{4\hbar}\frac{D_u N_D G_j \Sigma_{j'} A_{ug}(\omega_{m'}-\omega_{m''};jj')\chi_\sigma^{pop}(t,\omega_{m'};cv\mathbf{k}_g j')}{\omega_{m'}-\omega_{m''}+i(T_g^{j'}+R_g^{j'})}E_{m'}E_{m''}^* e^{i(\mathbf{q}_{m'}-\mathbf{q}_{m''})\cdot\mathbf{r}}, \tag{156}$$

where $A_{ug}(\omega_{m'}-\omega_{m''};jj')=A_{ug}^c(\omega_{m'}-\omega_{m''};jj')=A_{ug}^v(\omega_{m'}-\omega_{m''};jj')$.

By substituting Eqs. (155) and (156) to Eq. (154) and using Eqs. (A4) and (A9) in the Appendix, we obtain the susceptibility of Eq. (107) as

$$\eta^{wet}(z,T,\omega_m)=\sum_{\substack{m',m''m'''\\(m'\neq m''>0)}}\sum_{j=1}^{2M+1}\eta^{wet}(z,T,\omega_m;j)R_{m'}(z,T)R_{m''}^*(z,T)R_{m'''}(z,T)R_m^{-1}(z,T)e^{i(q_{m'}-q_{m''}+q_{m'''}-q_m)z}, \tag{157}$$

where

$$\eta^{wet}(z,T,\omega_m;j)=i\frac{\omega_m}{n_{\text{eff}}(\omega_m)c}N_D\Gamma_2\chi_\sigma^{wet}(N_w,\omega_m=\omega_{m'}-\omega_{m''}+\omega_{m'''};j)G_j, \tag{158}$$

$$\chi_\sigma^{wet}(N_w,\omega_m=\omega_{m'}-\omega_{m''}+\omega_{m'''};j)=-\frac{\varepsilon_0 n_{\text{eff}}(\omega_{m'''})cD_u A_{m'''}}{4\hbar\omega_{m'''}}\sum_{j'}Q(\omega_{m'},\omega_{m''};jj')[\chi_\sigma^{pop}(t,\omega_{m'};cv\mathbf{k}_g j')$$
$$-\chi_\sigma^{pop*}(t,\omega_{m''};cv\mathbf{k}_g j')], \tag{159}$$

$$Q(\omega_{m'},\omega_{m''};jj')=i\frac{(\alpha+i)T_{wu}}{[\omega_{m'}-\omega_{m''}+iT_w][\omega_{m'}-\omega_{m''}+i(T_g^{j'}+R_g^{j'})]}A_{ug}(\omega_{m'}-\omega_{m''};jj'), \tag{160}$$

and

$$\Gamma_2=\frac{\int_{act}|H(x,y)|^4dxdy}{\int_{act}|H(x,y)|^2dxdy}. \tag{161}$$

We assumed that N_w is constant in the cross section of the active region, which holds when the cross-sectional dimension of the wetting layer is smaller than the diffusion length of carriers. In Eq. (160), α is the alpha parameter in Eq. (A4), and $A_{m'''}$ is the differential gain of Eq. (A9).

IV. OPTICAL SIGNAL AMPLIFICATION AND SWITCHING

Based on the theory of light propagation in Sec. II and the model of carrier relaxation of Sec. III, we describe the operation of quantum-dot SOA's by presenting a set of equations for various operation schemes and by numerical simulation under random distribution approximation. We also simulate the operation of bulk SOA's for comparison, using the theory in the Appendix.

Parameters we used in the calculation are as follows. The active region has ten dot layers with the 1% optical confinement factor per one dot layer, i.e., $\Gamma_m=10\%$ in total. We suppose the columnar-shaped quantum dots with the radius of $R_D=10$ nm, the height of $L_D=5$ nm, and the volume of $V_D=\pi R_D^2 L_D$. The quantum dots are randomly distributed in the active region with the coverage of $\xi=N_D V_D$. We use the coverage of $\xi=6\%$ and $\xi=10\%$. The coverage of $\xi=10\%$ gives the area density of $N_D L_D=3.2\times10^{10}$ cm^{-2}. We assume the inhomogeneous broadening of the Gaussian shape with the full width at half maximum of $\hbar\Gamma_{inh}=20$ meV and $\hbar\Gamma_{inh}=40$ meV. We suppose the wetting layer or the layer covering dots with the thickness of 5 nm and with the density of states, D_w, of the 5 nm quantum well. We use the degeneracy of the ground state as $D_g=1$, the excited state as $D_e=3$ and the upper continuum state as $D_u=10$. We use the polarization relaxation time of $(\Gamma_g^j)^{-1}=130$ fs, which corresponds to the homogeneous broadening of the optical gain at the ground state of $2\hbar\Gamma_g^j=10$ meV. We use the carrier relaxation lifetime of $\tau_{e\to g,0}=\tau_{u\to g,0}=\tau_{u\to e,0}=3.4$ ps independent of the dot group, which gives the population relaxation time of $(T_g^j)^{-1}=260$ fs in Eq. (151) when the excited states and the upper continuum states are fully occupied by carriers. We use the carrier capture time of $\tau_{w\to u,0}=1$ ps, the emission time of $\tau_{u\to w,0}=10$ ps, and the carrier recombination lifetime of $R_w=R_u^j=R_e^j=R_g^j=0.4$ ns. In Eqs. (A13)–(A15), we assume the energy separation between the discrete states as $\Delta E_{eg}=70$ meV and $\Delta E_{ug}=150$ meV, which corresponds to the excited state energy and the third state energy. We consider the operation at room temperature of $T=295$ K. Note that the parameters used here suppose 1.3-micron InGaAs self-assembled dots on GaAs substrates (see Ref. 28 and discussion in Sec. III).

The propagation equation of the light pulse is described by Eqs. (96) and (104) as

$$\frac{\partial}{\partial z}R_m(z,T)=\frac{\Gamma_m}{2}[\eta^{pop}(z,T,\omega_m)+\eta^{dshb}(z,T,\omega_m)$$
$$+\eta^{cdp}(z,T,\omega_m)+\eta^{wet}(z,T,\omega_m)]R_m(z,T)$$
$$-\frac{\alpha_{loss}(\omega_m)}{2}R_m(z,T). \tag{162}$$

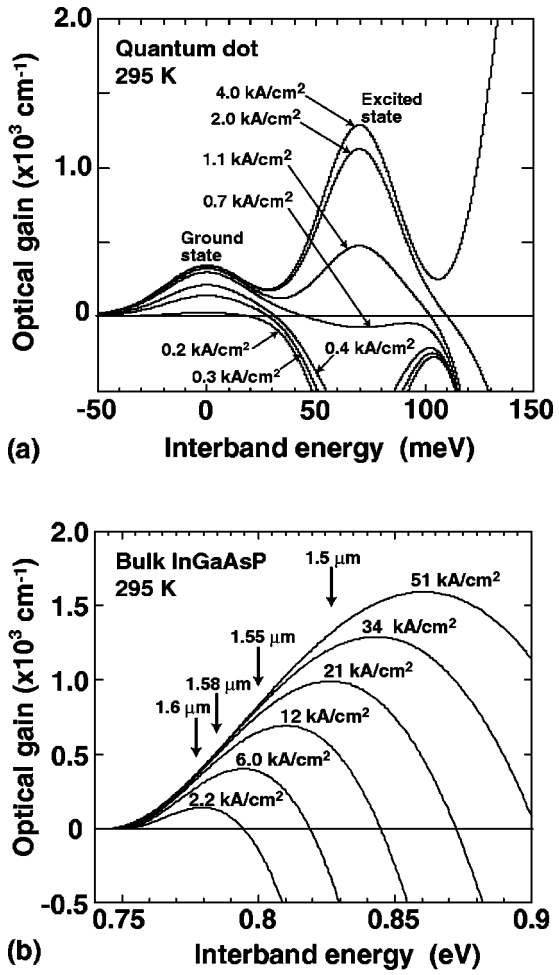

FIG. 5. (a) Calculated linear gain spectra of quantum dots, $g^{(1)}(\omega_m)$, as a function of $\hbar\omega_m-\hbar\omega^0_{cv,\mathbf{k}_g}$. (b) Calculated linear optical gain of bulk InGaAsP lattice matched to InP using the empirical gain formula in Appendix Sec. 3.

We can classify the operation of SOA's by whether it is under the single mode or multimodes.

A. Single-mode amplification

When there is only one light mode, the coherent terms in Eq. (162) vanish, resulting in the propagation equation of

$$\frac{\partial}{\partial z}R_m(z,T)=\frac{1}{2}[\Gamma_m\eta^{pop}(z,T,\omega_m)-\alpha_{loss}(\omega_m)]R_m(z,T). \tag{163}$$

The amplitude of $R_m(z,T)$ can be written as

$$R_m(z,T)=|R_m(z,T)|e^{i\phi_m(z,T)} \tag{164}$$

using the phase of $\phi_m(z,T)$. Substituting Eq. (164) into Eq. (163), we obtain the propagation equation of the photon flux density as

$$\frac{\partial}{\partial z}S_m(z,T)=[\Gamma_m g(z,T,\omega_m)-\alpha_{loss}(\omega_m)]S_m(z,T) \tag{165}$$

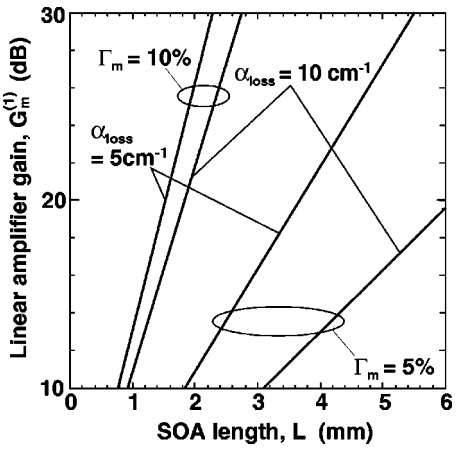

FIG. 6. Calculated maximum linear amplifier gain in the quantum-dot SOA at the ground state maximum of $\omega_m=\omega^0_{cv,\mathbf{k}_g}$ as a function of the length, L, when $g^{(1)}(\omega_m)=350\ \mathrm{cm}^{-1}$, $\alpha_{loss}(\omega_m)=5\ \mathrm{cm}^{-1}$ or $10\ \mathrm{cm}^{-1}$, and $\Gamma_m=5\%$ or 10%.

and that of the phase as

$$\frac{\partial}{\partial z}\phi_m(z,T)=\frac{\Gamma_m}{2}\xi(z,T,\omega_m). \tag{166}$$

The rate equations of carriers in Sec. III A with a single light mode, and Eqs. (163)–(166) give the amplified intensity and phase of the optical signal.

Figure 5 shows the linear gain spectra of (a) quantum dots calculated by Eqs. (123) and (140)–(153) with $S_m=0$ in Eq. (148), i.e., $g^{(1)}(\omega_m)$ as a function of $\hbar\omega_m-\hbar\omega^0_{cv,\mathbf{k}_g}$, and (b) bulk InGaAsP lattice matched to InP calculated by the empirical gain formula in Appendix Sec. 3 at various injection current densities. In quantum dots, we used $\xi=10\%$ and $\hbar\Gamma_{inh}=40$ meV. The bulk InGaAsP shows continuous gain spectra whose maximum goes toward higher energies as current increases. Quantum dots have discrete peaky gain spectra, where the ground-state gain reaches its maximum at low current densities of about 1–2 kA/cm^2. The maximum optical gain of $g^{(1)}(\omega_m)=350\ \mathrm{cm}^{-1}$ at the ground state agrees with real InGaAs/GaAs self-assembled dots.[39] The inhomogeneous broadening in conjunction with the low density of states due to the low dot density results in broader gain spectrum than in bulk semiconductors. For example, the gain spectrum width defined as the energy width to give more than -3 dB of the ground-state maximum is 121 meV at 2 kA/cm^2 in the quantum-dot SOA, while that in the bulk SOA defined as the -3 dB width of the maximum gain is only 25 meV at 2.2 kA/cm^2.

Figure 6 shows the maximum linear amplifier gain of

$$G^{(1)}_m=\exp\{L[\Gamma_m g^{(1)}(\omega_m)-\alpha_{loss}(\omega_m)]\} \tag{167}$$

in the quantum-dot SOA at the ground state maximum of $\omega_m=\omega^0_{cv,\mathbf{k}_g}$ as a function of the length, L, when $g^{(1)}(\omega_m)=350\ \mathrm{cm}^{-1}$, $\alpha_{loss}(\omega_m)=5\ \mathrm{cm}^{-1}$ or $10\ \mathrm{cm}^{-1}$, and $\Gamma_m=5\%$ or 10%. The length of the quantum-dot SOA needed to realize 10 to 20 dB linear amplifier gain ranges approximately between 1 and 6 mm, depending on the confinement

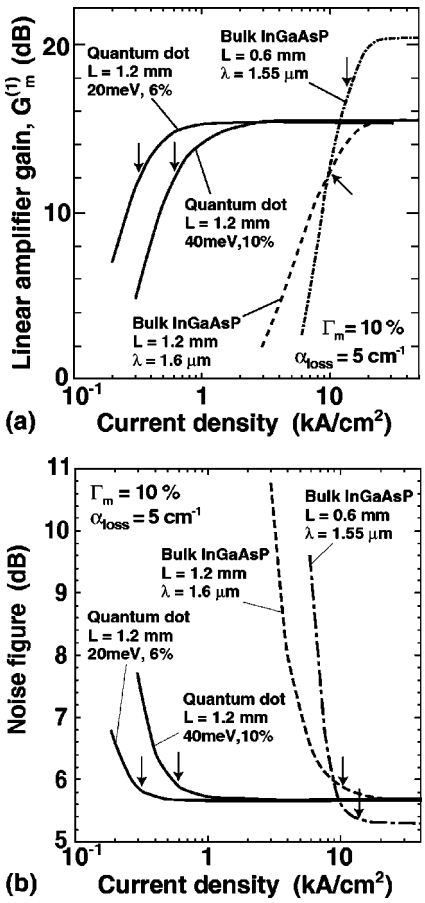

FIG. 7. (a) Calculated linear amplifier gain of $G_m^{(1)}$ as a function of the current density. The optical confinement factor is $\Gamma_m = 10\%$, and the internal loss is $\alpha_{loss}(\omega_m) = 5\ \mathrm{cm}^{-1}$ for both SOA's. (b) Calculated noise figure as a function of the current density. We assumed the input coupling coefficient of $\eta_{in} = -2$ dB.

factor and the loss. When $\Gamma_m = 10\%$, the length is 1.5–2 mm for 20 dB amplifier gain, and 2.3–2.7 mm for 30 dB.

Figure 7(a) shows the calculated linear amplifier gain of $G_m^{(1)}$ as a function of the current density. For quantum-dot SOA's, we used (i) $\hbar\Gamma_{inh} = 40$ meV and $\xi = 10\%$, and (ii) $\hbar\Gamma_{inh} = 20$ meV and $\xi = 6\%$. For the bulk SOA, we used the gain at $\lambda = 1.55\ \mu$m and $\lambda = 1.6\ \mu$m [see Fig. 5(b)]. The optical confinement factor is $\Gamma_m = 10\%$, and the internal loss is $\alpha_{loss} = 5\ \mathrm{cm}^{-1}$ for both SOA's. The amplifier gain of the quantum-dot SOA's appears even below 1 kA/cm^2, and reaches its maximum above 1 to 2 kA/cm^2. The bulk SOA's start to have the amplifier gain at about ten times larger current density than quantum dots, and need the current density of more than 20 kA/cm^2 for the maximum gain. The arrows represents -3 dB of the maximum amplifier gain.

Figure 7(b) shows the noise figure as a function of the current density calculated by Eq. (115). We assumed the input coupling coefficient of $\eta_{in} = -2$ dB. The noise figure decreases to reach its minimum value of 5 to 6 dB as the current density increases because the population inversion factor approaches one. The minimum value of the noise figure is determined by the 2 dB coupling loss and the internal loss. In order to achieve the minimum noise figure, we need current density to realize the maximum amplifier gain. From this point of view, the arrows for -3 dB amplifier gain is a measure of the lowest operation current density for low-noise operation in each SOA. We see that quantum-dot SOA's operate as low-noise amplifiers under current densities less than tenth of those of bulk SOA's.

Figure 8 shows the calculated continuous-wave amplifier gain of $G_m = S_m(L)/S_m(0)$ as a function of the output power of $S_m(L)$ in the quantum-dot SOA with $L = 1.2$ mm, $\hbar\Gamma_{inh} = 40$ meV, and $\xi = 10\%$ at the ground state maximum of $\omega_m = \omega_{cv,\mathbf{k}_g}^0$, and in the bulk InGaAsP SOA with $L = 0.6$ mm at the wavelength of 1.55 μm. We used Eqs. (123), (140)–(153), and (165). The current density is 24 kA/cm^2, the optical confinement factor is $\Gamma_m = 10\%$, and the internal loss is $\alpha_{loss} = 5\ \mathrm{cm}^{-1}$ for both SOA's. The linear optical gain is 15.5 dB in the quantum-dot SOA and 20.3 dB in the bulk InGaAsP SOA. As the output power increases, the amplifier gain starts to decrease, which is called gain saturation. The numbers next to the closed and open circles on the gain vs output power curve represents the magnitude of gain saturation. We define the output power at the 3 dB gain saturation as the 3 dB saturation power, $P_{sat}^{3\,\mathrm{dB}}$, which is shown by an arrow for each SOA.

Figure 8(b) shows the eye diagram of the 40 Gb/s non-return-to-zero (NRZ) 124-bit random-pattern input and those of the output from the quantum-dot SOA at the operation points marked by solid circles in Fig. 8(a). Note that, as the gain saturation increases from -0.4 dB to -4.1 dB, the crossing points rise. Even under a gain saturation as large as 2.2 dB, there is no fluctuation of the mark level. The mark level fluctuation, which is called the pattern effect, starts to appear at the saturation of -4.1 dB. This is in striking contrast to the case of the bulk InGaAsP SOA's, where the mark level starts to fluctuate even at -0.5 dB and splits into many traces due to the pattern effect as seen in Fig. 8(c). Let us define the pattern-effect saturation power, P_{sat}^{p}, where the fluctuation of the mark level exceeds the 10% of the continuous-wave output power. The pattern-effect-free amplification in the quantum-dot SOA under gain saturation occurs because the gain saturation is dominated by the incoherent spectral hole burning as seen in Fig. 8(d) and the spectral hole is repeatedly compensated by the carriers relaxing from the excited state.[6] The pattern effect appears as the carriers are lost in the excited and the upper continuum states that work as carrier reservoirs. The maximum response time of this process is the population relaxation time of $(T_g^j)^{-1} = 260$ fs with the excited and the upper continuum states are fully occupied. This response time is less than tenth of the 6.25-ps bit interval of the 160 Gb/s pulse trains, and is fast enough for their amplification and processing even at this high bit rate.

Figure 9 shows the saturation power of $P_{sat}^{3\,\mathrm{dB}}$ and P_{sat}^{p} as a function of the current density for the four cases in Fig. 7. The plots are shown above the current density indicated by the arrow (-3 dB gain) in Fig. 7. The saturation power increases in every case as the current density increases. In bulk SOA's, the saturation power increases as we go from $\lambda = 1.55\ \mu$m to $\lambda = 1.6\ \mu$m due to the decrease in the differ-

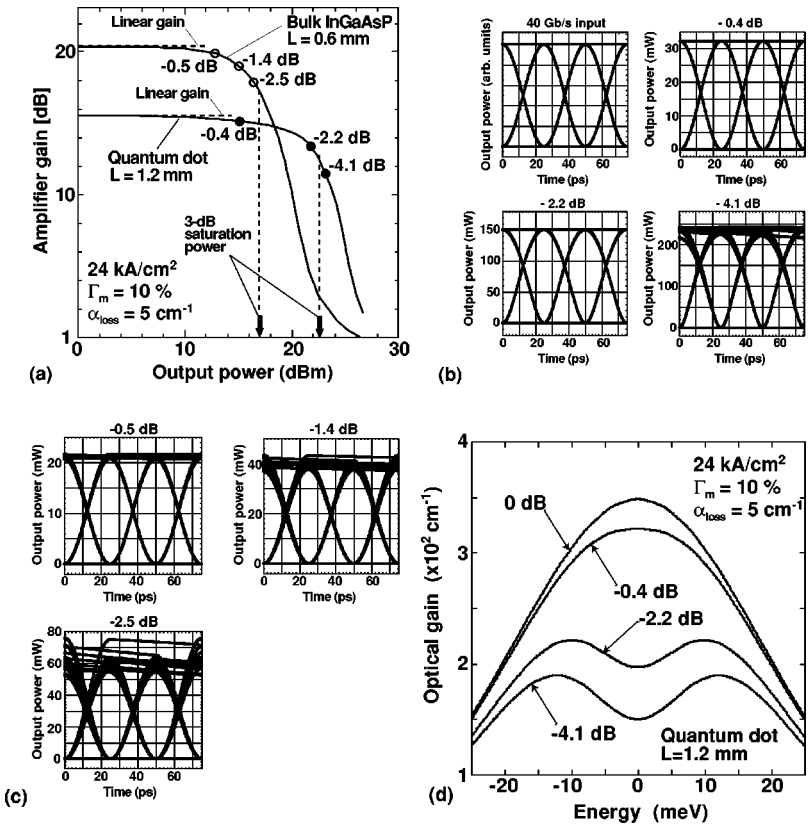

FIG. 8. (a) Calculated continuous-wave amplifier gain of G_m as a function of the output power in the quantum-dot SOA with $L=1.2$ mm, $\hbar\Gamma_{inh}=40$ meV, and $\xi=10\%$ at the ground state maximum of $\omega_m=\omega^0_{cv,\mathbf{k}_g}$, and in the bulk InGaAsP SOA with $L=0.6$ mm at the wavelength of 1.55 μm. (b) Eye diagram of the 40 Gb/s NRZ 128-bit random-pattern input and those of the output from the quantum-dot SOA at the operation points marked by solid circles in Fig. 8. (c) Eye diagram of the 40 Gb/s NRZ 128-bit random-pattern input and those of the output from the bulk InGaAsP SOA's. (d) Optical gain spectrum of the quantum-dot SOA.

ential gain, which is realized at the expense of the amplifier gain and/or the length [see Eq. (A37)]. The quantum-dot SOA's, having the same amplifier gain and length as the bulk SOA at $\lambda=1.6$ μm, have the improved saturation power vs current density curve, i.e., larger saturation power and lower operation current density than the bulk SOA. This is partly due to discrete quantized energy states, and partly due to the volume effect, i.e., the smaller crystal volume of the quantum-dot ensemble than bulk: The quantization causes larger optical gain than bulk at lower carrier density, and the combination of the volume effect and the quantization enables deeper Fermi level than bulk, leading to lower differential gain at a given current density, and thus, higher saturation power.

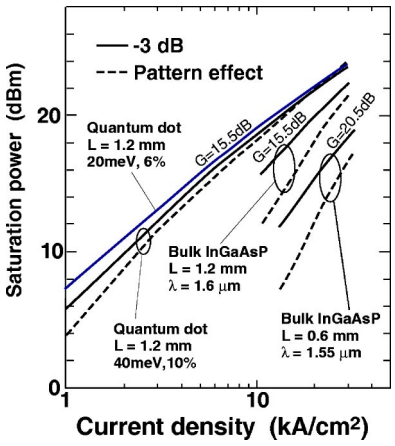

FIG. 9. Saturation power of $P^{3\,\mathrm{dB}}_{sat}$ (3 dB) and P^{p}_{sat} (pattern effect) as a function of the current density for the four cases in Fig. 7. The plots are shown above the current density indicated by the arrow (-3 dB gain) in Fig. 7.

From the practical point of view, quantum-dot SOA's have two attractive operation modes as seen in Fig. 9; one is low power consumption operation, for example, with the low noise of NF<6 dB, $P^{3\,\mathrm{dB}}_{sat}$, $P^{pat}_{sat}\geqslant 10$ dBm, $G=15$ dB at the current density of 3 kA/cm^2. The other is the operation under high saturation power, for example, of 23 dBm at 30 kA/cm^2, with broad gain bandwidth. The saturation power can be further increased by reducing the layer number and/or the dot area coverage at the expense of the amplifier gain or the length. See Eq. (A36) for simple understanding. In addition, we can expect the quantum dot SOA is less sensitive to temperature than the bulk SOA due to discrete energy states and lower carrier density under operation, which is good for coolerless applications.

B. Multimode operation: multimode amplification, cross-gain and cross-phase modulation, and four-wave mixing

The multimode operation can be further classified by the frequency separation between each mode. When the mode separation is sufficiently larger than the polarization relaxation rate ($|\omega_{m'}-\omega_{m''}|\gg\Gamma^j_g$), we can neglect the coherent terms in Eq. (162), leading to multimode amplification. When the mode separation is comparable to or less than the polarization relaxation rate ($|\omega_{m'}-\omega_{m''}|\leqslant\Gamma^j_g$), the coherent terms cause intermode interaction like cross-gain and cross-phase modulation and four-wave mixing.

1. Multimode amplification ($|\omega_{m'}-\omega_{m''}| \gg \Gamma_g^j$)

The propagation of each optical mode is described by Eqs. (163)–(166) in conjunction with the rate equations of carriers in Sec. III A. As the optical power increases, gain saturation occurs due to the incoherent spectral hole burning caused by the stimulated emission. The incoherent spectral hole burning due to each optical mode occurs in different dot groups, resulting in negligible cross talk between different modes.[6]

Using the high-saturation power characteristics as well as the broad gain bandwidth characteristics of quantum-dot SOA's discussed in Sec. IV A, we proposed and designed an ultrabroadband multimode amplifier, which enables low-noise amplification of up to 8 channels over the entire wavelength range of 1.3–1.6 micron with the 40 nm channel interval.[40] We proposed adopting the multisection electrode to realize nonuniform current injection in order to suppress gain saturation due to amplified spontaneous emission and reduce the gain difference among the discrete bound states. By simulation, we demonstrated the amplification of 40 Gb/s non-return-to zero (NRZ) 8-channel signals with negligible cross talk. This device is highly suitable in the course wavelength division multiplexing networks.

2. Intermode interaction ($|\omega_{m'}-\omega_{m''}| \leqslant \Gamma_g^j$)

Let us consider the case where we input the strong pump pulse with the frequency of ω_p and the signal pulse with the frequency of ω_s into the quantum-dot SOA. The beating between the pump and the signal causes coherent nonlinear polarization via the four different processes as $\omega_s=\omega_s-\omega_p+\omega_p$, $\omega_p=\omega_p-\omega_s+\omega_s$, $\omega_f=\omega_p-\omega_s+\omega_p$, and $\omega_f=\omega_s-\omega_p+\omega_s$. The combination of $\omega_s=\omega_s-\omega_p+\omega_p$ and $\omega_p=\omega_p-\omega_s+\omega_s$ causes cross-gain modulation and cross-phase modulation, and the combination of $\omega_f=\omega_p-\omega_s+\omega_p$ and $\omega_f=\omega_s-\omega_p+\omega_s$ causes four-wave mixing. These processes occur simultaneously.

From Eq. (162), the propagation equation of the pump is approximately given by

$$\frac{\partial R_p(z,T)}{\partial z}=\frac{1}{2}[\Gamma_p \eta^{pop}(z,T,\omega_p)-\alpha_{loss}(\omega_p)]R_p(z,T), \tag{168}$$

where the term under the combination of $\omega_p=\omega_p-\omega_s+\omega_s$ is neglected due to the strong pump pulse intensity.

(a) Cross-gain and cross-phase modulation ($\omega_s=\omega_s-\omega_p+\omega_p$). When the pump beam with a frequency of ω_p conveys a bit pattern, the intensity and the phase of the continuous-wave signal with a frequency of ω_s is modulated according to the bit pattern, each of which is called cross-gain and cross-phase modulation. We suppose that only the ground state has the dynamic spectral hole burning term.

Using Eqs. (119)–(122), (126)–(131), (157)–(61), and (162), the propagation equation of the ω_s mode is

$$\frac{\partial}{\partial z}R_s(z,T)=i\frac{\omega_s\Gamma_s}{2n_{\text{eff}}(\omega_s)c}\sum_{j=1}^{2M+1}\Omega(z,T,\omega_s;j)G_jR_s(z,T) - \frac{\alpha_{loss}(\omega_s)}{2}R_s(z,T), \tag{169}$$

where

$$\begin{aligned}\Omega(z,T,\omega_s;j) &= N_D(z)\sum_{l=g,e,c}D_l\chi_\sigma^{pop}(z,T,\omega_s;cvlj)+N_D^{coh}(z)\\ &\times\Bigg[D_g\chi_\sigma^{dshb}(z,T,\omega_s=\omega_s-\omega_p+\omega_p;cvgj)\\ &+\sum_{l=g,e,c}D_l\chi_\sigma^{cdp}(z,T,\omega_s=\omega_s-\omega_p+\omega_p;cvlj)\\ &+\chi_\sigma^{wet}(N_w,\omega_s=\omega_s-\omega_p+\omega_p;j)\Bigg]|R_p(z,T)|^2\end{aligned} \tag{170}$$

using $N_D^{coh}(z)\cong\Gamma_2 N_D(z)$.

From Eq. (169), the propagation equation of the photon flux density of the ω_s mode is given as (when $\sigma=\sigma'$)

$$\begin{aligned}\frac{\partial S_s(z,T)}{\partial z} &= \Gamma_s\sum_{j=1}^{2M+1}g_\sigma(z,T,\omega_s;cvgj)[1-\varepsilon_l(\omega_s,\omega_p,\omega_q\\ &=\omega_s;j)\Gamma_p S_p(z,T)]S_s(z,T)-\alpha_{loss}(\omega_s)S_s(z,T),\end{aligned} \tag{171}$$

where

$$\begin{aligned}\varepsilon_l(\omega_s,\omega_p,\omega_q=\omega_s;j) &= -\beta^j(\omega_p)A_{p,j}\Bigg\{\frac{\Gamma_g^j\{(\omega_q-\omega_{cv,\mathbf{k}_g}^j)(\omega_s-\omega_p)-\Gamma_g^jT_g^j\}}{[(\omega_q-\omega_{cv,\mathbf{k}_g}^j)^2+\Gamma_g^{j^2}][(\omega_s-\omega_p)^2+T_g^{j^2}]}\Bigg|_{\omega_q=\omega_s}\\ &-\sum_{j'}\sum_{l=g,e,u}\varsigma(\omega_s;jj')\frac{D_l}{D_g}\frac{\alpha_l(\omega_s,\omega_p,\omega_q=\omega_s;jj')(\omega_s-\omega_p)+T_g^j\gamma_l(\omega_s,\omega_p,\omega_q=\omega_s;jj')}{(\omega_s-\omega_p)^2+T_g^{j'^2}}\Bigg\}\\ &+D_uA_p\sum_{j'}\varsigma(\omega_s;jj')\mathrm{Re}\,Q(\omega_s,\omega_p;jj'),\end{aligned} \tag{172}$$

$$A_{p,j}=\frac{\omega_p C_p}{n_{\rm eff}(\omega_p)c\Gamma_g^j\beta^j(\omega_p)}, \tag{173}$$

is the differential gain at ω_p by the jth group [see Eqs. (124) and (125)],

$$C_m=\frac{2e^2|P_{cv}^{\sigma}|^2}{\varepsilon_0\hbar m_0^2\omega_m\omega_{cv,\mathbf{k}_g}^j}, \tag{174}$$

$$\alpha_l(\omega_s,\omega_p,\omega_q;jj')=-\frac{\Gamma_g^j[\Gamma_l^j\,{\rm Im}\,A_{lg}(\omega_s-\omega_p;jj')+(\omega_q-\omega_{cv,\mathbf{k}_l}^j){\rm Re}\,A_{lg}(\omega_s-\omega_p;jj')]}{(\omega_q-\omega_{cv,\mathbf{k}_l}^j)^2+\Gamma_l^{j^2}}, \tag{175}$$

$$\beta^j(\omega_p)=\left[\frac{\Gamma_{cv,g}^{j^2}}{(\omega_p-\omega_{cv,\mathbf{k}_g}^j)^2+\Gamma_{cv,g}^{j^2}}\right]^{-1}, \tag{176}$$

$$\gamma_l(\omega_s,\omega_p,\omega_q;jj')=-\frac{\Gamma_g^j[(\omega_q-\omega_{cv,\mathbf{k}_l}^j){\rm Im}\,A_{lg}(\omega_s-\omega_p;jj')-\Gamma_l^j\,{\rm Re}\,A_{lg}(\omega_s-\omega_p;jj')]}{(\omega_q-\omega_{cv,\mathbf{k}_l}^j)^2+\Gamma_l^{j^2}}, \tag{177}$$

and

$$\varsigma(\omega_s;jj')=\frac{{\rm Im}\,\chi_{\sigma}^{pop}(z,T,\omega_s;cvgj')}{{\rm Im}\,\chi_{\sigma}^{pop}(z,T,\omega_s;cvgj)}. \tag{178}$$

Here, we used $\chi_{\sigma}^{pop}(z,T,\omega_s;cvgj)-\chi_{\sigma}^{pop}(z,T,\omega_p;cvgj)^*\cong 2\,{\rm Im}\,\chi_{\sigma}^{pop}(z,T,\omega_s;cvgj)$, $\omega_{cv,\mathbf{k}_g}^j\cong\omega_{cv,\mathbf{k}_l}^j$, $T_g^j\gg R_g^j$, $|P_{cv,\mathbf{k}_g}^{\sigma}|^2\cong|P_{cv,\mathbf{k}_l}^{\sigma}|^2\equiv|P_{cv}^{\sigma}|^2$, and

$$\Gamma_p=N_D^{coh}(z)D/N_D(z)\textstyle\int_{cav}|H(x,y)|^2dxdy.$$

The first term of the right-hand side of Eq. (172) is due to the imaginary part of χ_{σ}^{dshb}, the second term is that of χ_{σ}^{cdp}, and the third term is that of χ_{σ}^{wet}. We neglected that the contribution of the excited states to the optical gain.

As the first order approximation of the successive solution of $A_{lg}(\omega_s-\omega_p;jj')$ from Eq. (132), we take

$$A_{lg}(\omega_s-\omega_p;jj)\cong i\frac{T_{lg}^j}{\omega_s-\omega_p+i(T_l^j+R_l^j)}\frac{D_g}{D_e+D_u} \tag{179}$$

for $l=e,u$, and other terms as zero. This means that we neglect the interdot interaction via the wetting layer within the population beating period, and the kickback to the population beating at the ground state from the upper states.

We can calculate the optical pulse propagation under the cross gain modulation by the rate equations of carriers [Eqs. (140)–(153)] with $m=s,p$, and Eqs. (168) and (169). The cross-gain modulation enables wavelength conversion from ω_p to ω_s with the bit pattern inverted.

Figure 10(a) shows the calculated continuous-wave amplifier gain at the frequency of ω_s (probe) and ω_p (pump) as a function of the input pump power, $P_p(0)=\hbar\omega_p DS_p(0)$, in the quantum-dot SOA with $L=1.2$ mm, $\hbar\Gamma_{inh}=40$ meV, and $\xi=10\%$. The pump is at the ground-state gain maximum of $\omega_p=\omega_{cv,\mathbf{k}_g}^0$ and the detuning of $\Delta\omega/2\pi=(\omega_p-\omega_s)/2\pi$ is 500 GHz. The current density is 24 kA/cm^2, the optical confinement factor is $\Gamma_m=10\%$, and the internal loss is $\alpha_{loss}=5\ {\rm cm}^{-1}$. The amplifier gain of the probe decreases as the pump power increases, which is the cross gain modulation.

Figure 10(b) shows the linear, incoherent, and total optical gain spectrum at the exit of the SOA when $P_p(0)=10$ dBm. We see the dimple in the gain spectrum denoted by incoherent gain which comes from $g_{\sigma}(z,T,\omega_s;cvgj)$. The "total" gain spectrum includes the gain saturation which comes from $\varepsilon_l(\omega_s,\omega_p,\omega_q=\omega_s;j)$ in Eq. (171). The saturated optical gain is almost symmetric due to dominant spectral hole burning, and negligible contribution of the carrier density pulsation, which is in contrast to the bulk SOA in Fig. 14(a).

Figure 10(c) shows eye diagrams of the output pump beam and the amplifier gain of the probe beam when the input pump is the NRZ random pattern at a bit rate of 40

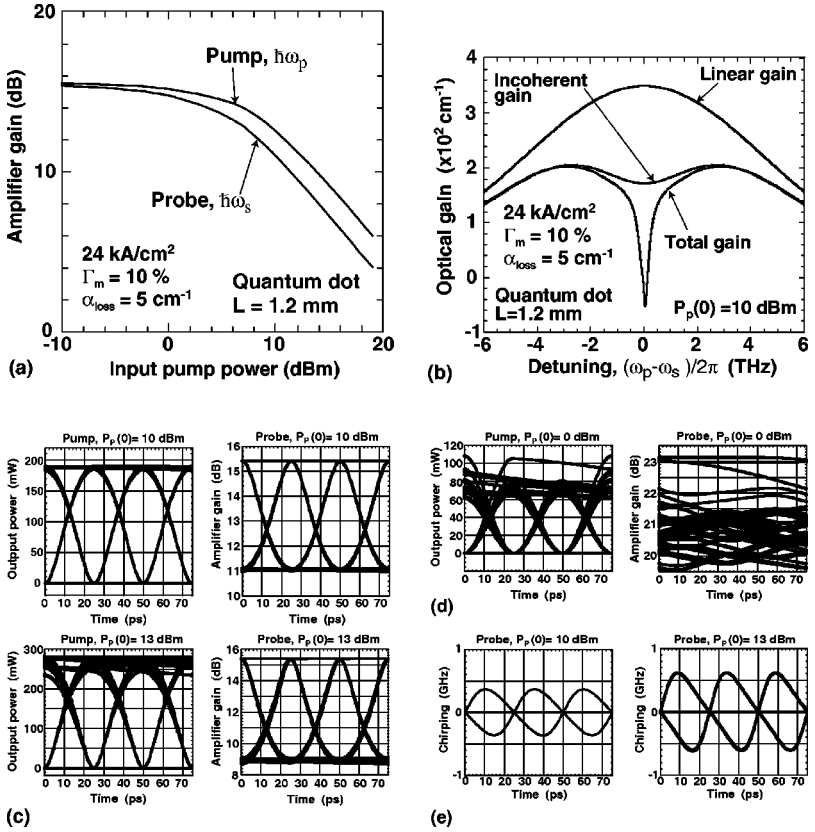

FIG. 10. (a) Calculated continuous-wave amplifier gain at the frequency of ω_s (probe) and ω_p (pump) as a function of the input pump power, $P_p(0)$, in the quantum-dot SOA with $L=1.2$ mm, $\hbar\Gamma_{inh}=40$ meV, and $\xi=10\%$. The pump is at the ground-state gain maximum of $\omega_p=\omega^0_{cv,\mathbf{k}_q}$ and the detuning of $\Delta\omega/2\pi=(\omega_p-\omega_s)/2\pi$ is 500 GHz. (b) Linear, incoherent, and total optical gain spectrum at the exit of the SOA when $P_p(0)=10$ dBm. (c) Eye diagrams of the output pump beam and the amplifier gain of the probe beam when the input pump is the NRZ random pattern at a bit rate of 40 Gb/s and the input probe is weak continuous wave. The input pump power is $P_p(0)=10$ dBm and 13 dBm. The input wave form is the same as Fig. 8(b). (d) The same calculation at 40 Gb/s in the bulk InGaAsP SOA with $L=0.6$ mm at the wavelength of 1.55 μm as (c). The input pump power is $P_p(0)=0$ dBm. (e) Calculated frequency chirping of the probe output from the quantum-dot SOA when the SOA is under the cross-gain modulation at 40 Gb/s with $P_p(0)=10$ dBm and 13 dBm shown in (b).

Gb/s and the input probe is weak continuous wave. The input pump power is 10 and 13 dBm. The input wave form is the same as Fig. 8(b). We see clear eye opening with the extinction ratio of 4.4 dB at $P_p(0)=10$ dBm and 6.6 dB at $P_p(0)=13$ dBm. The high-speed response is due to the high-speed repeated response of the incoherent spectral hole burning.

Figure 10(d) shows the same calculation at 40 Gb/s in the bulk InGaAsP SOA with $L=0.6$ mm at the wavelength of 1.55 μm as Fig. 10(c). The input pump power is 0 dBm. The slow response of gain saturation dominated by the carrier recombination lifetime in Eq. (A23) results in the pattern effect in the pump, and the undetectable signal in the probe beam. The response is 2.5 Gb/s at most [see Fig. 15(b)].

To summarize the cross-gain modulation, the 40 Gb/s response is possible due to the gain saturation under the incoherent and dynamic spectral hole burning by numerical calculation. The upper speed limit is 160 Gb/s or above owing to the intraband relaxation rate of 260 fs (as discussed in Sec. III, the intraband relaxation rate is 100 to 300 fs in self-assembled dots with optical gain). The extinction ratio of 6.6 dB in the present calculation at $P_p(0)=13$ dBm and 24 kA/cm^2 can be further increased above 10 dB without pattern effect using the SOA's with decreased optical confinement factor or dot area density and with longer cavity length.

From Eq. (169), the propagation equation of the phase of the mode ω_s is given as (when $\sigma'=\sigma$)

$$\frac{\partial}{\partial z}\phi_s(z,T)=-\frac{\Gamma_s}{2}\sum_{j=1}^{2M+1} D_g g_\sigma(z,T,\omega_s;cvgj)[\alpha_g^j(\omega_s)+\varepsilon_R(\omega_s,\omega_p,\omega_q=\omega_s;j)\Gamma_p S_p(z,T)]$$
$$-\frac{\Gamma_s}{2}\sum_{l=e,u}\sum_{j=1}^{2M+1} D_l g_\sigma(z,T,\omega_s;cvlj)\alpha_l^j(\omega_s), \tag{180}$$

where

$$\alpha_l^j(\omega_s)=\frac{\omega^j_{cv,\mathbf{k}_l}-\omega_s}{\Gamma_{cv,l}} \tag{181}$$

and

$$\varepsilon_R(\omega_s,\omega_p,\omega_q=\omega_s;j)=\beta^j(\omega_p)A_{p,j}\left\{\left.\frac{\Gamma_g^j[\Gamma_g^j(\omega_s-\omega_p)+T_g^j(\omega_q-\omega_{cv,\mathbf{k}_g}^j)]}{[(\omega_q-\omega_{cv,\mathbf{k}_g}^j)^2+\Gamma_g^{j^2}][(\omega_s-\omega_p)^2+T_g^{j^2}]}\right|_{\omega_q=\omega_s}\right.$$

$$\left.+\sum_{j'}\sum_{l=g,e,u}\varsigma(\omega_s;jj')\frac{D_l}{D_g}\frac{(\omega_s-\omega_p)\gamma_l(\omega_s,\omega_p,\omega_q=\omega_s;jj')-T_g^j\alpha_l(\omega_s,\omega_p,\omega_q=\omega_s;jj')}{(\omega_s-\omega_p)^2+(T_g^j)^2}\right\}$$

$$+D_uA_p\sum_{j'}\varsigma(\omega_s;jj')\mathrm{Im}\,Q(\omega_s,\omega_p;jj'). \tag{182}$$

The first term of the right-hand side of Eq. (182) is due to the real part of χ_σ^{dshb}, the second term is that of χ_σ^{cdp}, and the third term is that of χ_σ^{wet}.

We can calculate the phase of the signal under the cross phase modulation by the rate equations of carriers [Eqs. (140)–(153)] with $m=s,p$, and Eqs. (168) and (180).

Figure 10(e) shows the calculated frequency chirping of the probe output from the quantum-dot SOA when the SOA is under the cross-gain modulation at 40 Gb/s with $P_{in}(0)=10$ dBm and 13 dBm shown in Fig. 10(b). The chirping is given by

$$\Delta f_s=-\frac{1}{2\pi}\frac{\partial\phi_s(L,T)}{\partial T}, \tag{183}$$

where $\phi_s(L,T)$ is the phase at the exit. We see that the frequency chirping is less than 0.4 GHz at $P_{in}(0)=10$ dBm and 0.7 GHz at $P_{in}(0)=13$ Bm during the cross-gain modulation, which are only 1–2% of the signal bandwidth of about 40 GHz or more. This small chirping is partly because the contribution of the dots with $\omega_{cv,\mathbf{k}_g}^j>\omega_s$ and the dots with $\omega_{cv,\mathbf{k}_g}^j<\omega_s$ almost cancels out when $\omega_s\cong\omega_{cv,\mathbf{k}_g}^0$ due to the symmetric ground-state gain spectrum, and partly because the contribution of the excited and the upper continuum states is negligible due to their energy separation from the ground state.

(b) Four-wave mixing ($\omega_f=\omega_p-\omega_s+\omega_p$ and $\omega_{f'}=\omega_s-\omega_p+\omega_s$). Using Eqs. (119)–(122), (126)–(131), (157)–(161), and (162), the propagation equation of the ω_f mode is

$$\frac{\partial}{\partial z}R_f(z,T)=i\frac{\omega_f\Gamma_f}{2n_{\mathrm{eff}}(\omega_f)c}\sum_{j=1}^{2M+1}\Omega(z,T,\omega_f;j)G_jR_f(z,T)-\frac{\alpha_{loss}(\omega_c)}{2}R_f(z,T), \tag{184}$$

where

$$\Omega(z,T,\omega_f;j)=N_D(z)D_g\chi_\sigma^{pop}(z,T,\omega_f;cvgj)+N_D^{coh}(z)\left[D_g\chi_\sigma^{dshb}(z,T,\omega_f=\omega_p-\omega_s+\omega_p;cvgj)+\sum_{l=g,e,c}D_l\chi_\sigma^{cdp}(z,T,\omega_f=\omega_p\right.$$

$$\left.-\omega_s+\omega_p;cvlj)+\chi_\sigma^{wet}(N_w,\omega_f=\omega_p-\omega_s+\omega_p;j)\right]R_p^2(z,T)R_s^*(z,T)R_f^{-1}(z,T)e^{i(2q_p-q_s-q_f)z}. \tag{185}$$

From Eqs. (184) and (185), we obtain

$$\frac{\partial}{\partial z}R_f(z,T)=i\frac{\omega_f\Gamma_f}{2n_{\mathrm{eff}}(\omega_f)c}\sum_{j=1}^{2M+1}N_D(z)D_g\chi_\sigma^{pop}k(z,T,\omega_f;cvgj)G_jR_f(z,T)+\frac{\Gamma_f}{2}\Theta(\omega_p,\omega_s)R_p^2(z,T)R_s^*(z,T)e^{i(2q_p-q_s-q_f)z}$$

$$\cong\frac{\Gamma_f}{2}\sum_{j=1}^{2M+1}g_\sigma(z,T,\omega_f;cvgj)R_f(z,T)+\frac{\Gamma_f}{2}\Theta(\omega_p,\omega_s)R_p^2(z,T)R_s^*(z,T)e^{i(2q_p-q_s-q_f)z}, \tag{186}$$

where

$$\Theta(\omega_p,\omega_s)=-\frac{\varepsilon_0n_{\mathrm{eff}}(\omega_p)c}{2\hbar\omega_p}\Gamma_2\sum_{j=1}^{2M+1}W_j(\omega_p,\omega_s;j)gk(z,T,\omega_p;cvgj) \tag{187}$$

and

$$W_j(\omega_p,\omega_s;j)=\varepsilon_l(\omega_p,\omega_s,\omega_q=\omega_f;j)+\varepsilon_R(\omega_p,\omega_s,\omega_q=\omega_f;j). \tag{188}$$

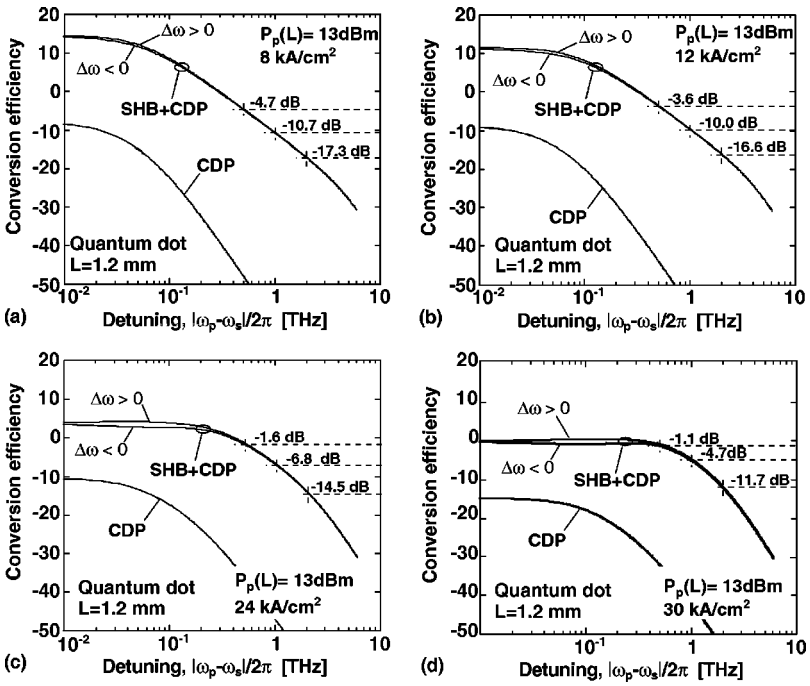

FIG. 11. Calculation of conversion efficiency, $\eta_{con}(\omega_p,\omega_s)$, as a function of the absolute value of detuning, $\Delta\omega/2\pi=(\omega_p-\omega_s)/2\pi$, in the quantum-dot SOA under different current density. The pump is at the top of the ground state gain, i.e., $\omega_p=\omega^0_{cv,\mathbf{k}_g}$, with the power of $P_p(L)=13$ dBm. We used the same parameters as Fig. 10 in calculating $W_f(\omega_p,\omega_s;j)$ and $g(\omega_p;cvgj)$, and the amplifier gain of $G_f=15.5$ dB independent of the current density since the SOA is almost in the linear region above 8 kA/cm^2.

The amplified intensity and phase of $R_f(z,T)$ can be calculated by the rate equations of carriers [Eqs. (140)–(153)] with $m=p,s,c$, and Eqs. (168), (169), and (186).

Instead of solving Eq. (186) by numerical calculations, we present here an approximate analytical solution for semiquantitative understanding of the conversion efficiency, the signal-to-background ratio (SBR$_f$), the signal-to-noise ratio (SNR$_f$) and the noise figure (NF$_f$) of the wavelength conversion by four-wave mixing. We suppose the condition of the continuous wave operation, a constant gain over the cavity, and the complete phase matching condition of $q_f=2q_p-q_s$. We use the signal amplitude of $R_s(L)$ at the exit and the pump amplitude of $R_p(L)$ at the exit in the second term of the right-hand side of Eq. (186). Then, by integrating Eq. (186) over the waveguide, we obtain the conversion efficiency of

$$\eta_{con}(\omega_p,\omega_s)=\frac{S_f(L)}{S_s(0)}\cong\Gamma_p^2G_f^2\left|\sum_{j=1}^{2M+1}W_j(\omega_p,\omega_s;j)\times g(\omega_p;cvgj)/g(\omega_p)\right|^2 S_p(L)^2, \quad (189)$$

where we use $g(\omega_p)$ and $g(\omega_p;cvgj)$ in Eq. (123) at the exit of the SOA under $S_p(L)$, and G_f is the amplifier gain. Using Eq. (109) with $S_{sp}(0,T,\omega_c)=0$, the SBR$_f$ of the converted signal with the ASE background is given as

$$\mathrm{SBR}_f=\frac{S_f(L)}{S_{sp}(L,\omega_f)}=\frac{\eta_{con}(\omega_p,\omega_s)S_s(0)}{[G_f-1]n_{sp}(\omega_f)S_{vac}(\omega_f)}. \quad (190)$$

The SNR$_f$ of the converted signal against the shot noise and the beating noise with the amplified spontaneous emission is given as

$$\mathrm{SNR}_f=\frac{\eta_{in}\eta_{out}DS_f(L)}{2\Delta v\left[1+\frac{4\pi\eta_{out}}{\Delta\omega_{sp}}DS_{sp}(L,\omega_f)\right]}. \quad (191)$$

The noise figure defined as the ratio of SNR$_{in}$ of Eq. (129) with $m=s$ and $S_{sp}(0,T,\omega_s)=0$ and SNR$_f$ of Eq. (191) is given as

$$\mathrm{NF}_f=\frac{1+2\eta_{out}[G_f-1]n_{sp}(\omega_f)}{\eta_{in}\eta_{out}\eta_{con}(\omega_p,\omega_s)}. \quad (192)$$

Equations (190) to (192) show that the high conversion efficiency is a key to high signal quality.

Figure 11(a) shows the calculation of $\eta_{con}(\omega_p,\omega_s)$ as a function of the absolute value of detuning, $\Delta\omega/2\pi=(\omega_p-\omega_s)/2\pi$, in the quantum-dot SOA under different current density. The pump is at the top of the ground state gain, i.e., $\omega_p=\omega^0_{cv,\mathbf{k}_g}$, with the power of $P_p(L)=13$ dBm. We used the same parameters as Fig. 10 in calculating $W_j(\omega_p,\omega_s;j)$ and $g(\omega_p;cvgj)$, and the amplifier gain of $G_f=15.5$ dB independent of the current density since the SOA is almost in the linear region above 8 kA/cm^2. We see that the total conversion efficiency is almost symmetric, i.e., independent of the conversion direction, which is a striking contrast to the bulk SOA [Fig. 17(a)]. This is because the coherent nonlinearity is dominated not by the carrier density pulsation but by the dynamic spectral hole burning, which is partly due to slower population and polarization relaxation than bulk semiconductors and partly due to the separated excited, upper and the wetting layer states from the ground state. The latter effect leads to small alpha parameter discussed in the Appendix.

As the current density increases from (a) to (d), the conversion bandwidth increases due to the increased relaxation rate of T_g^j, since the carriers occupy the excited and the

upper continuum states [see Eq. (151)]. As a result, the conversion efficiency at 0.5 to 2 THz, which corresponds to 8 to 32 nm wavelength dispersion in the 1.55 μm wavelength range for the optical transmission system, increases as the current density increases. For example, the conversion efficiency at 30 kA/cm^2 is -1.1 dB for 0.5 THz (8 nm conversion), -4.7 dB for 1 THz (16 nm conversion), and -11.7 dB for 2 THz (32 nm conversion). When $\Delta f_{sp}=100$ GHz ($\Delta\omega_{sp}=2\pi\Delta f_{sp}$), $G_f=15.5$ dB, $n_{sp}(\omega_f)=1$, $P_s(0)=-2.5$ dBm, and $\hbar\omega_s=0.8$ eV, Eq. (190) gives $\mathrm{SBR}_f\cong 31+\eta_f(\omega_p,\omega_s)$ in dB. When $\eta_{in}=-2$ dB, Eq. (192) gives $\mathrm{NF}_f\cong 20.5-\eta_f(\omega_p,\omega_s)$ in dB. The conversion efficiency of -4.7 dB at 30 kA/cm^2 gives $\mathrm{SBR}_f\cong 26.3$ dB and $\mathrm{NF}_f\cong 25.2$ dB.

One way to further improve NF_f of the four-wave mixing wavelength conversion by quantum-dot SOA's is to increase the optical gain of dots by increasing the dot density or reducing the inhomogeneous broadening width. The other one is to increase the pump power and the amplifier gain by increasing the SOA length. Figure 12 shows the conversion efficiency calculated by Eq. (189) and the noise figure calculated by Eq. (192) as a function of the amplifier gain, G_f, when the output pump power is (a) $P_p(L)=10$ dBm and (b) $P_p(L)=13$ dBm. The detuning is 0.5, 1.0, and 2.0 THz. The current density is 24 kA/cm^2. The solid lines represent the calculation as long as the converted signal power is less than -10 dB of the output signal, which is an approximate criteria for the spectrum distortion not to occur. The minimum noise figure is shown by the solid circle at each detuning. When the output signal power is equal to the pump power, which is also an approximate criteria for the spectrum distortion not to occur, the maximum signal-to-background-ratio at the minimum noise figure is $\mathrm{SBR}_f=27$ dB at 0.5 THz, $\mathrm{SBR}_f=22$ dB at 1.0 THz, and $\mathrm{SBR}_f=14$ dB at 2.0 THz when $P_p(L)=10$ dBm, and $\mathrm{SBR}_f=45$ dB at 0.5 THz, $\mathrm{SBR}_f=39$ dB at 1.0 THz, and $\mathrm{SBR}_f=33$ dB at 2.0 THz when $P_p(L)=13$ dBm. Comparing Figs. 12(a) and 12(b), we see that increasing the pump power is more effective for lower noise figure than increasing the amplifier gain. Note that $\mathrm{NF}_f=19$ dB with $\mathrm{SBR}_f=33$ dB even at the detuning of 2 THz is accomplished under $P_p(L)=13$ dBm and $G_f=18.6$ dB.

Since the detuing of 2 THz corresponds to 32 nm wavelength conversion at the 1.55 micron wavelength range, the quantum-dot SOA enables wavelength conversion over the entire range of the *C* band of the fiber transmission system. This enables the 20-channel 40 Gb/s system with a single channel bandwidth of 100 GHz and the 8-channel 160 Gb/s system with a single channel bandwidth of 500 GHz. We have proposed, designed, and assembled a tunable wavelength conversion module over the entire range of the *C* band by the combination of a quantum-dot SOA, a wavelength tunable laser as pump source and the dispersion diversity configuration for polarization insensitivity.[41]

C. Current states of experiments

We have done experiments on optical signal amplification and switching at the wavelength of 1.3 micron using SOA's

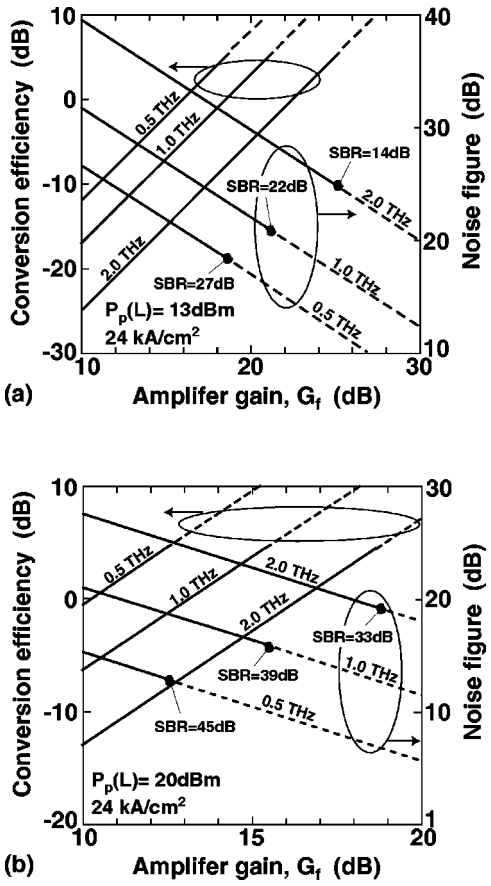

FIG. 12. Calculated conversion efficiency and the noise figure as a function of the amplifier gain, G_f, when the output pump power is (a) $P_p(L)=10$ dBm and (b) $P_p(L)=13$ dBm. The detuning is 0.5, 1.0, and 2.0 THz. The calculation is done until the converted signal power reaches -10 dB of the output signal.

with InGaAs/GaAs self-assembled quantum dots in the active region, and demonstrated their various unique characteristics discussed in this theoretical work. Among them are 10–40 Gb/s pattern-effect-free amplification,[11–15] 10–40 Gb/s pattern-effect-free wavelength conversion by the cross-gain modulation,[11–15] and the symmetric wavelength conversion by nondegenerate four-wave mixing.[16,17] We also fabricated quantum-dot SOA's with InGaAs/InP self-assembled quantum dots in the active region and succeeded in demonstrating high saturation power above 20 dBm at 1.55 micron.[42] We are now working to demonstrate the remaining promising features like low power-consumption amplification, multichannel amplification on broad gain bandwidth with negligible cross talk, and less than 20 dB noise figure as four-wave mixing wavelength converter.

We took the population relaxation rate (260 fs) and the polarization relaxation rate (130 fs) in the calculation from previous experimental studies on carrier dynamics. This slower relaxation time in quantum dots than bulk and quantum-well semiconductors can be attributed to the discrete energy states and spatial localization of quantum dots to limit the relaxation via carrier-LO phonon scattering, carrier-LA phonon scattering, and carrier-carrier scattering to some extent. This is the phonon bottleneck in the sense that

available electronic energy states to satisfy the energy conservation rule for relaxation are limited.

We can expect the relaxation rates can be controlled to some extent by tuning the size, shape, strain, density, and potential depth of quantum dots. Generally speaking, faster relaxation rates than those of 1.3-micron InGaAs/GaAs self-assembled quantum dots will be advantageous to linear operations as optical amplifiers, and slower rates to nonlinear operations as optical switches. The InGaAs/InP quantum dots with 1.55 micron we are now working on[42] have the diameter of about 40 nm, about twice that of 1.3-micron InGaAs/GaAs self-assembled quantum dots, and have denser discrete energy states. We expect these 1.55-micron dots will have faster relaxation rates than the 1.3-micron dots, and thus might work as linear optical amplifiers more efficiently than as nonlinear optical switches. An arbitrary control of the population and polarization relaxation rates via the dot structures will enable us to design the best performance amplifiers or switches we need.

V. SUMMARY

We presented a theory of optical signal amplification and processing by quantum-dot semiconductor optical amplifiers. The theory includes the linear optical response as well as the incoherent and coherent nonlinear response of the quantum-dot SOA's with arbitrary spectral and spatial distribution of quantum dots in the active region under the multimode light. Based on the theory, we numerically simulated the operation of quantum-dot SOA's to show diverse promising features as amplifiers with low power consumption, high-saturation power, broad gain bandwidth, pattern-effect-free operation under gain saturation, and also, as signal processing devices to realize high-speed (40–160 Gb/s) pattern-effect-free wavelength conversion by the cross-gain modulation with low frequency chirping, and the symmetric highly-efficient 1 to 2 THz wavelength conversion by nondegenerate four-wave mixing. The high performance as amplifiers is primarily based on discrete quantized energy states and relatively low dot density, and switching functions owes to dominant incoherent and dynamic spectral hole burning. Our previous theoretical prediction, experimental demonstration, and the development of devices and modules in progress are now supported by a rigid framework of the present theory. This work will help not only design practical quantum-dot devices working in the photonic networks but also understand how carrier dynamics in quantum dots relates to the optical response of quantum dots under current injection.

ACKNOWLEDGMENTS

This work is supported by ''Photonic Network Project'' which OITDA contracted with Ministry of Economy, Trade and Industry of Japan, and by ''Focused Research and Development Project'' for the Realization of the World's Most Advanced IT Nation, IT Program, MEXT of Japan.

APPENDIX: THEORY OF BULK AND QUANTUM-WELL SEMICONDUCTOR OPTICAL AMPLIFIERS

In this appendix, we present a theory of the single- and multimode optical pulse propagation in traveling-type semiconductor optical amplifiers (SOA's) with bulk or quantum-well active regions and show how the introduction of quantum dots into the active region will improve the performance of SOA's within the framework of the theory. Here, the quantum-dot active region is characterized as a continuum medium with the discrete density of states, small crystal volume, zero alpha parameter, and slower population and polarization relaxation rates than bulk or quantum well active region. This comparative approach will help highlight features of our quantum-dot theory in the main text.

As in the main text, we clarify the operation modes of the SOA's into the single-mode amplification, multimode amplification, and intermode interaction for optical switching. Though many papers on theoretical treatments of SOA operations have been published,[43–48] this appendix is the first, to our knowledge, to treat all the aspects of their operations in a unified manner. In this sense, this appendix will also help readers with an interest in conventional SOA's.

We use the density matrix equation to treat the interaction between the photon and the two-level electron system consisting of the conduction-band and valence-band **k** states, $|c,\mathbf{k}\rangle$ and $|v,\mathbf{k}\rangle$, respectively, as in the main text. The equation includes the relaxation rate of the polarization and that of the intraband and interband population at each **k** state, giving analytical expressions for the linear and nonlinear susceptibilities with the summation of the contribution of each **k** state. The nonlinear susceptibility includes the population term to describe the incoherent polarization, the dynamic spectral hole burning term, and the carrier density pulsation term. We also present approximate expressions of the susceptibilities as linear functions of the carrier density, N. This approximation, though taken primarily due to the difficulty in treating the intraband population relaxation at each **k** state in the continuous band under the electron-photon interaction, holds well as long as the optical power is such that the intraband population relaxation rate is much faster than the stimulated emission rate, and that the carrier distribution in the bands obeys Fermi-Dirac distribution function.

1. Propagation equation of optical pulse

We rewrite Eq. (162) of the propagation equation of the optical pulse with the wave form of Eq. (91) as

$$\frac{\partial}{\partial z}R_m(z,T)=\frac{\Gamma_m}{2}[\,\tilde{\eta}^{pop}(N,\omega_m)+\tilde{\eta}^{dshb}(N,\omega_m)+\tilde{\eta}^{cdp}(N,\omega_m)]R_m(z,T)-\frac{\alpha_{loss}(\omega_m)}{2}R_m(z,T). \tag{A1}$$

The direction of the wave guide with the length of L is taken as the z axis and its perpendicular direction is in the x-y plane. The frame of reference moving with the pulse at the

group velocity is employed by making the transformation of $T=t-q_0(\omega_m)z$. The terms in the parenthesis of the right-hand side of Eq. (A1) include the population term, $\tilde{\eta}_\sigma^{pop}(N,\omega_m)$, the dynamic spectral hole burning term, $\tilde{\eta}_\sigma^{dshb}(N,\omega_m)$, and the carrier density pulsation term, $\tilde{\eta}_\sigma^{cdp}(N,\omega_m)$ with the carrier density explicitly written. These susceptibility terms are given as follows.

A. Population term, $\tilde{\eta}_\sigma^{pop}(N,\omega_m)$

Assuming that N is constant in the cross section of the active region (this assumption holds when the cross-sectional dimension of the active region is smaller than the diffusion length of carriers, and is used throughout this appendix), we obtain from Eq. (98)

$$\tilde{\eta}^{pop}(N,\omega_m)=i\frac{\omega_m}{n_{\rm eff}(\omega_m)c}\tilde{\chi}_\sigma^{pop}(N,\omega_m). \tag{A2}$$

From Eqs. (47) and (48) with the dot serial number of s omitted, we obtain

$$\begin{aligned}\tilde{\chi}_\sigma^{pop}(N,\omega_m)&=\sum_{c,v,\mathbf{k}}\tilde{\chi}_\sigma^{pop}(N,\omega_m:cv\mathbf{k})\\&=\sum_{c,v,\mathbf{k}}\frac{2e^2|P_{cv,\mathbf{k}}^\sigma|^2[\rho_{cc,\mathbf{k}}^{pop}-\rho_{vv,\mathbf{k}}^{pop}]}{\varepsilon_0\hbar m_0^2\omega_m\omega_{cv,\mathbf{k}}}\\&\times\left[\frac{1}{\omega_m-\omega_{cv,\mathbf{k}}+i\Gamma_{cv,\mathbf{k}}}\right.\\&\left.+\frac{1}{\omega_m+\omega_{cv,\mathbf{k}}+i\Gamma_{cv,\mathbf{k}}}\right],\end{aligned} \tag{A3}$$

where $\Gamma_{cv,\mathbf{k}}$ is the relaxation rate of the polarization formed by the $|c,\mathbf{k}\rangle$ and $|v,\mathbf{k}\rangle$ states. The summation of $\tilde{\chi}_\sigma^{pop}(N,\omega_m:cv\mathbf{k})$ in $\mathbf{k}$ space in Eq. (A3) is done per unit volume. Note that $\rho_{cc,\mathbf{k}}^{pop}$ is the population at the $|c,\mathbf{k}\rangle$ state without beating, and $\rho_{cc,\mathbf{k}}^{pop}$ is that at the $|v,\mathbf{k}\rangle$ state, each of which is often represented by the Fermi-Dirac distribution function in each band due to ultrafast intraband population relaxation. For simplicity, we do the following: By neglecting the dispersion of $\omega_{cv,\mathbf{k}}$, $P_{cv,\mathbf{k}}^\sigma$, and $\Gamma_{cv,\mathbf{k}}$, introducing the gain spectrum width of Δ and the gain peak frequency of ω_0, and assuming the neutral condition of $\rho_{cc,\mathbf{k}}^{pop}=1-\rho_{vv,\mathbf{k}}^{pop}$, we obtain an approximate expression of Eq. (A3) as

$$\tilde{\chi}_\sigma^{pop}(N,\omega_m)\cong-\frac{(\alpha+i)C_m\Delta[N-N_{tr}]}{(\omega_m-\omega_0)^2+\Delta^2}. \tag{A4}$$

Here, the carrier density is given by taking the summation of $\rho_{cc,\mathbf{k}}^{pop}$ on the conduction-band $\mathbf{k}$ states including spin degeneracy per unit volume as

$$N=2\sum_{c,\mathbf{k}}\rho_{cc,\mathbf{k}}^{pop}, \tag{A5}$$

$$C_m=\frac{2e^2|P_{cv}^\sigma|^2}{\varepsilon_0\hbar m_0^2\omega_m\omega_0} \tag{A6}$$

is a constant,

$$\alpha=\frac{\dfrac{\partial\,\mathrm{Re}\,\tilde{\chi}_\sigma^{pop}(N,\omega_m)}{\partial N}}{\dfrac{\partial\,\mathrm{Im}\,\tilde{\chi}_\sigma^{pop}(N,\omega_m)}{\partial N}} \tag{A7}$$

is the alpha parameter, and N_{tr} is the carrier density for transparency.

Using Eq. (A4), the optical gain of Eq. (101) is

$$\tilde{g}_\sigma(N,\omega_m)=-\frac{\omega_m}{n_{\rm eff}(\omega_m)c}\,\mathrm{Im}\,\tilde{\chi}_\sigma^{pop}(N,\omega_m)=A_m[N-N_{tr}], \tag{A8}$$

where

$$A_m=\frac{\omega_m}{n_{\rm eff}(\omega_m)c}\frac{C_m\Delta}{(\omega_m-\omega_0)^2+\Delta^2} \tag{A9}$$

is the differential gain.

B. Coherent nonlinear polarization term due to dynamic spectral hole burning, $\tilde{\eta}_\sigma^{dshb}(N,\omega_m)$

From Eqs. (62) and (63) with the dot serial number of s omitted and Eq. (99), the coherent nonlinear term of $\tilde{\eta}^{dshb}(N,\omega_m)$ is given as

$$\begin{aligned}\tilde{\eta}^{dshb}(N,\omega_m)=i\frac{\omega_m}{n_{\rm eff}(\omega_m)c}\Gamma_2\sum_{\substack{m',m'',m'''\\(m'\neq m'',>0)}}&\tilde{\chi}_\sigma^{dshb}(N,\omega_m=\omega_{m'}-\omega_{m''}+\omega_{m'''})\\&\times R_{m'}(z,T)R_{m''}^*(z,T)R_{m'''}(z,T)R_m^{-1}(z,T)e^{i(q_{m'}-q_{m''}+q_{m'''}-q_m)z},\end{aligned} \tag{A10}$$

where

$$\tilde{\chi}_{\sigma}^{cshb}(N,\omega_m=\omega_{m'}-\omega_{m''}+\omega_{m'''})=\sum_{c,v,\mathbf{k}}\frac{e^2|P_{cv,\mathbf{k}}^{\sigma}|^2}{4m_0^2\omega_{m''}\omega_{cv,\mathbf{k}}\hbar^2}\frac{\tilde{\chi}_{\sigma'}^{pop}(N,\omega_{m'};cv\mathbf{k})-\tilde{\chi}_{\sigma'}^{pop}(N,\omega_{m''};cv\mathbf{k})^*}{\omega_{m'}-\omega_{m''}+\omega_{m'''}-\omega_{cv,\mathbf{k}}+i\Gamma_{cv,\mathbf{k}}}$$
$$\times\left\{\frac{1}{\omega_{m'}-\omega_{m''}+i(T_{cc,\mathbf{k}}+R_{cc,\mathbf{k}})}+\frac{1}{\omega_{m'}-\omega_{m''}+i(T_{vv,\mathbf{k}}+R_{vv,\mathbf{k}})}\right\}, \tag{A11}$$

$$\Gamma_2=\frac{\int_{act}|H(x,y)|^4dxdy}{\int_{act}|H(x,y)|^2dxdy}, \tag{A12}$$

$T_{cc,\mathbf{k}}$ is the intraband relaxation rate of the electron population of the $|c,\mathbf{k}\rangle$ state toward quasithermal equilibrium, $T_{vv,\mathbf{k}}$ is that of the $|v,\mathbf{k}\rangle$ state, $R_{cc,\mathbf{k}}$ is the interband relaxation rate of the electron population of the $|c,\mathbf{k}\rangle$ state toward thermal equilibrium state, i.e., the recombination rate, and $R_{vv,\mathbf{k}}$ is that of the $|v,\mathbf{k}\rangle$ state. The polarization of the m'' mode, σ, can be different from that of the m' and m'' modes, σ'.

Using the same procedure as we derived Eq. (A4), Eq. (A11) becomes

$$\tilde{\chi}_{\sigma}^{dshb}(N,\omega_m=\omega_{m'}-\omega_{m''}+\omega_{m'''})\cong\frac{\varepsilon_0}{4\hbar}C_{m'''}\frac{\tilde{\chi}_{\sigma'}^{pop}(N,\omega_{m'})-\tilde{\chi}_{\sigma'}^{pop}(N,\omega_{m''})^*}{(\omega_{m'}-\omega_{m''}+\omega_{m'''}-\omega_0+i\Gamma_{cv})[\omega_{m'}-\omega_{m''}+i(T_{in}+R_{rec})]}, \tag{A13}$$

where we adopted the polarization relaxation rate of Γ_{cv}, the intraband population relaxation rate of T_{in}, and the recombination rate of R_{rec} in common at each $\mathbf{k}$ state in both bands.

C. Coherent nonlinear polarization term due to carrier density pulsation, $\tilde{\eta}_{\sigma}^{cdp}(N,\omega_m)$

From Eqs. (50) and (53) with the dot serial number of s omitted, the time derivative of the diagonal term of the density matrix is

$$\dot{\rho}_{cc,\mathbf{k}}(\mathbf{r},t)\cong\frac{\varepsilon_0}{4\hbar}\sum_{v}\sum_{\substack{m\\(>0)}}\mathrm{Im}\,\tilde{\chi}_{\sigma}^{pop}(N,\omega_m;cv\mathbf{k})|E_m(\mathbf{r},t)|^2$$
$$-\frac{\varepsilon_0 i}{8\hbar}\sum_{v}\sum_{\substack{m,m'\\(m\neq m'>0)}}\tilde{\chi}_{\sigma}^{pop}(N,\omega_m;cv\mathbf{k})E_m(\mathbf{r},t)$$
$$\times E_{m'}^*(\mathbf{r},t)e^{i(q_m-q_{m'})z}e^{-i(\omega_m-\omega_{m'})t}+\text{c.c.} \tag{A14}$$

Taking the summation in $\mathbf{k}$ space per unit volume, using Eq. (A3), and adding the recombination term and the current injection term, Eq. (A14) becomes

$$\frac{\partial N^{\mathrm{tot}}}{\partial t}=\frac{\varepsilon_0}{2\hbar}\sum_{\substack{m\\(>0)}}\mathrm{Im}\,\tilde{\chi}_{\sigma}^{pop}(N,\omega_m)|E_m(\mathbf{r},t)|^2$$
$$-\frac{\varepsilon_0 i}{4\hbar}\sum_{\substack{m,m'\\(m\neq m'>0)}}\tilde{\chi}_{\sigma}^{pop}(N,\omega_m)E_m(\mathbf{r},t)E_{m'}^*(\mathbf{r},t)$$
$$\times e^{i(q_m-q_{m'})z}e^{-i(\omega_m-\omega_{m'})t}+\text{c.c.}-R_{rec}(N^{\mathrm{tot}}-N_0), \tag{A15}$$

where $N^{\mathrm{tot}}=2\Sigma_{c,\mathbf{k}}\rho_{cc,\mathbf{k}}(\mathbf{r},t)$ is the total carrier density including the beating under the charge neutrality condition, $N_0=J/R_{rec}ed$ is the quasithermal equilibrium carrier density under a given injection current density, J, and d is the active layer thickness. The thermal-equilibrium carrier density is neglected. By substituting

$$N^{\mathrm{tot}}=N+\sum_{\substack{m',m''\\(m\neq m'>0)}}\Delta N(\omega_{m'}-\omega_{m''})e^{-i(\omega_{m'}-\omega_{m''})t}+\text{c.c.} \tag{A16}$$

into Eq. (A15), we obtain the amplitude of beating as

$$\Delta N(\omega_{m'}-\omega_{m''})=\frac{\varepsilon_0}{4\hbar}\frac{\tilde{\chi}_{\sigma}^{pop}(N,\omega_{m'})}{\omega_{m'}-\omega_{m''}+i[R_{rec}+R_{stim}]}$$
$$\times E_{m'}(\mathbf{r},t)E_{m''}^*(\mathbf{r},t)e^{i(q_{m'}-q_{m''})z}, \tag{A17}$$

where

$$R_{stim}=-\frac{\varepsilon_0}{2\hbar}\sum_{m>0}\frac{\partial\,\mathrm{Im}\,\tilde{\chi}_{\sigma}^{pop}(N,\omega_m)}{\partial N}|E_m(\mathbf{r},t)|^2 \tag{A18}$$

is the stimulated emission rate. By taking average of Eq. (A18) in the xy plane, and using Eqs. (A4) and (A9), Eq. (A18) becomes

$$R_{stim}=\sum_{m>0}\Gamma_m A_m S_m, \tag{A19}$$

where S_m is the photon flux density given by Eq. (95).

By substituting Eq. (A17) into [see Eq. (96)]

$$\frac{\partial}{\partial z}R_m(z,T)=i\frac{\omega_m}{2n_{\mathrm{eff}}(\omega_m)c}\times\frac{\int_{act}\frac{\partial\tilde{\chi}_\sigma^{pop}(N,\omega_{m'''})}{\partial N}[\Delta N(\omega_{m'}-\omega_{m''})+\Delta N^*(\omega_{m''}-\omega_{m'})]|H(x,y)|^2dxdy}{\int_{cav}|H(x,y)|^2dxdy}R_{m'''}(z,T)e^{i(q_{m'''}-q_m)z},\tag{A20}$$

we obtain

$$\tilde{\eta}^{cdp}(N,\omega_m)=i\frac{\omega_m}{n_{\mathrm{eff}}(\omega_m)c}\Gamma_2\sum_{\substack{m',m'',m'''\\(m'\neq m'',>0)}}\tilde{\chi}_\sigma^{cdp}(N,\omega_m=\omega_{m'}-\omega_{m''}+\omega_{m'''})\times R_{m'}(z,T)R_{m''}^*(z,T)R_{m'''}(z,T)R_m^{-1}(z,T)e^{i(q_{m'}-q_{m''}+q_{m'''}-q_m)z},\tag{A21}$$

where

$$\tilde{\chi}_\sigma^{cdp}(N,\omega_m=\omega_{m'}-\omega_{m''}+\omega_{m'''})=-\frac{\varepsilon_0}{4\hbar}\frac{n_{\mathrm{eff}}(\omega_{m'''})c}{\omega_{m'''}}(\alpha+i)A_{m'''}\frac{\tilde{\chi}_{\sigma'}^{pop}(N,\omega_{m'})-\tilde{\chi}_{\sigma'}^{pop}(N,\omega_{m''})^*}{\omega_{m'}-\omega_{m''}+i[R_{rec}+R_{stim}]}.\tag{A22}$$

The polarization of the m'' mode, σ, can be different from that of the m' and m'' modes, σ'.

D. Rate equations of carrier density and gain

By averaging Eq. (A15) in the xy plane and omitting the beating term and introducing $T=t-q_0(\omega_m)z$, we obtain the equation of the carrier density as

$$\frac{\partial N}{\partial T}=-R_{rec}[N-N_0]-\sum_{m>0}\Gamma_m\tilde{g}_\sigma(N,\omega_m)S_m(z,T).\tag{A23}$$

From Eqs. (A8) and (A23), we obtain the rate equation of gain as

$$\frac{\partial\tilde{g}_\sigma(N,\omega_m)}{\partial T}=-R_{rec}[\tilde{g}_\sigma(N,\omega_m)-\tilde{g}_\sigma^{(1)}(N,\omega_m)]-A_m\sum_{m'>0}\Gamma_{m'}\tilde{g}_\sigma(N,\omega_{m'})S_{m'}(z,T),\tag{A24}$$

where the linear gain is

$$\tilde{g}_\sigma^{(1)}(N,\omega_m)=A_mN_{tr}(J/J_{tr}-1)\tag{A25}$$

and $J_{tr}=edR_{rec}N_{tr}$.

2. Optical amplification and switching

The operation of SOA's can be described by Eqs. (A1), (A2), (A10), (A21), and (A23) [or Eq. (A24)]. We can classify the operation by whether it is under the single mode or multimodes. The multimode operation can be further classified by the frequency separation between each mode. When the mode separation is sufficiently larger than the polarization relaxation rate ($|\omega_{m'}-\omega_{m''}|\gg\Gamma_{cv}$), we can neglect the coherent terms in Eq. (A1), leading to multimode amplification. When the mode separation is comparable to or less than the polarization relaxation rate ($|\omega_{m'}-\omega_{m''}|\leqslant\Gamma_{cv}$), the coherent terms cause intermode interaction including cross-gain and cross-phase modulation and four-wave mixing.

A. Single-mode amplification

When there is only one light mode, the coherent terms in Eq. (A1) vanish, resulting in the propagation equation of

$$\frac{\partial}{\partial z}R_m(z,T)=\frac{1}{2}[\Gamma_m\tilde{\eta}^{pop}(N,\omega_m)-\alpha_{loss}(\omega_m)]R_m(z,T).\tag{A26}$$

The amplitude of $R_m(z,T)$ can be written as

$$R_m(z,T)=|R_m(z,T)|e^{i\phi_m(z,T)}\tag{A27}$$

using the phase of $\phi_m(z,T)$. Substituting Eq. (A27) into Eq. (A26), we obtain the propagation equation of the photon flux density as

$$\frac{\partial}{\partial z}S_m(z,T)=[\Gamma_m\tilde{g}_\sigma(N,\omega_m)-\alpha_{loss}(\omega_m)]S_m(z,T)\tag{A28}$$

and that of the phase as

$$\frac{\partial}{\partial z}\phi_m(z,T)=\frac{\Gamma_m}{2}\tilde{\xi}_\sigma(N,\omega_m),\tag{A29}$$

where

$$\tilde{\xi}_\sigma(N,\omega_m)=\frac{\omega_m}{n_{\mathrm{eff}}(\omega_m)c}\mathrm{Re}\,\tilde{\chi}_\sigma^{pop}(N,\omega_m)=-\alpha_m\tilde{g}_\sigma(N,\omega_m).\tag{A30}$$

Under the continuous-wave operation, Eq. (A28) becomes

$$\frac{\partial S_m(z)}{\partial z} = [\Gamma_m \tilde{g}_\sigma(N,\omega_m) - \alpha_{loss}(\omega_m)] S_m(z) \quad \text{(A31)}$$

by replacing $S_m(z,T)$ with $S_m(z)$. Similarly, Eq. (A24) gives the gain of

$$\tilde{g}_\sigma(N,\omega_m) \equiv \frac{\tilde{g}_\sigma^{(1)}(N,\omega_m)}{1+S_m(z)/S_m^{sat}}, \quad \text{(A32)}$$

where

$$S_m^{sat} = \frac{R_{rec}}{A_m \Gamma_m} \quad \text{(A33)}$$

is the saturation photon flux density. Equation (A32) tells us that the gain saturation occurs when $S_m(z)$ exceeds S_m^{sat}. Integrating Eq. (A31) with Eq. (A32) and neglecting the internal loss, we obtain the amplifier gain as

$$G_m = \frac{S_m(L)}{S_m(0)} = G_m^{(1)} \exp\left\{ -\frac{[G_m - 1] S_m(L)}{G_m S_m^{sat}} \right\}, \quad \text{(A34)}$$

where the linear or unsaturated single-pass amplifier gain without the loss is

$$G_m^{(1)} = \exp[\Gamma_m \tilde{g}_\sigma^{(1)}(N,\omega_m) L]. \quad \text{(A35)}$$

If we define the saturation power of P_m^{sat} as the output power to give $G_m = G_m^{(1)}/2$ in Eq. (A34), we obtain

$$P_m^{sat} \cong (\ln 2) \frac{\hbar \omega_m R_{rec} D}{\Gamma_m A_m}, \quad \text{(A36)}$$

where we used the optical power of $P_m = \hbar \omega_m D S_m$, and D is the cross section area of the active region. From Eqs. (A25), (A35), and (A36), we obtain the product of the unsaturated gain and the saturation output power divided by the SOA length as

$$P_m^{sat} \cdot \ln G_m^{(1)}/L = \frac{(\ln 2)\hbar \omega_m D}{ed} J(J/J_{tr} - 1). \quad \text{(A37)}$$

Equation (A37) tells us that the saturation power, the amplifier gain and the length of SOA's is under trade off at a given current density. In some applications, where high saturation power is essential, we should increase the saturation power at the expense of the length, i.e., the consumption power, or the amplifier gain. In order to increase the saturation power, we know from Eq. (A36) that we should reduce the optical confinement factor of Γ_m, the differential gain of A_m, and the recombination rate of R_{rec}. The active region area of D should be designed to maximize the coupling efficiency to optical fibers.

Figure 13 compares the active-region structures and the density of states of a bulk semiconductor and quantum nanostructures like quantum wells, quantum wires, and quantum dots. Let us assume the filling factor of the hatched region in the active region as ξ_2 in the quantum wells, ξ_1 in the quantum wires, and ξ_0 in the quantum dots. Generally speaking, the filling factor decreases as the dimension of the quantization increases, i.e., $1 > \xi_2 > \xi_1 > \xi_0$. As a result, the optical confinement factor decreases from $\Gamma_m = \Gamma_b$ in the bulk active region approximately to $\Gamma_b \xi_2$ in the quantum-well, $\Gamma_b \xi_1$ the quantum-wire and $\Gamma_b \xi_0$ in the quantum-dot active region. Also, since quantum dots have the density of states which is discrete due to the complete quantization as well as small due to the low filling factor, the Fermi level goes into the band deeper than in other semiconductors at a given carrier density, causing smaller differential gain. Owing to these two factors, i.e., low confinement factor and small differential gain, we can expect higher saturation power in quantum-dot SOA's than in other conventional SOA's.

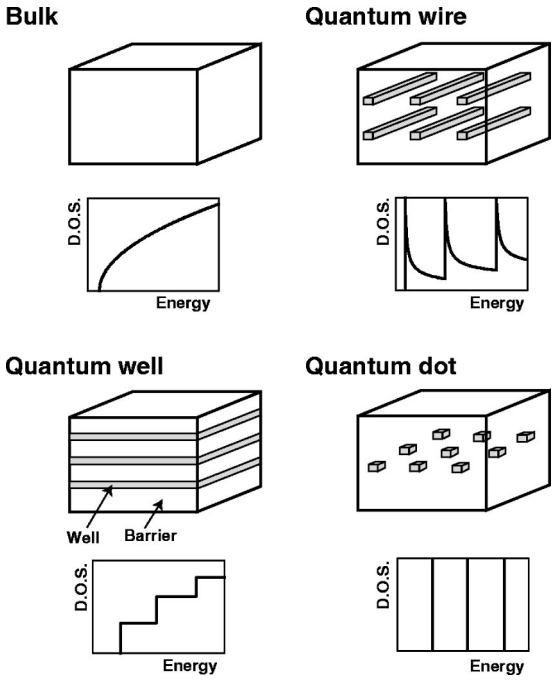

FIG. 13. Active-region structures and density of states of a bulk semiconductor and quantum nanostructures like quantum wells, quantum wires, and quantum dots.

Note that the combination of the deep Fermi level and the inhomogeneous broadening due to size distribution also causes broader gain bandwidth than other conventional SOA's.

B. Multimode amplification ($|\omega_m - \omega_{m'}| \gg \Gamma_{cv}$)

The propagation of each optical mode is described by Eqs. (A8), (A23), and (A28)–(A30). The intermode interaction appears via the $\tilde{g}_\sigma(N,\omega_m)$ in Eqs. (A28) and (A30), i.e., the gain saturation due to the reduction in the carrier density results in the cross talk between different modes as the optical power increases. In quantum-dot SOA's multimode amplification with negligible cross talk even under gain saturation is possible due to the inhomogeneous broadening and spatial isolation of quantum dots as discussed in the main text.

C. Intermode interaction ($|\omega_m - \omega_{m'}| \leqslant \Gamma_{cv}$)

Let us consider the case where we input the strong pump light with a frequency of ω_p and the signal or probe light

with a frequency of ω_s into the SOA. The beating between the ω_p and ω_s light causes coherent nonlinear polarization via the four different processes as $\omega_s=\omega_s-\omega_p+\omega_p$, $\omega_p=\omega_p-\omega_s+\omega_s$, $\omega_f=\omega_p-\omega_s+\omega_p$, and $\omega_{f'}=\omega_s-\omega_p+\omega_s$. The combination of $\omega_s=\omega_s-\omega_p+\omega_p$ and $\omega_p=\omega_p-\omega_s+\omega_s$ causes cross-gain modulation and cross-phase modulation, and the combination of $\omega_f=\omega_p-\omega_s+\omega_p$ and $\omega_{f'}=\omega_s-\omega_p+\omega_s$ causes four-wave mixing where frequency or wavelength conversion occurs. These processes occur simultaneously.

From Eq. (A1), the propagation equation of the pump is approximately given by

$$\frac{\partial}{\partial z}R_p(z,T)=\frac{1}{2}[\Gamma_p\tilde{\eta}^{pop}(N,\omega_p)-\alpha_{loss}(\omega_p)]R_p(z,T), \tag{A38}$$

where the coherent term under the combination of $\omega_p=\omega_p-\omega_s+\omega_s$ is neglected due to the strong pump pulse intensity.

(1) Cross-gain modulation ($\omega_s=\omega_s-\omega_p+\omega_p$). When the pump beam with a frequency of ω_p conveys a bit pattern, the intensity and the phase of the continuous-wave signal with a frequency of ω_s is modulated according to the bit pattern, each of which is called cross-gain and cross-phase modulation.

The propagation equation of the mode with a frequency of ω_s is

$$\frac{\partial}{\partial z}R_s(z,T)=\frac{\Gamma_s}{2}[\tilde{\eta}^{pop}(N,\omega_s)+\tilde{\eta}^{dshb}(N,\omega_s)+\tilde{\eta}^{cdp}(N,\omega_s)]R_s(z,T)-\frac{\alpha_{loss}(\omega_s)}{2}R_s(z,T). \tag{A39}$$

Using the results in Sec. 1, we obtain

$$\tilde{\eta}^{pop}(N,\omega_s)=i\frac{\omega_s}{n_{\rm eff}(\omega_s)c}\tilde{\chi}_\sigma^{pop}(N,\omega_s), \tag{A40}$$

$$\tilde{\eta}_\sigma^{dshb}(N,\omega_s)=i\frac{\omega_s}{n_{\rm eff}(\omega_s)c}\Gamma_2\tilde{\chi}_\sigma^{dshb}(N,\omega_s=\omega_s-\omega_p+\omega_p)\times|R_p(z,T)|^2 \tag{A41}$$

with

$$\tilde{\chi}_\sigma^{dshb}(N,\omega_s=\omega_s-\omega_p+\omega_p)=\frac{\varepsilon_0}{4\hbar}C_p\frac{\tilde{\chi}_{\sigma'}^{pop}(N,\omega_s)-\tilde{\chi}_{\sigma'}^{pop}(N,\omega_p)^*}{(\omega_s-\omega_0+i\Gamma_{cv})[\omega_s-\omega_p+i(T_{in}+R_{rec})]}, \tag{A42}$$

and

$$\tilde{\eta}_\sigma^{cdp}(N,\omega_s)=i\frac{\omega_s}{n_{\rm eff}(\omega_s)c}\Gamma_2\tilde{\chi}_\sigma^{cdp}(N,\omega_s=\omega_s-\omega_p+\omega_p)|R_p(z,T)|^2 \tag{A43}$$

with

$$\tilde{\chi}_\sigma^{cdp}(N,\omega_s=\omega_s-\omega_p+\omega_p)=-\frac{\varepsilon_0}{4\hbar}\frac{n_{\rm eff}(\omega_p)c}{\omega_p}(\alpha+i)A_p\frac{\tilde{\chi}_{\sigma'}^{pop}(N,\omega_s)-\tilde{\chi}_{\sigma'}^{pop}(N,\omega_p)^*}{\omega_s-\omega_p+i(R_{rec}+R_{stim})}. \tag{A44}$$

From Eq. (A39), the propagation equation of the photon flux density of the mode ω_s is given as (where $\sigma'=\sigma$)

$$\frac{\partial}{\partial z}S_s(z,T)=\Gamma_s\tilde{g}_\sigma(N,\omega_s)[1-\varepsilon_l(\omega_s,\omega_p,\omega_q=\omega_s)\Gamma_pS_p(z,T)]S_s(z,T)-\alpha_{loss}(\omega_s)S_s(z,T), \tag{A45}$$

where

$$\varepsilon_l(\omega_s,\omega_p,\omega_q=\omega_s)=-A_p\left\{\frac{\beta_p\Delta\{(\omega_q-\omega_0)(\omega_s-\omega_p)-\Gamma_{cv}T_{in}\}}{[(\omega_q-\omega_0)^2+\Gamma_{cv}^2][(\omega_s-\omega_p)^2+T_{in}^2]}-\frac{\alpha(\omega_s-\omega_p)+(R_{rec}+R_{stim})}{[(\omega_s-\omega_p)^2+(R_{rec}+R_{stim})^2]}\right|_{\omega_q=\omega_s} \tag{A46}$$

and

$$\beta_p=\frac{\omega_pC_p}{n_{\rm eff}(\omega_p)cA_p\Delta}. \tag{A47}$$

We used $\Gamma_p\cong\Gamma_2D/\int_{cav}|H(x,y)|^2dxdy$. The first term of the right-hand side of Eq. (A46) is due to the imaginary part of $\tilde{\chi}_\sigma^{dshb}$, and the second term is that of $\tilde{\chi}_\sigma^{cdp}$.

We can calculate the optical pulse propagation under the cross-gain modulation by the combination of Eq. (A23) with $m=p$, s, Eq. (A38), and Eq. (A45). The cross-gain modulation enables wavelength conversion from ω_p to ω_s with the bit pattern inverted.

Figure 14(a) shows the calculation of $1-\varepsilon_l(\omega_s,\omega_p,\omega_q=\omega_s)\Gamma_pS_p$ as a function of the detuning of $\Delta\omega/2\pi=(\omega_p-\omega_s)/2\pi$ in bulk InGaAsP, using the parameters of $\alpha=2$, $\Gamma_{cv}^{-1}=30$ fs, $T_{in}^{-1}=60$ fs, $R_{rec}^{-1}=0.4$ ns, $P_p=\hbar\omega_pDS_p$

$=20$ nW, $\Gamma_p=0.1$, $N=2.35\times10^{18}$ cm^{-3}, $D=1.5\times10^{-9}$ cm^2, and $\lambda_p=2\pi c/\omega_p=1.55$ μm, and $\omega_p=\omega_0$. We used the empirical gain formula of bulk InGaAsP in Sec. 3, which gives the differential gain of $A_p=2.22\times10^{-16}$ cm^2 when $N=2.35\times10^{18}$ cm^{-3} at 1.55 μm. See the optical gain curve in Fig. 5(b). We see that the asymmetry of gain around the pump frequency appears, which is due the carrier density pulsation. Figure 14(b) shows the calculation when $\alpha=0$, $\Gamma_{cv}^{-1}=130$ fs, and $T_{in}^{-1}=260$ fs with other parameters fixed, where we suppose that the active region consists of quantum dots. Note that we used these values of Γ_{cv}^{-1} and T_{in}^{-1} in the main text. The magnitude of gain saturation due to the dynamic spectral hole burning around $\Delta\omega=0$ is about 20 times larger than that in Fig. 14(a) due to slower relaxation. The asymmetric gain due to the carrier density pulsation disappears due to the zero alpha parameter.

Figure 15(a) shows the calculated amplifier gain at the frequency of ω_s (probe) and ω_p (pump) as a function of the input pump power, $P_p(0)=\hbar\omega_p DS_p(0)$. The wavelengths are $\lambda_s=1.54$ μm and $\lambda_p=1.55$ μm, and thus the detuning is $\Delta\omega/2\pi=-1.26$ THz. We suppose the bulk InGaAsP SOA with $L=0.6$ mm, $\alpha_{loss}(\omega_m)=5$ cm^{-1}, and the empirical gain of Sec. 3. The amplifier gain of the probe decreases as the pump power increases, which is the cross gain modulation. Figure 5(b) shows the eye diagram of the amplifier gain of the probe beam when the input pump is the non-return-to-zero (NRZ) random pattern at a bit rate of 2.5 Gb/s with the power of 1 mW [see Fig. 8(b) for the input waveform]. Though we see eye opening, the response speed is almost near its limit at this bit rate.

The switching speed is dominated by the response time of the gain saturation, which is R_{rec}^{-1} as seen in Eq. (A24). Since R_{rec}^{-1} ranges between 0.1 and 1 ns in direct-transition semiconductors, the switching speed is 10 Gb/s at most. See the eye diagram with distorted waveforms of Fig. 10(d) at 40 Gb/s in the main text. In quantum dots, the incoherent and dynamic spectral hole burning enhanced by the retarded carrier relaxation enables pattern-effect-free and high-speed cross-gain modulation as seen in the eye diagram of Fig. 10(c).

(2) Cross-phase modulation ($\omega_s=\omega_s-\omega_p+\omega_p$). From Eq. (A39), the propagation equation of the phase of the mode with a frequency of ω_s is given as (when $\sigma'=\sigma$)

$$\frac{\partial}{\partial z}\phi_s(z,T)=-\frac{\Gamma_s}{2}\tilde{g}_\sigma(N,\omega_s)\times[\alpha+\varepsilon_R(\omega_s,\omega_p,\omega_q=\omega_s)\Gamma_p S_p(z,T)], \tag{A48}$$

where

$$\varepsilon_R(\omega_s,\omega_p,\omega_q=\omega_s)=A_p\left\{\frac{\beta_P\Delta[\Gamma_{cv}(\omega_s-\omega_p)+T_{in}(\omega_q-\omega_0)]}{[(\omega_q-\omega_0)^2+\Gamma_{cv}^2][(\omega_s-\omega_p)^2+\Gamma_{in}^2]}+\frac{(\omega_s-\omega_p)-\alpha(\Gamma_{rec}+\Gamma_{stim})}{(\omega_s-\omega_p)^2+(\Gamma_{rec}+\Gamma_{stim})^2}\right\}\Bigg|_{\omega_q=\omega_s}. \tag{A49}$$

The first term of the right-hand side of Eq. (A49) is due to the real part of $\tilde{\chi}_\sigma^{cshb}$, and the second term is that of $\tilde{\chi}_\sigma^{cdp}$.

We can calculate the optical pulse propagation under the cross-phase modulation by the combination of Eq. (A23) with $m=p$, s, Eq. (A38), and Eq. (A48). The cross-phase modulation in the interferometer like Mach-Zehnder interferometric waveguide with SOA's on both branches enables the wavelength conversion from ω_p to ω_s without the bit pattern inverted.[49] With the continuous light of ω_s passing through both branches, the phase change in one SOA caused by the input of the one-bit pump pulse of ω_p results in the constructive interference of the ω_s light at the exit of the interferometer, generating a one-bit optical pulse on ω_s. As in the case of the cross gain modulation, the switching speed of the conversion is dominated by the response time of the gain saturation, which is R_{rec}^{-1} as seen in Eq. (A24). Since R_{rec}^{-1} ranges between 0.1 and 1 ns, the switching speed is 10 Gb/s at most. In order to overcome this material-limited speed, the so-called push pull operation has been adopted with the time-offset control pulses injected into both SOA's in order to cancel out the slow recovery of the phase change.[50] However, since the amount of phase change for one bit depends on bit patterns, this scheme is not free of pattern effect, either.

Figure 16(a) shows the calculation of $\alpha+\varepsilon_R(\omega_s,\omega_p,\omega_q=\omega_s)\Gamma_p S_p$ as a function of the detuning of $\Delta\omega/2\pi=(\omega_p-\omega_s)/2\pi$ in bulk InGaAsP, using the same parameters of Fig. 14(a). We see that the carrier density pulsation causes the refractive index change just around the pump frequency, and that the dynamic spectral hole burning causes the extended refractive index change of a few percent of $\alpha=2$. Figure 16(b) shows the calculation using the same parameters of Fig. 14(b), which corresponds to quantum dots. We see that the contribution of the dynamic spectral hole burning increases due to the decrease in the relaxation rates. However, the value of $\alpha+\varepsilon_R(\omega_s,\omega_p,\omega_q=\omega_s)\Gamma_p S_p$ is much smaller than in the case of Fig. 16(a), which shows that quantum-dot SOA's are not suitable for the optical signal switching by the cross-phase modulation.

Figure 15(c) shows the calculated frequency chirping of the probe output from the bulk InGaAsP SOA when the SOA is under the cross-gain modulation at 2.5 Gb/s shown in Fig. 15(b). The chirping is given by Eq. (183). We see that the frequency chirping up to about 24 MHz occurs during the cross-gain modulation. A merit of quantum-dot SOA's concerning the cross-phase modulation is that the chirping at the exit of the SOA can be restricted at the onset and offset of the light pulse, when the wavelength conversion is done via the cross-gain modulation.

(3) Four-wave mixing ($\omega_f=\omega_p-\omega_s+\omega_p$ and $\omega_{f'}=\omega_s-\omega_p+\omega_s$). Basic understanding of nondegenerate four-wave mixing in traveling-type semiconductor optical amplifiers has been reached by Agrawal[46] and Kikuchi *et al.*[47] Agrawal derived coupled wave equations of the four-wave mixing including nonlinear susceptibilities due to both carrier density pulsation and spectral hole burning as dominant processes, discussed their bandwidth, and found asymmetric gain around the pump frequency caused by the nonzero alpha

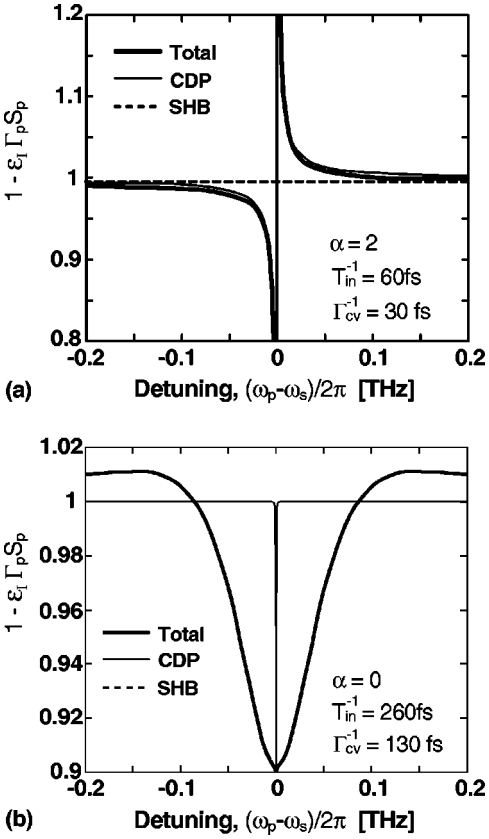

FIG. 14. Calculation of $1-\varepsilon_l(\omega_s,\omega_p,\omega_q=\omega_s)\Gamma_p S_p$ as a function of the detuning of $\Delta\omega/2\pi=(\omega_p-\omega_s)/2\pi$ when (a) $\alpha=2$, $\Gamma_{cv}^{-1}=30$ fs, $T_{in}^{-1}=60$ fs, and (b) $\alpha=0$, $\Gamma_{cv}^{-1}=130$ fs, and $T_{in}^{-1}=260$ fs. The contribution of the dynamic spectral hole burning (SBH), and carrier density pulsation (CDP) are also shown, though the SHB almost coincides with the total in (b).

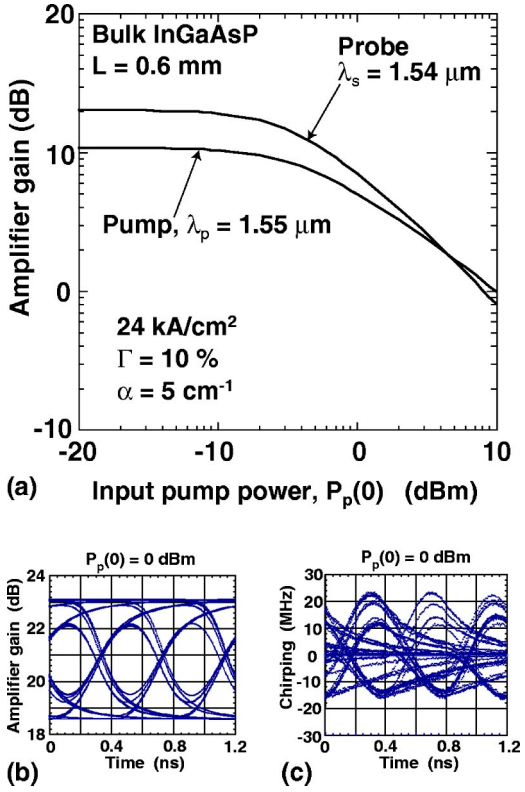

FIG. 15. (a) Calculation of the amplifier gain at the frequency of ω_s (probe) and ω_p (pump) as a function of the input pump power, $P_p(0)$. We suppose the bulk InGaAsP SOA with $L=0.6$ mm, and $\alpha_{loss}(\omega_m)=5\ \mathrm{cm}^{-1}$. (b) Calculated eye diagram of the amplifier gain of the probe beam at the NRZ random pattern at bit rate of 2.5 Gb/s [see Fig. 8(b) for the input waveform]. (c) Calculated frequency chirping of the probe output from the bulk InGaAsP SOA under the cross-gain modulation at 2.5 Gb/s of (b).

parameter. Kikuchi *et al.* measured the wavelength conversion efficiency as a function of the pump and probe detuning to find asymmetric efficiency with a dip under the negative detuning (when the pump frequency is lower than the probe frequency), and attributed this asymmetry to the interference of the two nonlinear processes.

The propagation equation of the mode with a frequency of ω_f is

$$\frac{\partial}{\partial z}R_f(z,T)=\frac{\Gamma_c}{2}[\tilde{\eta}^{pop}(N,\omega_f)+\tilde{\eta}^{cshb}(N,\omega_f)+\tilde{\eta}^{cdp}(N,\omega_f)]R_f(z,T)-\frac{\alpha_{loss}(\omega_f)}{2}R_f(z,T), \tag{A50}$$

where

$$\tilde{\eta}^{pop}(N,\omega_f)=i\frac{\omega_f}{n_{\mathrm{eff}}(\omega_f)c}\tilde{\chi}_\sigma^{pop}(N,\omega_f), \tag{A51}$$

$$\tilde{\eta}^{dshb}(N,\omega_f)=i\frac{\omega_f}{n_{\mathrm{eff}}(\omega_f)c}\Gamma_2\tilde{\chi}_\sigma^{dshb}(N,\omega_f=\omega_p-\omega_s+\omega_p)\times R_p^2(z,T)R_s^*(z,T)R_f^{-1}(z,T)e^{i(2q_p-q_s-q_f)z} \tag{A52}$$

with

$$\tilde{\chi}_\sigma^{dshb}(N,\omega_f=\omega_p-\omega_s+\omega_p)=\frac{\varepsilon_0}{4\hbar}C_p\frac{\tilde{\chi}_{\sigma'}^{pop}(N,\omega_p)-\tilde{\chi}_{\sigma'}^{pop}(N,\omega_s)^*}{(\omega_f-\omega_0+i\Gamma_{cv})(\omega_p-\omega_s+iT_{in})}, \tag{A53}$$

and

$$\tilde{\eta}^{cdp}(N,\omega_f)=i\frac{\omega_f}{n_{\mathrm{eff}}(\omega_f)c}\Gamma_2\tilde{\chi}_\sigma^{cdp}(N,\omega_f=\omega_p-\omega_s+\omega_p)\times R_p^2(z,T)R_s^*(z,T)R_f^{-1}(z,T)e^{i(2q_p-q_s-q_f)z} \tag{A54}$$

with

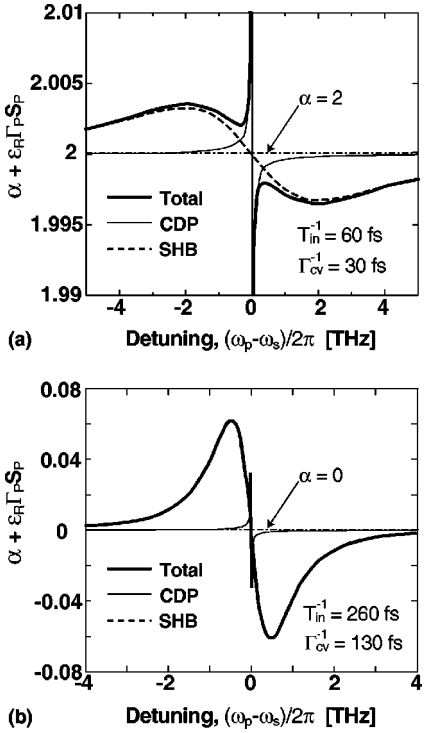

FIG. 16. Calculation of $\alpha+\varepsilon_R(\omega_s,\omega_p,\omega_q=\omega_s)\Gamma_p S_p$ as a function of the detuning of $\Delta\omega/2\pi=(\omega_p-\omega_s)/2\pi$ when (a) $\alpha=2$, $\Gamma_{cv}^{-1}=30$ fs, $T_{in}^{-1}=60$ fs, and (b) $\alpha=0$, $\Gamma_{cv}^{-1}=130$ fs, and $T_{in}^{-1}=260$ fs. The contribution of the dynamic spectral hole burning (SBH), and carrier density pulsation (CDP) are also shown.

$$\tilde{\chi}_{\sigma}^{cdp}(N,\omega_f=\omega_p-\omega_s+\omega_p) = -\frac{\varepsilon_0}{4\hbar}\frac{(\alpha+i)C_p\Delta}{(\omega_p-\omega_0)^2+\Delta^2}\frac{\tilde{\chi}_{\sigma'}^{pop}(N,\omega_p)-\tilde{\chi}_{\sigma'}^{pop}(N,\omega_s)^*}{\omega_p-\omega_s+i(T_{rec}+T_{stim})}. \tag{A55}$$

The propagation of $R_f(z,T)$ can be calculated using Eqs. (A23) with $m=p$, s,f, Eqs. (A38), (A39), and (A50).

From Eqs. (A50)–(A55) with the phase term in $\tilde{\eta}^{pop}(N,\omega_c)$ neglected, we obtain (when $\sigma'=\sigma$)

$$\frac{\partial}{\partial z}R_f(z,T)\cong\frac{1}{2}[\Gamma_f\tilde{g}_{\sigma}(N,\omega_f)-\alpha_{loss}(\omega_f)]R_f(z,T)+\frac{\Gamma_f}{2}\times\Theta_{\sigma}(\omega_p,\omega_s)R_p^2(z,T)R_s^*(z,T)e^{i(2q_p-q_s-q_f)z}, \tag{A56}$$

where

$$\Theta_{\sigma}(\omega_p,\omega_s)=-\frac{\varepsilon_0 n_{\text{eff}}(\omega_p)c}{2\hbar\omega_p}\Gamma_2\tilde{g}_{\sigma}(N,\omega_p)\times W(\omega_p,\omega_s,\omega_q=\omega_f) \tag{A57}$$

and

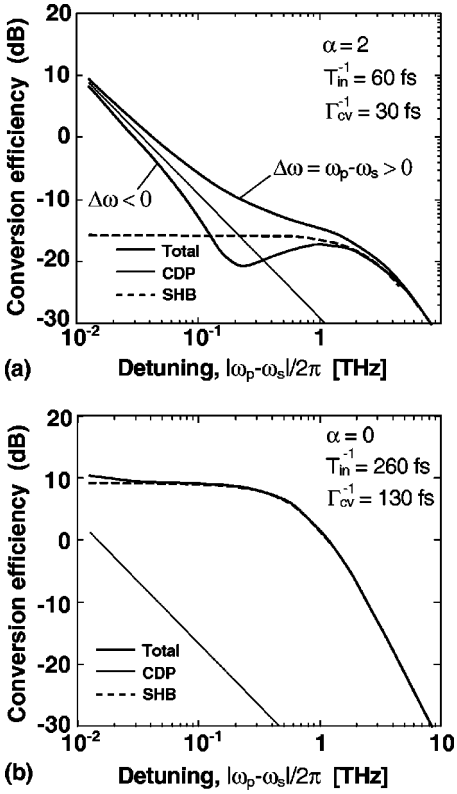

FIG. 17. Calculation of the conversion efficiency, $\eta_{con}(\omega_p,\omega_s)$, as a function of the absolute value of the detuning, $\Delta\omega/2\pi=(\omega_p-\omega_s)/2\pi$ when (a) $\alpha=2$, $\Gamma_{cv}^{-1}=30$ fs $T_{in}^{-1}=60$ fs, and (b) $\alpha=0$, $\Gamma_{cv}^{-1}=130$ fs, and $T_{in}^{-1}=260$ fs. The contribution of the dynamic spectral hole burning (SBH), and carrier density pulsation (CDP) are also shown.

$$W(\omega_p,\omega_s,\omega_q=\omega_f)=\varepsilon_I(\omega_p,\omega_s,\omega_q=\omega_f)+i\varepsilon_R(\omega_p,\omega_s,\omega_q=\omega_f). \tag{A58}$$

The first and third term of the right-hand side of Eq. (A58) originates from the imaginary and real part of $\tilde{\chi}_{\sigma}^{dshb}$, respectively. The second and fourth term originates from the imaginary and real part of $\tilde{\chi}_{\sigma}^{cdp}$, respectively.

Instead of solving Eq. (A56) by numerical calculations, we present here an approximate analytical solution for semiquantitative understanding of the conversion efficiency, the signal-to-background ratio (SBR_f), the signal-to-noise ratio (SNR_f) and the noise figure (NF_f) of the wavelength conversion by four-wave mixing. We suppose the condition of the continuous wave operation, a constant gain over the cavity, and the complete phase matching condition of $q_f=2q_p-q_s$. We use the signal amplitude of $R_s(L)$ and the pump amplitude of $R_p(L)$ at the exit in the second term of the right-hand side of Eq. (A56). Then, by integrating Eq. (A56) over the waveguide, we obtain the conversion efficiency of

$$\eta_{con}(\omega_p,\omega_s)=\frac{S_f(L)}{S_s(0)}\cong\Gamma_p^2G_f^2|W(\omega_p,\omega_s,\omega_q=\omega_f)|^2S_p(L)^2, \tag{A59}$$

where G_f is the amplifier gain of the converted signal. The SBR_f of the converted signal with the ASE background is given by Eq. (190), the SNR_f of the converted signal against the shot noise and the beating noise with the amplified spontaneous emission is given by Eq. (191), and the noise figure is given by Eq. (192). The high conversion efficiency is a key to high signal quality.

Figure 17(a) shows the calculation of $\eta_{con}(\omega_p,\omega_s)$ as a function of the absolute value of $\Delta\omega/2\pi=(\omega_p-\omega_s)/2\pi$ in the InGaAsP SOA, using the same parameters of Figs. 14(a) and 16(a), and $G_f=17$ dB. We see that the conversion efficiency is asymmetric around the pump frequency, and has a dip at the detuning of $\Delta\omega/2\pi=0.23$ THz under the negative detuning ($\omega_p<\omega_s$) where the contribution of the spectral-hole burning and the carrier density pulsation crosses. This dip results in more than 10 dB difference in the conversion efficiency depending on the direction of conversion. The asymmetry is due to the constructive or destructive interference of the dynamic spectral hole burning and the carrier density pulsation when the detuning is positive ($\omega_p>\omega_s$) or negative ($\omega_p<\omega_s$), respectively. Equation (A58) tells us that the asymmetry of conversion efficiency around the pump frequency becomes remarkable as α increases due to the carrier density pulsation.

Figure 17(b) shows the calculation using the same parameters of Figs. 14(b) and 16(b), where we suppose that the active region consists of quantum dots. We see that the asymmetric gain due to the interference of the two nonlinear components disappears due to $\alpha=0$ [see Eq. (A58) with $\omega_p=\omega_0$]. Compared to Fig. 17(a), we also see that the magnitude of the dynamic spectral hole burning increases by about 25 dB due to the decrease in the relaxation rates at the expense of the bandwidth, and that the magnitude of the carrier density pulsation decreases due to $\alpha=0$. The conversion efficiency of 7 dB is obtained at the detuning of 0.5 THz corresponding to 8 nm wavelength conversion around 1.55 μm and 1.5 dB at the detuning of 1 THz corresponding to 16 nm wavelength conversion.

For example, when $\Delta f_{sp}=500$ GHz ($\Delta\omega_{sp}=2\pi\Delta f_{sp}$), $G_f=17$ dB, $n_{sp}(\omega_f)=1$, $P_s(0)=0$ dBm, and $\hbar\omega_s=0.8$ eV, Eq. (190) gives $\mathrm{SBR}_f=27+\eta_{con}(\omega_p,\omega_s)$ in dB. When $\eta_{in}=\eta_{out}=-2$ dB, Eq. (192) gives $\mathrm{NF}_f=22-\eta_{con}(\omega_p,\omega_s)$ in dB. Then, the conversion efficiency of 0 dB gives $\mathrm{SBR}_f=27$ dB and $\mathrm{NF}_c=22$ dB. The conversion efficiency of 10 dB gives $\mathrm{SBR}_c=37$ dB and $\mathrm{NF}_c=12$ dB, which are promising values for the optical transmission.

3. Empirical gain formula in InGaAsP

The empirical optical gain of bulk InGaAsP we use in the calculation is given as[51]

$$\tilde{g}_\sigma(N,\lambda_m)=\begin{cases}A_N[\lambda_m-\lambda_z(N)]^2+B_N[\lambda_m-\lambda_z(N)]^3 & \lambda<\lambda_z(N),\\ 0 & \lambda>\lambda_z(N),\end{cases} \tag{A60}$$

with

$$A_N=3g_p(N)/[\lambda_z(N)-\lambda_p(N)]^2 \tag{A61}$$

and

$$B_N=2g_p(N)/[\lambda_z(N)-\lambda_p(N)]^3, \tag{A62}$$

where the peak gain is

$$g_p(N)=a_0(N-N_0)+a_1a_0N_0\exp(-N/N_0), \tag{A63}$$

the light wavelength to give the peak gain is

$$\lambda_p(N)=\lambda_0-b_0(N-N_0), \tag{A64}$$

and the light wavelength below which the optical gain appears is

$$\lambda_z(N)=\lambda_{z0}-c_0(N-N_0). \tag{A65}$$

Parameters are $N_0=7.0\times10^{17}$ [cm^{-3}], $a_0=3.0\times10^{-16}$ [cm^2], $a_1=1.0$, $\lambda_0=1.6$ [μm], $b_0=3.0\times10^{-20}$ [$\mathrm{cm}^3\mu$m], $\lambda_{z0}=16.5$ [μm], and $c_0=-3.0\times10^{-21}$ [$\mathrm{cm}^3\mu$m].

*Email address: msuga@iis.u-tokyo.ac.jp

[1] T. Akiyama, T. Simoyama, H. Kuwatsuka, Y. Nakata, K. Mukai, M. Sugawara, O. Wada, and H. Ishikawa, in *Proceedings of the 25th European Conference on Optical Communication (ECOC), 1999* (IEEE, New York, 1999), p. II-76.

[2] T. Akiyama, H. Kuwatsuka, T. Simoyama, Y. Nakata, K. Mukai, M. Sugawara, O. Wada, and H. Ishikawa, IEEE Photonics Technol. Lett. **12**, 1261 (2000).

[3] P. Borri, W. Langbein, J. M. Hvam, F. Heinrichsdorff, M.-H. Mao, and D. Bimberg, IEEE J. Sel. Top. Quantum Electron. **6**, 544 (2000).

[4] P. Borri, W. Langbein, J. M. Hvam, F. Heinrichsdorff, M.-H. Mao, and D. Bimberg, IEEE Photonics Technol. Lett. **12**, 594 (2000).

[5] T. Akiyama, H. Kuwatsuka, T. Simoyama, Y. Nakata, K. Mukai, M. Sugawara, O. Wada, and H. Ishikawa, IEEE J. Quantum Electron. **37**, 1059 (2001).

[6] M. Sugawara, N. Hatori, T. Akiyama, Y. Nakata, and H. Ishikawa, Jpn. J. Appl. Phys., Part 2 **40**, L488 (2001).

[7] M. Sugawara, N. Hatori, T. Akiyama, and Y. Nakata, in *Proceedings of the 13th International Conference on Indium Phosphide and Related Materials 2001* (Nara, 2001), p. 358.

[8] M. Sugawara, N. Hatori, T. Akiyama, and Y. Nakata, in *Proceedings of the 13th International Conference on Indium Phosphide and Related Materials 2001* (Nara, 2001), p. 471.

[9] M. Sugawara, N. Hatori, T. Akiyama, Y. Nakata, and H. Ishikawa, in *Proceedings of the 4th Pacific Rim Conference on Lasers and Electro-Optics* (Makuhari, 2001), p. I-260.

[10] M. Sugawara, T. Akiyama, N. Hatori, and Y. Nakata, in *Proceedings of Contemporary Photonics Technology 2002* (Tokyo, 2002), p. 133.

[11] T. Akiyama, N. Hatori, Y. Nakata, H. Ebe, and M. Sugawara, post deadline paper of the 14th International Conference on Indium Phosphide and Related Materials, Stockholm, 2002.

[12] T. Akiyama, H. Kuwatsuka, N. Hatori, Y. Nakata, H. Ebe, and M.

Sugawara, Electron. Lett. **38**, 1133 (2002).
[13] T. Akiyama, H. Kuwatsuka, N. Hatori, Y. Nakata, H. Ebe, and M. Sugawara, in *Proceedings of Semiconductor Quantum Dots 2002* (Tokyo, 2002), H-4.
[14] M. Sugawara, in *Proceedings of NanOp-Workshop 2002* (Berlin, 2002).
[15] T. Akiyama, N. Hatori, Y. Nakata, H. Ebe, and M. Sugawara, in *Proceedings of the 28th European Conference on Optical Communication (ECOC), Amsterdam, 2002* (IEEE, New York, 2002), p. II-76.
[16] T. Akiyama, H. Kuwatsuka, N. Hatori, Y. Nakata, H. Ebe, and M. Sugawara, IEEE Photonics Technol. Lett. **14**, 1133 (2002).
[17] M. Sugawara, T. Akiyama, N. Hatori, Y. Nakata, K. Otsubo, and H. Ebe, in *APOC 02, Materials and Devices for Optical and Wireless Communications, Shanghai*, SPIE Vol. 4905 (SPIE, Bellingham, WA, 2002), p. 259.
[18] M. Sugawara, T. Akiyama, N. Hatori, Y. Nakata, H. Ebe, and H. Ishikawa, Meas. Sci. Technol. **13**, 1433 (2002).
[19] A. Bilenca, R. Alizon, D. Dahan, and G. Eisenstein, in *Proceedings of the Optical Fiber Communication 2003* (Atlanta, 2003), ThO2.
[20] T. Kita, O. Wada, H. Ebe, Y. Nakara, and M. Sugawara, Jpn. J. Appl. Phys., Part 2 **41**, L1143 (2002).
[21] K. Mukai and M. Sugawara, in *Semiconductors & Semimetals*, edited by M. Sugawara (Academic, San Diego, 1999), Vol. 60, Chap. 5.
[22] A. V. Uskov and J. McInerney, Appl. Phys. Lett. **72**, 58 (1998).
[23] P. Bhattacharya *et al.*, J. Select. Topics Quantum Electron. **6**, 426 (2000).
[24] A. Sakamoto and M. Sugawara, Photon. Tech. Lett. **12**, 107 (2000).
[25] M. Sugawara, K. Mukai, Y. Nakata, and H. Ishikawa, Phys. Rev. B **61**, 7595 (2000).
[26] M. Sargent III, M. O. Scully, and W. E. Lamb, Jr., *Laser Physics* (Addison-Wesley, Reading, 1974).
[27] H. Haug and S. Koch, *Quantum Theory of the Optical and Electronic Properties of Semiconductors*, 3rd ed. (World Scientific, Singapore, 1994).
[28] M. Sugawara, in *Semiconductors & Semimetals*, edited by M. Sugawara (Ref. 21), Vol. 60, Chap. 1.
[29] G. P. Agrawal, *Nonlinear Fiber Optics*, 2nd ed. (Academic, San Diego, 1995).
[30] V. Weisskopf and E. P. Wigner, Z. Phys. **63**, 54 (1930).
[31] A. Yariv, Opt. Lett. **15**, 1064 (1990); H. Kogelink and A. Yariv, Proc. IEEE **52**, 165 (1964).
[32] A. Yariv, *Optical Electronics in Modern Communications* (Oxford University Press, New York, 1997).
[33] E. V. Goldstein and P. Meystre, in *Spontaneous Emission and Laser Oscillation in Microcavities*, edited by H. Yokoyama and K. Ujihara (CRC Press, New York, 1995), Chap. 1.
[34] E. V. Tsiper, Phys. Rev. B **54**, 1959 (1996).
[35] P. Borri, S. Schneider, W. Langbein, U. Woggon, A. E. Zhukov, V. M. Ustinov, N. N. Ledentsov, Zh. I. Alferov, D. Ouyang, and D. Bimberg, Appl. Phys. Lett. **79**, 2633 (2001).
[36] L. Zhang, T. F. Boggess, D. G. Deppe, D. L. Huffaker, O. B. Shchekin, and C. Cao, Appl. Phys. Lett. **76**, 1222 (2000); T. F. Boggess, L. Zhang, D. G. Deppe, D. L. Huffaker, and C. Cao, *ibid.* **78**, 276 (2001).
[37] S. Seki, K. Yokoyama, and P. Sotirelis, Phys. Rev. B **50**, 1663 (1994).
[38] H. Kuwatsuka, T. Simoyama, and H. Ishikawa, IEEE J. Quantum Electron. **35**, 1817 (1999).
[39] N. Hatori, M. Sugawara, K. Mukai, Y. Nakata, and H. Ishikawa, Appl. Phys. Lett. **77**, 773 (2000).
[40] T. Akiyama, M. Sugawara, H. Ebe, and Y. Arakawa (unpublished).
[41] N. Hatori, H. Kuwatsuka, T. Akiyama, K. Otsubo, H. Ebe, Y. Nakata, and M. Sugawara, in *Proceedings of Semiconductor Quantum Dots 2002* (Tokyo, Japan, 2002), G-22.
[42] T. Akiyama, K. Kawaguchi, M. Sugawara, H. Sudo, M. Ekawa, H. Ebe, A. Kuramata, K. Otsubo, K. Morito, and Y. Arakawa, post deadline paper in the 29th European Conference on Optical Communication, 2003.
[43] A. Mecozzi, S. Scotti, A. D'Ottavi, E. Iannone, and P. Spano, IEEE J. Quantum Electron. **31**, 689 (1995).
[44] A. Uskov, J. Mork, and J. Mark, IEEE J. Quantum Electron. **30**, 1769 (1994).
[45] J. Mork and A. Mecozzi, IEEE J. Quantum Electron. **33**, 545 (1997).
[46] G. P. Agrawal, J. Opt. Soc. Am. B **5**, 147 (1988).
[47] K. Kikuchi, M. Kakui, C-E Zah, and T-P Lee, IEEE J. Quantum Electron. **28**, 151 (1992).
[48] G. P. Agrawal and N. Andes Olsson, IEEE J. Quantum Electron. **25**, 2297 (1989).
[49] T. Durhuus, B. Mikkelsen, C. Joergensen, S. L. Danielsen, and K. E. Stubkjaer, J. Lightwave Technol. **14**, 942 (1996).
[50] K. Tajima, S. Nakamura, and Y. Ueno, Meas. Sci. Technol. **13**, 1692 (2002).
[51] J. Leuthold, in *Series in Quantum Electronics*, edited by H. Baltes (Hartung-Gorre Verlag, Konstanz, 1999), Vol. 12.